On Design and Control of Simulated Moving Bed Plants

Dissertation
zur Erlangung des akademischen Grades

Doktoringenieur
(Dr.-Ing.)

von MSc, BEng(HONS), Dipl.-Ing.(FH) Marco Fütterer

geb. am 03.05.1972 in Burg

Genehmigt durch die Fakultät Elektrotechnik und Informationstechnik

der Otto-von-Guericke-Universität Magdeburg.

Gutachter:

    Prof. Dr. A. Kienle

    Prof. Dr. A. Seidel-Morgenstern

    Prof. Dr. A. Vande Wouwer

Promotionskolloquium am: 26.04.2010

Kurzfassung

In vielen Zweigen der chemischen und pharmazeutischen Industrie ist man mit der Aufgabenstellung konfrontiert, Stoffgemische zu trennen. Hierfür existieren verschiedene Trennverfahren, die jeweils die unterschiedlichen Stoffeigenschaften der einzelnen Komponenten ausnutzen. Ein häufig benutztes Trennverfahren ist die Chromatographie. Diese nutzt das unterschiedliche Adsorptionsverhalten der in ein Lösungsmittel aufgelösten Stoffe aus. So bewegt sich die Konzentrationsfront einer stärker adsorbierten Komponente mit einer geringeren Geschwindigkeit durch eine chromatographische Säule als die Konzentrationsfront der schwächer adsorbierten Komponente. Um eine kontinuierliche Auftrennung eines Stoffgemisches zu realisieren, ist eine zyklische Verschaltung von chromatographischen Säulen notwendig. Eine solche Methode wurde von der Firma Universal Oil Products, UOP, in den 60-iger Jahren entwickelt, [1], und wird als Simulated- Moving- Bed, SMB, Verfahren bezeichnet. Seit dieser Zeit wurde diese Technologie in verschiedenen Bereichen zur Stofftrennung erfolgreich angewandt. Der Prozess ist jedoch sehr empfindlich gegenüber Änderungen in den einzustellenden Volumenströmen und Umschaltzeiten. Es ist daher notwendig die Volumenströme und die Umschaltzeit, die man zusammenfassend als Betriebspunkt bezeichnen kann, für einen störungsfreien Betrieb korrekt einzustellen.

Die Berechnung eines Betriebspunktes erfolgt heutzutage meist auf der Basis eines True- Moving- Bed, TMB, Prozesses. Bei diesem Prozess wird ein echter Gegenstrom des Adsorbtionsbetts angenommen. Der Grund hierfür liegt in der Tatsache, dass ein TMB- Prozess mathematisch einfacher zu analysieren ist als ein periodisch arbeitender SMB- Prozess. Auf Basis dieses Modells haben sich im Wesentlichen zwei Verfahren für die Berechnung von Betriebspunkten für vollständige Trennung und vollständige Regeneration etabliert. Das eine Verfahren bezeichnet man als *triangle theory*, [2], [3], und das andere als *standing wave design*, [4], [5]. Die mit diesem Verfahren berechneten Betriebspunkte für den TMB- Prozess werden anschließend in Betriebspunkte für den SMB- Prozess trans-

formiert. Zusätzlich wurden auch Anstrengungen unternommen, um Betriebspunkte für TMB- Prozesse bei geringeren Reinheitsanforderungen zu berechnen, [6], [7]. Der TMB- Prozess ist jedoch nicht in der Lage, die periodischen Konzentrationsänderungen an den Abzügen zu beschreiben.

Um den aktuellen Herausforderungen gerecht zu werden und auch weiterentwickelte Betriebsweisen, wie z.B. die asynchrone Umschaltung durch das VariCol-Konzept, [8], und die Variation des Stoffmengenflusses durch ModiCon, [9], und PowerFeed, [10], gut beschreiben zu können, ist es unabdingbar, neue Verfahren für die Bestimmung von Betriebspunkten zu entwickeln, die den tatsächlichen SMB- Prozess als Ausgangspunkt für die mathematische Analyse verwenden.

In dieser Arbeit wird eine neue Methode für die Berechnung der Stellgrößen des zyklisch-stationären Zustandes eines SMB- Prozesses unter idealisierten Bedingungen vorgestellt. Mit Hilfe dieses Ansatzes, lassen sich explizite Designformeln für eine vollständige Trennung der beteiligten Stoffkomponenten für die in der Praxis häufig verwendeten Langmuir- Isothermen und den daraus abgeleiteten Grenzfällen herleiten. Die periodischen Konzentrationsänderungen an den Abzügen lassen sich nun mathematisch sehr gut beschreiben. Weiterhin wird aufgezeigt, wie sich diese Methode auch bei reduzierter Produktreinheit anwenden lässt.

Zusätzlich wird diese Methode verwendet, um einfache, aber sehr robuste Regelungskonzepte für die automatische Einstellung von SMB- Anlagen zu entwickeln. Diese Regelungskonzepte lassen sich auch verwenden, um komplexe Modelle von SMB- Anlagen effektiv zu optimieren.

Abstract

In many branches of the chemical and pharmaceutical industry, one is confronted with the task of separating mixtures of substances. For this, various separating methods exist, which make use of the different properties of the individual components. A frequently-used separating procedure is chromatography. This exploits the different adsorption behaviors of the materials dissolved into a solvent. Thus, the concentration front of a component more strongly adsorbed moves with a lower velocity through a chromatographic column than the concentration front of the component more weakly adsorbed. In order to realize a continuous separation of a substance mixture, a special cyclical port shifting is necessary. Such a method was developed by Universal Oil Products, UOP, in the '60s, [1], and is called the simulated moving bed, SMB, method. Since that time, this technology has successfully been used for the separation of substances in different areas. However, this process is very sensitive to volumetric flow rates and switching time. Therefore, it is necessary to adjust the flow rates and switching time carefully for a faultless operation. In the following, the flow rates and switching time are summarized as an operating point.

Nowadays, the determination of an operating point is usually carried out on the basis of a true moving bed, TMB, process. Like a countercurrent heat exchanger, the TMB process assumes a countercurrent motion between adsorbed and liquid phase. This assumption allows a simpler mathematical analysis in comparison with a SMB process that works periodically. Based on the TMB model, two methods have been introduced for the calculation of operating points in the case of complete separation and complete regeneration. The first procedure is called *triangle theory*, [2], [3], and the second is called *standing wave design*, [4],[5]. The operating points for the TMB process calculated with one of these procedures are transformed into operating points for the SMB process. In addition, some efforts were made to also compute operating points for TMB processes under reduced purity requirements, [6], [7]. Unfortunately, the TMB process is only an approximation and is not able to describe the periodic changes in the concentrations at

the drains.

Many modern operations, like asynchronous switching of columns by the Vari-Col concept, [8], and the variation of the component flow rates by ModiCon, [9], and PowerFeed, [10], make use of the periodic behavior of the SMB process. In order to appropriately describe the cyclic processes mathematically, it is necessary to develop new tools that analyze the SMB process directly.

In this contribution, a new method for designing SMB plants is developed. It is based on an idealized model which neglects axial dispersion and assumes thermodynamic equilibrium. The periodic changes of the concentrations at the drains at cyclic steady state are appropriately described. Explicit design formulas are derived for the most popular isotherms, which mathematically describe the adsorption behavior. This work shows further how operating points can be determined under reduced purity requirements. In addition, this method is used to develop simple but very robust control concepts for an automatic adjustment of SMB plants. These control concepts may also be used to optimize more complex models of SMB plants effectively.

Acknowledgements

Contents

1 Introduction to Simulated Moving Bed Chromatography

Preparative chromatography is an important separation method. It uses the effect of different adsorption affinities of components dissolved into a solvent. Thus, the concentration front of a more strongly adsorbed component moves with a lower velocity through a chromatographic column than the concentration front of the more weakly adsorbed component. In the sixties, the company Universal Oil Products, UOP, developed the simulated moving bed, SMB, Technology, [1]. Chromatographic columns are interconnected to form a ring. The connections of the feeding and drains are cyclically changed to allow a continuous separation of a binary mixture.

1.1 Process Description

As shown in Fig. 1.1, the classical SMB process consists of four zones that are coupled through the volumetric flow rates of the liquid phase. Each zone can consist of several chromatographic columns. The binary mixture, which is fed in between the second and third zone, is called "feed". The stronger adsorbed component, B, is obtained at the "extract" between the first and second zone. On the other hand, the weaker adsorbed component, A, is obtained at the "raffinate" between the third and fourth zone. Additionally, a pure solvent stream is provided between the fourth and first zones. The volumetric flow rates are adjusted with the aid of the four pumps, U_I, U_{Ex}, U_{Fe} and U_{Ra}. The flow and port shift directions are indicated in Fig. 1.1. After a specific time, the connections together with the pumps are shifted synchronously in the direction of the liquid phase by one column length. The propagation velocity of the more strongly adsorbed component, B, must be smaller than the switching speed, so that this component moves in the direction of the extract. On the other hand, the propagation ve-
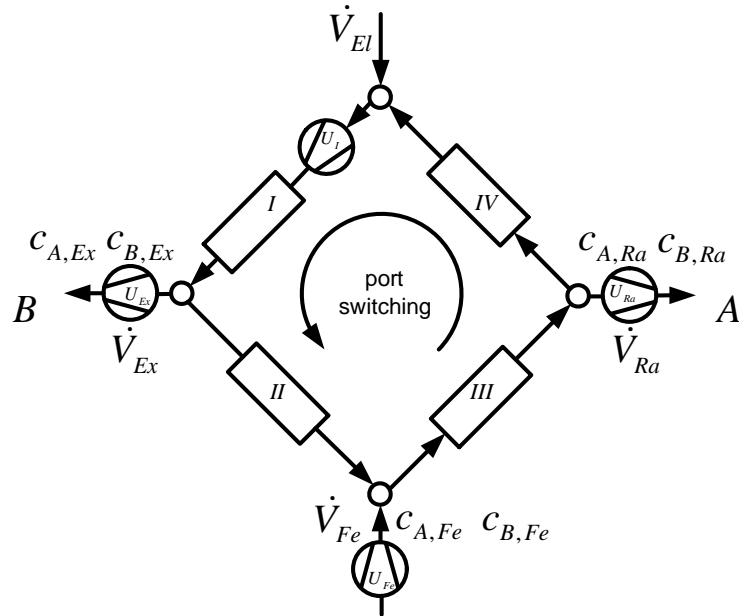
Figure 1.1: Configuration of a four zone SMB plant.

locity of the weaker adsorbed component, A, must be larger than the switching speed, so that this component moves in the direction of the raffinate. Therefore, a correct setting of the zone velocities is necessary for a faultless operation. As indicated in Fig. 1.2, the four zones may be arranged in a plane to plot the associated concentration profiles at cyclic steady state above the columns. The spatial coordinate is chosen such that it starts with zone I. Within a certain time interval, the concentration profiles move from the left to the right.

1.2 A Short Review on Design of SMB plants

The SMB process has a periodic behavior, which makes the mathematical analysis difficult. For this reason, one frequently uses an approximation. Thus, it is assumed that a real countercurrent flow exists between liquid and adsorbed phase. Such a process is called a true moving bed, TMB. The main reason for this approximation is that a suitable adjusted TMB process offers a real steady state, where all states are constant. A SMB process will only archive a cyclic steady state. The cyclic steady state still depends on space and time coordinates regardless if a rotating observer is used or not. This means that one still has to solve a partial differential equation, PDE, to determine its cyclic steady state profile,
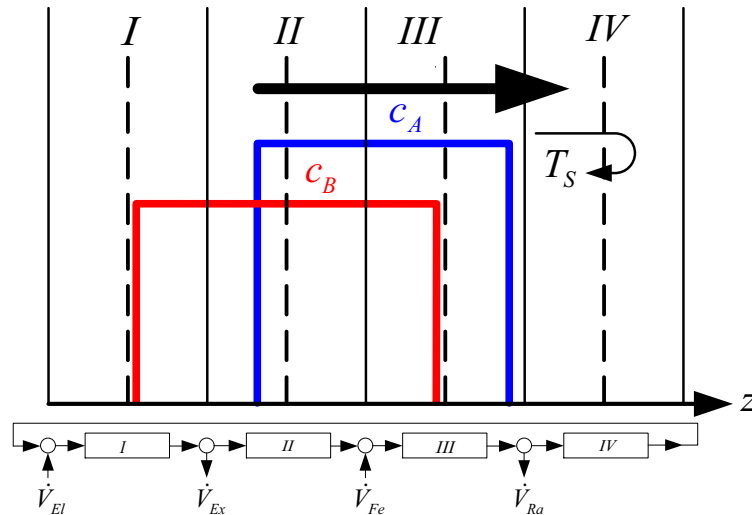
Figure 1.2: Idealized concentration profiles of an SMB plant moving from the left to the right.

which makes an analytic approach more demanding.

Nowadays, it is most common to use either the *triangle theory*, [2], [3], or the *standing wave design*, [4], [5], to find operating conditions for a TMB process.

The *triangle theory* is based on the classical approach to solve a ordinary differential equation, ODE, for the steady state profile. Since the standard TMB process consist of four section all four solutions together with the coupling equations leads to an algebraic set of equations that needs to be solved. For a dispersion-free model and for complete separation, the set of equations leads to explicit solutions for Henry and Langmuir isotherms.

The *standing wave design* uses the observation that at steady-state each wave front has a fixed location. With other words four standing waves are formed. Using the conditions for a standing wave, one can set-up a set of algebraic equations, which can be used to solve for the unknown flow rates.

Both methods only find operating conditions under idealized conditions and there may be a discrepancy to the real SMB process. Thus, the idealized operating conditions are often used as initial guess for a dynamic optimization, [11], [12]. A dynamic optimization is only usefully if a good dynamic model including its parameters is known. In practice, this is often not the case and therefore a closed loop control is of great interest.

A general review on design of SMB plants including the references to the most significant contributions can be found in [13], [14], [15].

1.3 A Short Review on Control of SMB plants

SMB technology is an attractive separation process for binary mixtures and has its applications in the fine chemical and pharmaceutical industry. Nowadays, most plants operate in open loop far away from the optimum to increase robustness. Since this process is very sensitive to disturbances and parameter changes, it is natural to require an automatic controller which is capable of always driving the system near the optimum.

Several contributions on this topic have been reported in the literature. The first concepts published are based on TMB models, [16], [17], [18], [19]. However, this model is not able to describe the periodic behavior of the concentrations at the drains. For this reason, the full SMB model is often suggested as a basis for the control design. In [20] and [21] a concept was introduced, which uses the linearization of the complete model around the trajectory of the cyclic steady state. The resulting linear time varying model of high order can then be used as a starting point for an arbitrary classical control design.

A predictive control strategy based on a numeric optimization of the future trajectory of the nonlinear model is also frequently suggested, [22], [23]. An advantage in this approach lies in the fact that this method is relatively universal and can be easily transferred to different process models. Furthermore, constraints in the control variables can also be taken into account explicitly. The drawback is that the necessary discretization of the partial differential equations often leads to a numeric model representation of high order. Usually, the parameters will enter into the model in a complex way. Furthermore, a high number of states of this model need to be reconstructed from a small number of inputs and measured outputs, which often leads to a slow convergence in the state estimates. Changes in the model parameters, e.g. by aging, have a great influence on the quality of the state estimates and the control performance. Therefore, it is necessary to adapt the process parameters.

The natural question arises if it would be possible to describe the essential dynamics with a low-order model. First concepts with this philosophy are published in [24], [25] and in [26], [27], [28]. In a first step, these works attempt to reconstruct the concentration fronts of the SMB profile in a different way. After the concentration fronts of the SMB profile are approximated, signals are derived for their positions. In a second step, an experimental model approach is used to establish a connection between the positions of the four concentration fronts and

the four control variables. Such a control design leads to simpler controllers of low order that are desired in practice. However, the concentration fronts can take very different shapes, especially during the startup phase. Through this, the reconstruction of the concentration front is very susceptible. It would therefore be favorable to find a control concept without the reconstruction of the complete concentration fronts. In [18] and [19] the static equations of the concentration velocities of the wave fronts of the TMB model are used in order to achieve a static decoupling. The dynamic behavior is also described by an experimental approach that leads again to time-consuming experiments. To avoid this, it would be favorably to find a more rigorous approach, which describes the relationship between the inputs and outputs. Furthermore, it should be tried to achieve an automatic adjustment of the model parameters from past measurements.

1.4 Outline of this Thesis

In this thesis, a new method for the analysis of SMB plants is presented. In a first chapter, the basics of chromatography are repeated to provide the reader the mathematical tools necessary in the subsequent chapters.

A second chapter deals with the determination of operating points for dispersion-free SMB models for the most used isotherms. Explicit equations are derived which have a great practical use for the design of SMB plants. These equations can be used as an ideal initial condition for a further dynamic optimization. In this way, the optimization time can be reduced considerably. In addition it is possible to predict the time trajectory of the concentrations at the drains at cyclic steady state almost exactly. Thus, one can judge the quality of different numeric solution methods for the simulation. A simple sensitivity analysis can be carried out with help of these equations. This leads to more insight into the process and to new ideas how one can optimize it.

A third chapter shows how one can use this knowledge for an adaptive control-strategy. Two control concepts are introduced. The first concept is a simple but extremely robust adaptive control strategy for SMB plants in case of complete separation. The second control concept indicates a simple extension to reduced purities and the control of four-column SMBs.

If you pretend to be good, the world takes you very seriously.
If you pretend to be bad, it doesn't. Such is the astounding
stupidity of optimism.

~ Oscar Wilde ~

2 Basics of Chromatography

This chapter will review the basic theory in chromatography, as it is needed throughout the thesis. It is written in such a style that it provides a good starting point to enter the field of chromatography. Experienced readers may skip this chapter.

2.1 Modeling of Chromatographic Columns

In this section, the basic model equations for chromatographic columns are derived from first principles, [29], [30], [31], [32], [33].

2.1.1 Liquid Phase Balance

To describe a chromatographic column in a simple way, an incompressible fluid is assumed, and thus the total mass balance reduces to an algebraic equation. Therefore, one may start directly with the component balance of the liquid phase in general integral form. To do this, the mole number per unit length is introduced and signed with an over bar. Further, all flow variables are indicated with an over dot. The balance equation simple states: that the temporal change of stored moles within the fixed domain of interest is equal to the in and out flow to this domain and the production rate. In this case, the production rate is the exchange rate between the liquid and adsorbed phase.

$$\frac{d}{dt} \int_a^b \bar{n}\left(t,z\right) dz = \dot{n}\left(t,a\right) - \dot{n}\left(t,b\right) + \int_a^b \dot{\bar{n}}_{ex}\left(t,z\right) dz \tag{2.1}$$

If continuity of component flow is assumed, the in and out flow can be expressed using the equivalent integral relationship.

$$\int_a^b \frac{\partial \bar{n}(t,z)}{\partial t} dz = -\int_a^b \frac{\partial \dot{n}(t,z)}{\partial z} dz + \int_a^b \dot{\bar{n}}_{ex}(t,z)\, dz \tag{2.2}$$

The volume concentration is used to substitute the mole number per unit length. The volume occupied by the liquid is expressed as product of void fraction, ε, and total volume, V.

$$\bar{n}(t,z) = c(t,z) \frac{\varepsilon V}{L} = c(t,z)\, \varepsilon A \tag{2.3}$$

The mole flow rate, within the domain, consists of a convective and a diffusive part. It is practical to use the measurable liquid volume flow rate to build up the convective part. Fick's law describes the diffusive part, which is proportional to the fluid cross section area.

$$\dot{n}(t,z) = c(t,z)\, \dot{V}_l - D\,\varepsilon\,A \frac{\partial c(t,z)}{\partial z} \tag{2.4}$$

A linear driving term is used to express the exchange between liquid and adsorbed phase. For simplicity, the chosen mass transfer resistance includes also the surface area. Further, an equilibrium relationship, $f(c(t,z))$, needs to be specified.

$$\dot{\bar{n}}_{ex}(t,z) = -\frac{1}{R}\left(f(c(t,z)) - q(t,z)\right) \tag{2.5}$$

All these terms are inserted in the integral balance equation, Eq. (2.2).

$$
\begin{aligned}
\int_a^b \frac{\partial c(t,z)}{\partial t}\,\varepsilon\,A dz = \ & -\int_a^b \left(\frac{\partial c(t,z)}{\partial z}\,\dot{V}_l - D\,\varepsilon\,A\,\frac{\partial^2 c(t,z)}{\partial z^2}\right) dz \\
& -\int_a^b \frac{1}{R}\left(f(c(t,z)) - q(t,z)\right) dz
\end{aligned}
\tag{2.6}
$$

Afterwards, all parts are collected under one integral.

$$\int_a^b \left[\begin{array}{c} \frac{\partial c(t,z)}{\partial t}\,\varepsilon\,A + \frac{\partial c(t,z)}{\partial z}\,\dot{V}_l - D\,\varepsilon\,A\,\frac{\partial^2 c(t,z)}{\partial z^2} \\ +\frac{1}{R}\left(f(c(t,z)) - q(t,z)\right) \end{array}\right] dz = 0 \tag{2.7}$$

Since the equation has to be satisfied for arbitrary fixed length, the term under the integral must be zero. As result, the differential description of the fluid phase concentration is obtained.

$$\varepsilon A \frac{\partial c(t,z)}{\partial t} + \dot{V}_l \frac{\partial c(t,z)}{\partial z} \quad - D \varepsilon A \frac{\partial^2 c(t,z)}{\partial z^2} \\ + \frac{1}{R} \left(f\left(c\left(t,z \right) \right) - q\left(t,z \right) \right) = 0 \tag{2.8}$$

2.1.2 Adsorbed Phase Balance

The same method can be used to derive the component balance for the adsorbed phase. Now the integral balance equation will not have a flow term.

$$\frac{d}{dt} \int_a^b \bar{n}_q\left(t,z \right) dz = - \int_a^b \dot{n}_{ex}\left(t,z \right) dz \tag{2.9}$$

Again, the mole numbers are substituted using volume concentration.

$$\int_a^b \frac{\partial q\left(t,z \right)}{\partial t} \left(1 - \varepsilon \right) A dz = \int_a^b \frac{1}{R} \left(f\left(c\left(t,z \right) \right) - q\left(t,z \right) \right) dz \tag{2.10}$$

All terms are collected under one integral and the equation needs to be satisfied for different fixed length. Therefore, the integrand must be zero.

$$\int_a^b \left[\frac{\partial q\left(t,z \right)}{\partial t} \left(1 - \varepsilon \right) A - \frac{1}{R} \left(f\left(c\left(t,z \right) \right) - q\left(t,z \right) \right) \right] dz = 0 \tag{2.11}$$

Finally, the differential description of the adsorbed phase concentration is obtained.

$$\frac{\partial q\left(t,z \right)}{\partial t} \left(1 - \varepsilon \right) A - \frac{1}{R} \left(f\left(c\left(t,z \right) \right) - q\left(t,z \right) \right) = 0 \tag{2.12}$$

2.1.3 Boundary Conditions

To complete the model, boundary conditions need to be defined. They describe the in and out flow through the boundary of the specified domain. For the liquid

phase, the integral description of the left boundary is formulated by Eq. (2.13).

$$\frac{d}{dt} \int_0^b \bar{n}\,(t,z)\,dz = \dot{n}_{in}\,(t) - \dot{n}\,(t,b) + \int_0^b \dot{\bar{n}}_{ex}\,(t,z)\,dz \qquad (2.13)$$

In the limit, $\lim_{b \to 0}$, the mole flow rates are coupled directly:

$$\dot{n}_{in}\,(t) = \dot{n}\,(t,0)\,. \qquad (2.14)$$

The mole flow rates are expressed in volume concentration. Therefore, the left boundary condition has following form:

$$c_{in}\,(t)\,\dot{V}_l = c\,(t,0)\,\dot{V}_l - D\,\varepsilon\,A\,\frac{\partial c\,(t,z)}{\partial z}\bigg|_{z=0}, \qquad \text{for } z = 0. \qquad (2.15)$$

The integral balance for the right boundary is derived in a similar manner.

$$\frac{d}{dt} \int_a^L \bar{n}\,(t,z)\,dz = \dot{n}\,(t,a) - \dot{n}_{out}\,(t) + \int_a^L \dot{\bar{n}}_{ex}\,(t,z)\,dz \qquad (2.16)$$

If taking the limit, $\lim_{a \to L}$, the inner and outer mole flow rates are coupled directly:

$$\dot{n}_{out}\,(t) = \dot{n}\,(t,L)\,, \qquad (2.17)$$

$$c_{out}\,(t)\,\dot{V}_l = c\,(t,L)\,\dot{V}_l - D\,\varepsilon\,A\,\frac{\partial c\,(t,z)}{\partial z}\bigg|_{z=L}, \qquad \text{for } z = L. \qquad (2.18)$$

Since the leaving concentration is equal to the concentration at the boundary, $c_{out}\,(t) = c\,(t,L)$, the right boundary condition, Eq. (2.18), is simple:

$$\frac{\partial c\,(t,z)}{\partial z}\bigg|_{z=L} = 0. \qquad (2.19)$$

There is no need to specify boundary conditions for the adsorbed phase, since no flow is present. The partial differential equation for the adsorbed phase concentration is in principle an ordinary differential equation where the space coordinate is treated as a parameter.

2.1.4 Summary of Governing Equations

For a quick overview, the governing model equations for single component chromatography are collected here:

$$\frac{\partial c(t,z)}{\partial t} = -\frac{\dot{V}_l}{\varepsilon A} \frac{\partial c(t,z)}{\partial z} + D \frac{\partial^2 c(t,z)}{\partial z^2} - \frac{1}{R\,\varepsilon\,A} \left(f\left(c\left(t,z\right)\right) - q\left(t,z\right)\right), \tag{2.20}$$

$$\frac{\partial q(t,z)}{\partial t} = \frac{1}{R\,(1-\varepsilon)\,A} \left(f\left(c\left(t,z\right)\right) - q\left(t,z\right)\right), \tag{2.21}$$

$z \in (0, L)$ and $t \in (0, \infty)$.

With boundary conditions:

$$c_{in}\left(t\right) = c\left(t, 0\right) - \frac{D\,\varepsilon\,A}{\dot{V}_l} \frac{\partial c(t,z)}{\partial z}\Big|_{z=0}, \qquad \frac{\partial c(t,z)}{\partial z}\Big|_{z=L} = 0, \tag{2.22}$$

and initial conditions:

$$c\left(0, z\right) = c_0\left(z\right), \quad q\left(0, z\right) = q_0\left(z\right). \tag{2.23}$$

If Eq. (2.21) is substituted in Eq. (2.20), following alternative form is derived:

$$\frac{\partial c(t,z)}{\partial t} + \frac{1-\varepsilon}{\varepsilon} \frac{\partial q(t,z)}{\partial t} = -\frac{\dot{V}_l}{\varepsilon\,A} \frac{\partial c(t,z)}{\partial z} + D \frac{\partial^2 c(t,z)}{\partial z^2}, \tag{2.24}$$

$$\frac{\partial q(t,z)}{\partial t} = \frac{1}{R\,(1-\varepsilon)\,A} \left(f\left(c\left(t,z\right)\right) - q\left(t,z\right)\right). \tag{2.25}$$

2.1.5 Simplification for Fast Adsorption

If the resistance for the exchange between the liquid and adsorbed phase approaches zero, the differential equation for the adsorbed phase becomes an algebraic equation. In this case, the adsorbed phase is expressed directly by the equilibrium relationship.

$$q\left(t, z\right) = f\left(c\left(t, z\right)\right) \tag{2.26}$$

As consequence, only one partial differential equation is needed to describe a single component chromatographic column.

$$\frac{\partial c\,(t,z)}{\partial t} + \frac{1-\varepsilon}{\varepsilon} \frac{\partial q\,(t,z)}{\partial t} = -\frac{\dot{V_l}}{\varepsilon\,A} \frac{\partial c\,(t,z)}{\partial z} + D\,\frac{\partial^2 c\,(t,z)}{\partial z^2} \tag{2.27}$$

2.1.6 Two Component Chromatography for Fast Adsorption

If chromatography with several components is used, one gets for each component one partial differential equation. The steady state adsorption relationship will in general depend on all components used. The governing equations for a two component chromatographic column for fast adsorption are given below:

$$\frac{\partial c_A}{\partial t} + \frac{1-\varepsilon}{\varepsilon} \frac{\partial q_A\,(c_A, c_B)}{\partial t} = -\frac{\dot{V_l}}{\varepsilon\,A} \frac{\partial c_A}{\partial z} + D\,\frac{\partial^2 c_A}{\partial z^2}, \tag{2.28}$$

$$\frac{\partial c_B}{\partial t} + \frac{1-\varepsilon}{\varepsilon} \frac{\partial q_B\,(c_A, c_B)}{\partial t} = -\frac{\dot{V_l}}{\varepsilon\,A} \frac{\partial c_B}{\partial z} + D\,\frac{\partial^2 c_B}{\partial z^2}, \tag{2.29}$$

for $z \in (0, L)$ and $t \in (0, \infty)$.

With boundary conditions:

$$c_{i,in}\,(t) = c_i\,(t,0) - \frac{D\,\varepsilon\,A}{\dot{V_l}} \left.\frac{\partial c_i(t,z)}{\partial z}\right|_{z=0}, \quad \left.\frac{\partial c_i(t,z)}{\partial z}\right|_{z=L} = 0, \quad i = A, B, \tag{2.30}$$

and initial conditions:

$$c_i\,(0,z) = c_{i,0}\,(z), \quad q_i\,(0,z) = q_{i,0}\,(z), \quad i = A, B. \tag{2.31}$$

2.1.7 Langmuir Isotherms

To describe the adsorption process on surfaces the simple model idea of Langmuir, [34], [35], is used. It assumes that molecules are adsorbed at a fixed number of adsorption sites of equal energy, where each site can hold one adsorbate molecule until mono layer coverage is achieved. It is further assumed that no interaction between adsorbate molecules takes place. A fractional coverage, ϑ, is introduced, which is defined as ratio of adsorbed covered sites of component A to the total number of sites available per unit volume. The exchange rates between adsorbed and liquid phase is described by the rate of adsorption and desorption.

The rate of adsorption is written in dependency of the liquid component concentration and the overall coverage.

$$r_{ad} = k_{ad} \, c_A \, (1 - \vartheta) \tag{2.32}$$

The rate of desorption is only written in dependency of the coverage with component A.

$$r_{des} = k_{des} \, \vartheta_A \tag{2.33}$$

At equilibrium, the overall rate is zero and following equation holds.

$$0 = r_{ad} - r_{des} = k_{ad} \, c_A \, (1 - \vartheta) - k_{des} \, \vartheta_A \tag{2.34}$$

The overall coverage is the sum of all component coverage's. For a single component A it is just:

$$\vartheta = \vartheta_A. \tag{2.35}$$

The resulting equation can now be solved for this component coverage.

$$\vartheta_A = \frac{\frac{k_{ad}}{k_{des}} \, c_A}{1 + \frac{k_{ad}}{k_{des}} \, c_A} = \frac{K_A \, c_A}{1 + K_A \, c_A} \tag{2.36}$$

Finally, the equation can be written in adsorbed concentrations by introducing the saturation limit also called mono layer capacity for the corresponding component for Langmuir isotherms:

$$q_A = q_S \frac{K_A \, c_A}{1 + K_A \, c_A}, \quad q_A \, (c_A \to \infty) = q_S. \tag{2.37}$$

The equilibrium constant, K_A, decreases with increasing temperature and can be modeled by the following ansatz:

$$K_A \, (T) = K_{A\infty} \, e^{\frac{Q}{RT}}. \tag{2.38}$$

The product of saturation limit and equilibrium rate constant may be combined

to the Henry constant.

$$H_A = q_S K_A \tag{2.39}$$

This reaction kinetic like modeling can be extended to more than one species. For two components and different saturation capacities, the Langmuir isotherms are given by Eq. (2.40) and Eq. (2.41).

$$q_A\left(c_A, c_B\right) = \frac{H_A c_A}{1 + K_A c_A + K_B c_B} \tag{2.40}$$

$$q_B\left(c_A, c_B\right) = \frac{H_B c_B}{1 + K_A c_A + K_B c_B} \tag{2.41}$$

2.1.8 Selectivity and Adsorbility

Adsorbility is defined as ratio of adsorbed to liquid concentration in steady state.

$$\gamma = \frac{q\left(c\right)}{c} \tag{2.42}$$

Selectivity between two components is defined as ratio of their adsorbilities.

$$S_{AB} = \frac{\gamma_A}{\gamma_B} = \frac{q\left(c_A\right) c_B}{q\left(c_B\right) c_A} \tag{2.43}$$

In case of Langmuir Isotherms, it follows that they have constant selectivity, [34].

$$\gamma = \frac{H}{1 + K c}, \quad S_{AB} = \frac{H_A}{H_B} \tag{2.44}$$

2.2 Analysis of a Single Component Chromatographic Column

The questions arise if some analytical approach can be made to get a deeper insight in the behavior of chromatography by using the model equations. To this, Some analysis techniques are introduced here as a basic tool to derive analytical equations that sufficiently describes chromatographic effects. A detailed treatment was given by [29].

2.2.1 Method of Characteristic

The method of characteristics, [36], is a powerful tool to derive analytical solutions for first-order partial differential equation. Since the original model is second order in space, one can only use this tool if diffusion is neglected. Therefore following partial differential equation for a single component chromatography is used as starting point.

$$\frac{\partial c}{\partial t} + F \frac{\partial q}{\partial t} = -v_l \frac{\partial c}{\partial z}, \quad z \in (0, L], \quad t \in (0, \infty) \tag{2.45}$$

with $q = q\left(c\left(t, z\right)\right)$ and $c_{in}\left(t\right) = c\left(t, 0\right)$, $c\left(0, z\right) = c_0\left(z\right)$.

This partial differential equation may be written in form of Eq. (2.46).

$$\left(1 + F \frac{dq}{dc}\right) \frac{\partial c}{\partial t} + v_l \frac{\partial c}{\partial z} = 0 \tag{2.46}$$

It is assumed that the concentration depends only on a single variable. If this is the case, following relationship is obtained.

$$c\left(t\left(s\right), z\left(s\right)\right) \quad \rightarrow \frac{dc}{ds} = \frac{\partial c}{\partial t} \frac{dt}{ds} + \frac{\partial c}{\partial z} \frac{dz}{ds} \tag{2.47}$$

A simple comparison of the coefficients results in a set of ordinary differential equations.

$$\begin{aligned} \frac{dc}{ds} &= 0 \\ \frac{dt}{ds} &= 1 + F \frac{dq}{dc} \\ \frac{dz}{ds} &= v_l \end{aligned} \tag{2.48}$$

This set is reduced by one equation if s is eliminated.

$$\left(1 + F \frac{dq}{dc}\right) \frac{dc}{dt} = 0, \quad \frac{dz}{dt} = \frac{v_l}{1 + F \frac{dq}{dc}} \tag{2.49}$$

The first equation is satisfied if either the concentration is constant or the bracket is zero. If the concentration is constant, the right hand side of the second differential equation, Eq. (2.49), is also constant and can be integrated.

$$c\left(t\right) = c_{ref}, \quad z - z_{ref} = \frac{v_l}{1 + F \frac{dq}{dc}} \left(t - t_{ref}\right) \tag{2.50}$$

The integration constants, c_{ref}, z_{ref}, and t_{ref}, are selected such that the initial or boundary conditions are satisfied. With, $c_{ref} = c(0, z_{ref}) = c_0(z_{ref})$, the propagation of any point of the initial profile can be described.

$$c(t,z) = c_0(z_{ref}) = c_0 \left(z - \frac{v_l}{1 + F\frac{dq}{dc}} t \right) \tag{2.51}$$

Taking, $c_{ref} = c(t_{ref}, 0) = c_{in}(t_{ref})$, any point of the boundary condition can also be described.

$$c(t,z) = c_{in}(t_{ref}) = c_{in} \left(t - \frac{1 + F\frac{dq}{dc}}{v_l} z \right) \tag{2.52}$$

There is still one special solution of Eq. (2.49) left, which is the root of following equation.

$$1 + F\frac{dq}{dc} = 0 \tag{2.53}$$

Since for most practical isotherms, $\frac{dq}{dc} \geq 0$, for all positive concentration it is not a physical solution and can be neglected.

2.2.2 Rarefaction Wave

The solution found by the method of characteristics describes the propagation of a concentration point along the characteristics. A problem arises if the characteristic lines are not parallel. Suppose the initial profile is piecewise constant. Assume further that the left side of the discontinuity is lower than the right side. In this case, there is a piece within the (t,z) space that is not directly related to any point of the initial profile and the equations from last section are not able to describe this area, [37].

$$\left(1 + \frac{FH}{(1 + Kc)^2} \right) \frac{\partial c}{\partial t} + v_l \frac{\partial c}{\partial z} = 0, \quad c(0,z) = \begin{cases} c_L & z < z_{ref} \\ c_R & z > z_{ref} \end{cases}, \quad c_L < c_R \tag{2.54}$$

Since the model describes a real physical system, there should be a unique solution for this area. The boundary of this area can be described by the left and
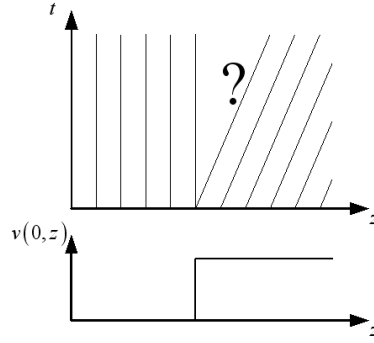
Figure 2.1: Creation of a rarefaction wave.

right state of the initial condition. One may assume that a smooth transition between these states is developed as time increases. In case of Langmuir isotherms, Eq. (2.40) and Eq. (2.41) on page 14, it is possible to solve the equation explicitly, which determines the characteristic for the concentration.

$$z - z_{ref} = \frac{v_l}{1 + F \frac{dq}{dc}} \left(t - t_{ref} \right) = \frac{v_l}{1 + F \frac{H}{(1+Kc)^2}} \left(t - t_{ref} \right) \tag{2.55}$$

$$c(t,z) = \frac{1}{K} \left(\sqrt{\left| \frac{FH}{v_l \frac{t-t_{ref}}{z-z_{ref}} - 1} \right|} - 1 \right) \tag{2.56}$$

To show that this is indeed a solution one has to plug it into the original PDE and prove that it can solve this equation. This kind of solution is called self-similarity solution since it does not depend separately on t and z. It depends on a similarity variable, $\eta(t,z) = \frac{t-t_{ref}}{z-z_{ref}}$. If the reference point is chosen to be the origin, which means, $t_{ref} = 0$ and $z_{ref} = 0$, one call this centered rarefaction. The full solution of this Riemann problem is stated below.

$$c(t,z) = \begin{cases} c_L & \frac{z-z_{ref}}{t-t_{ref}} < \frac{v_l}{1+F \frac{H}{(1+Kc_L)^2}} \\[3ex] \frac{1}{K} \left(\sqrt{\left| \frac{FH}{v_l \frac{t-t_{ref}}{z-z_{ref}} - 1} \right|} - 1 \right) & \frac{v_l}{1+F \frac{H}{(1+Kc_L)^2}} < \frac{z-z_{ref}}{t-t_{ref}} < \frac{v_l}{1+F \frac{H}{(1+Kc_R)^2}} \\[3ex] c_R & \frac{z-z_{ref}}{t-t_{ref}} > \frac{v_l}{1+F \frac{H}{(1+Kc_R)^2}} \end{cases}$$
$$\tag{2.57}$$

2.2.3 Shock Wave

Another problem arises if a piecewise constant initial profile is chosen with a discontinuity; where the right side is lower than the left side, [37]. In such cases the left side will travel with higher speed as the right side, which is pointed out by the intersections of characteristic lines. It seems that the shaded area is over determined.

$$
\frac{\partial}{\partial t} \left(c + F q \left(c \right) \right) + v_l \frac{\partial c}{\partial z} = 0, \quad c \left(0, z \right) = \begin{cases} c_L & z < z_{ref} \\ c_R & z > z_{ref} \end{cases}, \quad c_L > c_R \qquad (2.58)
$$

To deal with this problem, a general balance equation in differential form is
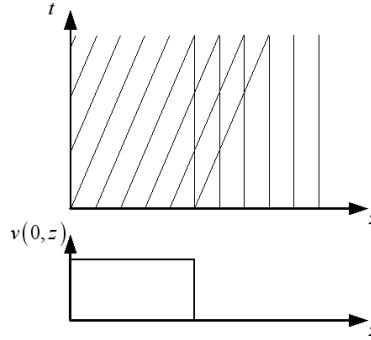
Figure 2.2: Creation of a shock wave.

investigated.

$$
\frac{\partial \tilde{\mathbf{q}} \left(\mathbf{v} \left(t, z \right) \right)}{\partial t} = -\frac{\partial \tilde{\mathbf{f}} \left(\mathbf{v} \left(t, z \right) \right)}{\partial z} \qquad (2.59)
$$

The variable, $\tilde{\mathbf{q}}$, is a stored quantity and, $\tilde{\mathbf{f}}$, is a flow density in dependency of a chosen state variable. Integration in space and time on both side of the equation is performed.

$$
\int_0^L \tilde{\mathbf{q}} \left(\mathbf{v} \left(t, \zeta \right) \right) d\zeta = -\int_0^t \tilde{\mathbf{f}} \left(\mathbf{v} \left(\tau, L \right) \right) - \tilde{\mathbf{f}} \left(\mathbf{v} \left(\tau, 0 \right) \right) d\tau = 0 \qquad (2.60)
$$

Taking the time derivative on both sides and neglecting initial conditions one obtains a general balance equation in integral form.

$$\frac{d}{dt} \int_0^L \tilde{\mathbf{q}} \left(\mathbf{v} \left(t, \zeta \right) \right) d\zeta = \tilde{\mathbf{f}} \left(\mathbf{v} \left(t, 0 \right) \right) - \tilde{\mathbf{f}} \left(\mathbf{v} \left(t, L \right) \right) \tag{2.61}$$

If a discontinuity exists, the integration needs to be divided in two parts. The position of this discontinuity may be time dependent and is described by following equation.

$$s = s \left(t \right) \tag{2.62}$$

Since the balance equation has to be valid for any arbitrary domain, some fixed values in space are used around the discontinuity. Therefore, following equation can be derived.

$$\frac{d}{dt} \int_{z_1}^{s(t)} \tilde{\mathbf{q}} \left(\mathbf{v} \left(t, \zeta \right) \right) d\zeta + \frac{d}{dt} \int_{s(t)}^{z_2} \tilde{\mathbf{q}} \left(\mathbf{v} \left(t, \zeta \right) \right) d\zeta = \tilde{\mathbf{f}} \left(\mathbf{v} \left(t, z_1 \right) \right) - \tilde{\mathbf{f}} \left(\mathbf{v} \left(t, z_2 \right) \right) \tag{2.63}$$

Changing the order of differentiation and integration and taking care about the time dependent boundary one obtains Eq. (2.64).

$$\int_{z_1}^{s(t)-0} \frac{d\tilde{\mathbf{q}}}{d\mathbf{v}} \frac{\partial \mathbf{v}(t,\zeta)}{\partial t} d\zeta + \dot{s} \left(t \right) \tilde{\mathbf{q}} \left(\mathbf{v} \left(t, s \left(t \right) - 0 \right) \right)$$
$$+ \int_{s(t)+0}^{z_2} \frac{d\tilde{\mathbf{q}}}{d\mathbf{v}} \frac{\partial \mathbf{v}(t,\zeta)}{\partial t} d\zeta - \dot{s} \left(t \right) \tilde{\mathbf{q}} \left(\mathbf{v} \left(t, s \left(t \right) + 0 \right) \right) = \tilde{\mathbf{f}} \left(\mathbf{v} \left(t, z_1 \right) \right) - \tilde{\mathbf{f}} \left(\mathbf{v} \left(t, z_2 \right) \right)$$

$$\tag{2.64}$$

Since the upper and lower fixed boundaries are arbitrary, the limits, $\lim\limits_{z_1 \to s(t)-0} z_1$ and $\lim\limits_{z_2 \to s(t)+0} z_2$, are taken which removes the integrals of the equation.

$$\dot{s} \left(t \right) \left(\tilde{\mathbf{q}} \left(\mathbf{v} \left(t, s \left(t \right) - 0 \right) \right) - \tilde{\mathbf{q}} \left(\mathbf{v} \left(t, s \left(t \right) + 0 \right) \right) \right)$$
$$= \tilde{\mathbf{f}} \left(\mathbf{v} \left(t, s \left(t \right) - 0 \right) \right) - \tilde{\mathbf{q}} \left(\mathbf{v} \left(t, s \left(t \right) + 0 \right) \right) \tag{2.65}$$

One may define the left state by: $\tilde{\mathbf{q}} \left(\mathbf{v} \left(t, s \left(t \right) - 0 \right) \right) = \tilde{\mathbf{q}} \left(\mathbf{v}_L \right)$ and the right state by: $\tilde{\mathbf{q}} \left(\mathbf{v} \left(t, s \left(t \right) + 0 \right) \right) = \tilde{\mathbf{q}} \left(\mathbf{v}_R \right)$. Now a simple equation for the shock velocity is

derived.

$$\dot{s}(t)\left(\tilde{\mathbf{q}}(\mathbf{v}_L) - \tilde{\mathbf{q}}(\mathbf{v}_R)\right) = \tilde{\mathbf{f}}(\mathbf{v}_L) - \tilde{\mathbf{f}}(\mathbf{v}_R) \tag{2.66}$$

Within the multi dimensional case, all scalar ratios needs to be satisfied by the shock velocity.

$$\dot{s}(t) = \frac{\tilde{f}(\mathbf{v}_L) - \tilde{f}(\mathbf{v}_R)}{\tilde{q}_1(\mathbf{v}_L) - \tilde{q}_1(\mathbf{v}_R)} = \quad \cdots = \frac{\tilde{f}_i(\mathbf{v}_L) - \tilde{f}_i(\mathbf{v}_R)}{\tilde{q}_i(\mathbf{v}_L) - \tilde{q}_i(\mathbf{v}_R)} \cdots$$

$$\cdots = \frac{\tilde{f}_n(\mathbf{v}_L) - \tilde{f}_n(\mathbf{v}_R)}{\tilde{q}_n(\mathbf{v}_L) - \tilde{q}_n(\mathbf{v}_R)} \tag{2.67}$$

This relation was derived by Rankine and Hugoniot for a problem arising in gas dynamics and is therefore signed after their names, [38]. In a simple scalar case, the shock velocity is determined by:

$$\dot{s}(t) = \frac{\tilde{f}(v_R) - \tilde{f}(v_L)}{\tilde{q}(v_R) - \tilde{q}(v_L)}. \tag{2.68}$$

Before a shock occurs, a compression of characteristic lines is needed. This condition due to Oleinik, [37], can be stated as follow.

$$\frac{\tilde{f}(v_R) - \tilde{f}(v)}{\tilde{q}(v_R) - \tilde{q}(v)} \leq \dot{s}(t) = \frac{\tilde{f}(v_R) - \tilde{f}(v_L)}{\tilde{q}(v_R) - \tilde{q}(v_L)} \leq \frac{\tilde{f}(v) - \tilde{f}(v_L)}{\tilde{q}(v) - \tilde{q}(v_L)} \tag{2.69}$$

Returning to the original problem of a single component chromatography following shock condition applies.

$$\frac{v_l(c_R - c)}{c_R + Fq(c_R) - c - Fq(c)} \leq \dot{s}(t) = \begin{array}{c} \frac{v_l(c_R - c_L)}{c_R + Fq(c_R) - c_L - Fq(c_L)} \\ \leq \frac{v_l(c - c_L)}{c + Fq(c) - c_L - Fq(c_L)} \end{array} \tag{2.70}$$

2.2.4 Traveling Wave Solution for Langmuir Isotherms

Traveling wave solutions gives answer how concentration profiles propagate through a specific medium, [39], [30], [40], [31], [41]. As an example, a single component is considered that travels through a chromatographic column with infinite length. The adsorption is described by a Langmuir isotherm.

$$\frac{\partial c}{\partial t} + F \frac{\partial q}{\partial t} = -v_l \frac{\partial c}{\partial z} + D \frac{\partial^2 c}{\partial z^2}, \quad \text{with} \quad q(c) = \frac{Hc}{1 + Kc} \tag{2.71}$$

An investigation is carried out if a solution, $c(t,z) = c(s)$, exists, where the concentration depends only on a single variable, $s = z - u\,t$. This single variable can be thought of as a moving coordinate, where the velocity, u, is the observer velocity. Further, it is assumed that the concentrations at the boundaries are constant. To simplify the analysis the right boundary is assumed to be zero. That means following boundary conditions are applied.

$$\lim_{s \to -\infty} c(s) = c_L, \quad \lim_{s \to +\infty} c(s) = c_R, \quad \frac{dc_L}{ds} = 0, \quad \frac{dc_R}{ds} = 0, \quad c_R = 0 \qquad (2.72)$$

If this ansatz is substituted in the partial differential equation, Eq. (2.71), it will reduce to an ordinary differential equation as it is shown below.

$$\frac{d}{ds}(c + F\,q)\frac{\partial s}{\partial t} + \frac{d}{ds}\left(v_l\,c - D\frac{dc}{ds}\frac{\partial s}{\partial z}\right)\frac{\partial s}{\partial z} = 0 \qquad (2.73)$$

$$-u\frac{d}{ds}(c + F\,q) + \frac{d}{ds}\left(v_l\,c - D\frac{dc}{ds}\right) = 0 \qquad (2.74)$$

This ODE can be integrated once.

$$-u\,(c + F\,q) + \left(v_l\,c - D\frac{dc}{ds}\right) + C_1 = 0 \qquad (2.75)$$

$$D\frac{dc}{ds} = -u\,(c + F\,q) + v_l\,c + C_1 \qquad (2.76)$$

The right boundary definition of Eq. (2.72) is now used to evaluate the integration constant.

$$0 = -u\,(c_R + F\,q_R) + v_l\,c_R + C_1 \quad \rightarrow \quad C_1 = 0 \qquad (2.77)$$

It is helpful to look at the special case of zero diffusion. The ordinary differential equation reduces to an algebraic equation, which is equivalent to Eq. (2.66) for $u = \dot{s}$ and the special adsorption isotherm.

$$0 = -u\,(c + F\,q) + v_l\,c \qquad (2.78)$$

Since, $q(0) = 0$, the equation is still valid for the right boundary condition. To be also valid for the left boundary condition, the observer velocity needs to be

chosen in the following way.

$$u = \frac{v_l}{1 + F \frac{q(c_L)}{c_L}} = \frac{v_l}{1 + \frac{FH}{1+Kc_L}} \tag{2.79}$$

The general case with diffusion is now investigated by substituting the Langmuir isotherm in the differential equation.

$$D \frac{dc}{ds} = \left(v_l - u \left(1 + \frac{FH}{1+Kc} \right) \right) c \tag{2.80}$$

Since concentration never can be negative and the equilibrium constant, K, is positive no singularity can occur. Separation of differentials can be done.

$$\frac{(1+Kc) \, D}{K \, (v_l - u) \, c^2 + (v_l - u - u \, F H) \, c} dc = ds \tag{2.81}$$

Both sides of the equation can be integrated and an implicit expression is obtained.

$$D \frac{\ln(c) \, (v_l - u) - u \, F H \ln(u \, F H - (1 + Kc) \, (v_l - u))}{(v_l - u - u \, F H) \, (v_l - u)} = s + C_2 \tag{2.82}$$

The observer velocity is chosen to be the same like for zero diffusion and the equation becomes:

$$-D \frac{\ln(c) - (1 + K c_L) \ln\left((c_L - c) \, \frac{v_l K F H}{1+K c_L + F H} \right)}{v_l \frac{FH}{1+K c_L + F H} K c_L} = s + C_2. \tag{2.83}$$

If the left boundary condition is applied the argument of the second natural logarithm becomes zero and therefore the equation will be satisfied for all finite C_2. The integration constant may be chosen to set the origin of the moving coordinate system to a specified value. It is natural to chose:

$$c(0) = \frac{c_L}{2}. \tag{2.84}$$

In this case, the concentration constant becomes:

$$C_2 = -D \frac{\ln\left(\frac{c_L}{2}\right) - (1 + K c_L) \ln\left(\frac{c_L}{2} \frac{v_l K F H}{1+K c_L + F H} \right)}{v_l \frac{FH}{1+K c_L + F H} K c_L}. \tag{2.85}$$

Some manipulation can be done to get the final implicit form.

$$\ln\left(\frac{2c}{c_L}\right) - (1 + Kc_L)\ln\left(2\frac{c_L - c}{c_L}\right) = -s\frac{v_l}{D}\frac{FHKc_L}{1 + Kc_L + FH} \tag{2.86}$$

$$\frac{2c}{c_L}\left(\frac{c_L}{2(c_L - c)}\right)^{(1+Kc_L)} = e^{-s\frac{v_l}{D}\frac{FHKc_L}{1+Kc_L+FH}} \tag{2.87}$$

The concentration profile of a traveling wave in case of Langmuir Isotherm can be determined using this formula, Fig. 2.3. A shock layer may be defined as
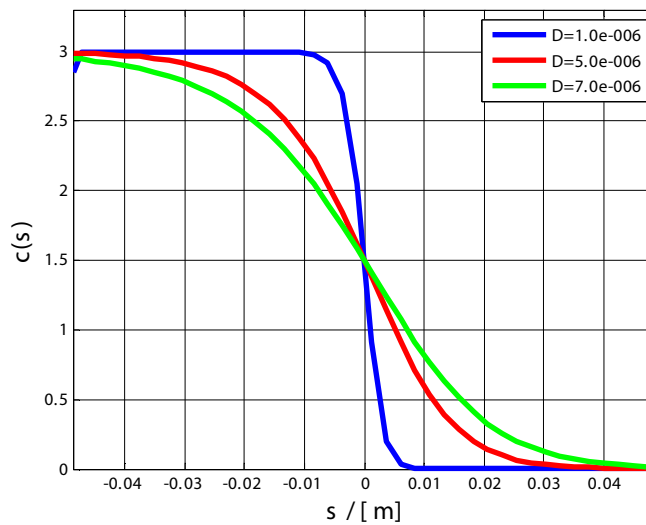
Figure 2.3: Traveling wave profile.

distance until $p\,100\,\%$ of both states is reached. This is the double size of **s** if $c = p\,c_L$ is substituted.

$$\delta(p) = 2\frac{D}{v_l}\frac{(1 + Kc_L + FH)}{FHKc_L}\ln\left(\frac{(2(1 - p))^{(1+Kc_L)}}{2p}\right) \tag{2.88}$$

2.2.5 Similarity Analysis of Rarefaction

Consider the partial differential equation for a single component chromatography with Langmuir isotherm.

$$\frac{\partial c}{\partial t} + F\frac{\partial q}{\partial t} = -v_l\frac{\partial c}{\partial z}, \quad \text{with } q(c) = \frac{Hc}{1 + Kc} \tag{2.89}$$

To find the general shape of the rarefaction, diffusion is neglected. Further, following similarity variable is defined, [40].

$$c(t, z) = c(\eta), \quad \eta = \frac{z - z_{ref}}{t - t_{ref}} \tag{2.90}$$

Plugging this into the partial differential equation, Eq. (2.89), it will reduce to an ordinary one.

$$-\frac{(z - z_{ref})}{(t - t_{ref})^2} \frac{dc}{d\eta} \left(1 + F \frac{dq}{dc}\right) = 0 \tag{2.91}$$

$$\left(v_l - \eta \left(1 + F \frac{dq}{dc}\right)\right) \frac{dc}{d\eta} = 0 \tag{2.92}$$

One solution of the equation above can be found by setting the bracket to zero and solve the algebraic equation.

$$v_l - \eta \left(1 + \frac{F H}{(1 + K c)^2}\right) = 0 \tag{2.93}$$

$$c(\eta) = \frac{1}{K} \left(\sqrt{F H \left|\frac{\eta}{v_l - \eta}\right|} - 1\right) \tag{2.94}$$

If the similarity variable, η, is substituted back, it results in a solution identical to Eq. (2.56) on page 17. Thus, with aid of the similarity ansatz the solution is found more quickly.

$$c\left(\frac{z - z_{ref}}{t - t_{ref}}\right) = \frac{1}{K} \left(\sqrt{\left|\frac{F H}{v_l \frac{t - t_{ref}}{z - z_{ref}} - 1}\right|} - 1\right) \tag{2.95}$$

2.3 Analysis of a Two Component Chromatographic Column

The method of characteristics can be extended to a system of first order equation and is therefore useful to derive analytical solutions for multi component chromatographic columns. In this thesis only two species are considered. Therefore, the analysis is presented for a two component chromatographic column, [29].

2.3.1 Matrix Description of a Column

Neglecting diffusion, the model equations of a two component chromatographic column can be written in following form.

$$\frac{\partial c_A}{\partial t} + \frac{1-\varepsilon}{\varepsilon} \frac{\partial q_A\left(c_A, c_B\right)}{\partial t} + \frac{\dot{V}_l}{\varepsilon A} \frac{\partial c_A}{\partial z} = 0 \tag{2.96}$$

$$\frac{\partial c_B}{\partial t} + \frac{1-\varepsilon}{\varepsilon} \frac{\partial q_B\left(c_A, c_B\right)}{\partial t} + \frac{\dot{V}_l}{\varepsilon A} \frac{\partial c_B}{\partial z} = 0 \tag{2.97}$$

Using the substitution, $F = \frac{1-\varepsilon}{\varepsilon}$ and $v_l = \frac{\dot{V}_l}{\varepsilon A}$, this model is written in matrix form.

$$\begin{pmatrix} 1 + F \frac{\partial q_A}{\partial c_A} & F \frac{\partial q_A}{\partial c_B} \\ F \frac{\partial q_B}{\partial c_A} & 1 + F \frac{\partial q_B}{\partial c_B} \end{pmatrix} \begin{pmatrix} \frac{\partial c_A}{\partial t} \\ \frac{\partial c_B}{\partial t} \end{pmatrix} + v_l \begin{pmatrix} \frac{\partial c_A}{\partial z} \\ \frac{\partial c_B}{\partial z} \end{pmatrix} = \begin{pmatrix} 0 \\ 0 \end{pmatrix} \tag{2.98}$$

The complete model may also be stated in a short matrix notation.

$$\mathbf{A} \frac{\partial \mathbf{c}}{\partial t} + v_l \frac{\partial \mathbf{c}}{\partial z} = \mathbf{0}, \quad z \in (0, L], \quad t \in (0, \infty) \tag{2.99}$$

with $\mathbf{c}\left(t, 0\right) = \mathbf{c}_{in}\left(t\right)$ and $\mathbf{c}\left(0, z\right) = \mathbf{c}_0\left(z\right)$.

2.3.2 Finding Riemann Invariants

To decouple the system in scalar equations, the matrix equation is pre multiplied by a transposed vector, [38], [29].

$$\mathbf{l}_i^T \mathbf{A} \frac{\partial \mathbf{c}}{\partial t} + v_l \mathbf{l}_i^T \frac{\partial \mathbf{c}}{\partial z} = \mathbf{0}, \quad i = 1, 2 \tag{2.100}$$

A decoupling is achieved if the vector is a left eigenvector of the matrix $\mathbf{A}$. To find such a vector following eigenvalue equation has to be solved.

$$\mathbf{l}_i^T \mathbf{A} = \lambda_i \mathbf{l}_i^T \tag{2.101}$$

Notice that by transposing this equation a standard right eigenvalue problem is obtained.

$$\mathbf{A}^T \mathbf{l}_i = \lambda_i \mathbf{l}_i \tag{2.102}$$

If such a vector and eigenvalue is found one gets following decoupled first order partial differential equations.

$$\mathbf{l}_i^T \left(\lambda_i \frac{\partial \mathbf{c}}{\partial t} + v_l \frac{\partial \mathbf{c}}{\partial z} \right) = \mathbf{0} \tag{2.103}$$

$$\lambda_i \mathbf{l}_i^T \left(\frac{\partial \mathbf{c}}{\partial t} + \frac{v_l}{\lambda_i} \frac{\partial \mathbf{c}}{\partial z} \right) = \mathbf{0} \tag{2.104}$$

To find a solution, it is realized that the bracket term is just the ordinary time derivative of the concentrations.

$$\frac{d\mathbf{c}}{dt} = \frac{\partial \mathbf{c}}{\partial t} + \frac{\partial \mathbf{c}}{\partial z} \frac{dz}{dt} = \frac{\partial \mathbf{c}}{\partial t} + \frac{v_l}{\lambda_i} \frac{\partial \mathbf{c}}{\partial z} \tag{2.105}$$

Therefore, the system is converted to a set of ordinary differential equations, [38].

$$\mathbf{l}_i^T \frac{d\mathbf{c}}{dt} = \mathbf{0}, \quad \frac{dz}{dt} = \frac{v_l}{\lambda_i}, \quad \lambda_i \neq 0 \tag{2.106}$$

The first equation describes the Riemann invariant. The second equation describes the characteristic line on which the Riemann invariants are constant. Since, $\mathbf{l}_i$, is unlikely a constant vector it is in general not easy to integrate these equations to find the algebraic relation which defines the Riemann invariant. However, the system under investigation is 2x2 and homogeneous. This means the differential equations can be converted always to the phase plane.

$$l_{1,i} \frac{dc_A}{dt} + l_{2,i} \frac{dc_B}{dt} = \mathbf{0} \quad \rightarrow \quad \frac{dc_A}{dc_B} = -\frac{l_{2,i}}{l_{1,i}} \tag{2.107}$$

Therefore, the Riemann invariants are found by solving this first order differential equation.

2.3.3 Solving the Eigenvalue Problem

The eigenvalue problem is solved by first determining the associated eigenvalues.

$$\det \left(\mathbf{A}^T - \lambda \, \mathbf{I}_2 \right) = \det \begin{pmatrix} 1 + F \frac{\partial q_A}{\partial c_A} - \lambda & F \frac{\partial q_B}{\partial c_A} \\ F \frac{\partial q_A}{\partial c_B} & 1 + F \frac{\partial q_B}{\partial c_B} - \lambda \end{pmatrix} \tag{2.108}$$

Following characteristic equation is obtained.

$$\left(1 + F\frac{\partial q_A}{\partial c_A} - \lambda\right)\left(1 + F\frac{\partial q_B}{\partial c_B} - \lambda\right) - F^2\frac{\partial q_A}{\partial c_B}\frac{\partial q_B}{\partial c_A} = 0 \tag{2.109}$$

The eigenvalue is determined by solving this quadratic equation.

$$\lambda_{1,2} = 1 + \frac{F}{2}\left(\frac{\partial q_A}{\partial c_A} + \frac{\partial q_B}{\partial c_B}\right) \pm \frac{F}{2}\sqrt{\left(\frac{\partial q_B}{\partial c_B} - \frac{\partial q_A}{\partial c_A}\right)^2 + 4\frac{\partial q_A}{\partial c_B}\frac{\partial q_B}{\partial c_A}} \tag{2.110}$$

Notice that the eigenvalues are real if the second part under the square root is of positive sign, which is often the case for practical isotherm relationships. The next step is to compute the associated eigenvectors. This is done with help of the eigenvalue equation.

$$\begin{pmatrix} 1 + F\frac{\partial q_A}{\partial c_A} & F\frac{\partial q_B}{\partial c_A} \\ F\frac{\partial q_A}{\partial c_B} & 1 + F\frac{\partial q_B}{\partial c_B} \end{pmatrix}\begin{pmatrix} l_{1,i} \\ l_{2,i} \end{pmatrix} = \lambda_i\begin{pmatrix} l_{1,i} \\ l_{2,i} \end{pmatrix} \tag{2.111}$$

Using the first equation and substituting the eigenvalue, a relationship for the elements of the eigenvectors is obtained.

$$F\frac{\partial q_B}{\partial c_A}l_{2,i} = \left(\lambda_i - 1 - F\frac{\partial q_A}{\partial c_A}\right)l_{1,i} \tag{2.112}$$

$$l_{1,i} = \frac{2\frac{\partial q_B}{\partial c_A}}{\left(\frac{\partial q_B}{\partial c_B} - \frac{\partial q_A}{\partial c_A}\right) \pm \sqrt{\left(\frac{\partial q_B}{\partial c_B} - \frac{\partial q_A}{\partial c_A}\right)^2 + 4\frac{\partial q_A}{\partial c_B}\frac{\partial q_B}{\partial c_A}}}l_{2,i} \tag{2.113}$$

Following choice can be made.

$$\mathbf{l}_i^T = \left[2\frac{\partial q_B}{\partial c_A}, \quad -\left(\frac{\partial q_A}{\partial c_A} - \frac{\partial q_B}{\partial c_B}\right) \pm \sqrt{\left(\frac{\partial q_A}{\partial c_A} - \frac{\partial q_B}{\partial c_B}\right)^2 + 4\frac{\partial q_A}{\partial c_B}\frac{\partial q_B}{\partial c_A}}\right] \tag{2.114}$$

This results in following differential equation for the Riemann invariants.

$$\left(\frac{dc_A}{dc_B}\right)_{1,2} = \frac{\left(\frac{\partial q_A}{\partial c_A} - \frac{\partial q_B}{\partial c_B}\right) \mp \sqrt{\left(\frac{\partial q_A}{\partial c_A} - \frac{\partial q_B}{\partial c_B}\right)^2 + 4\frac{\partial q_A}{\partial c_B}\frac{\partial q_B}{\partial c_A}}}{2\frac{\partial q_B}{\partial c_A}} \tag{2.115}$$

It is cumbersome to solve these two differential equations in this form. It is simpler to convert them in implicit form by noting that the left side can be thought of as a solution of following quadratic equation.

$$\left[\left(\frac{\partial q_B}{\partial c_A} \right) \left(\frac{dc_A}{dc_B} \right)^2 - \left(\frac{\partial q_A}{\partial c_A} - \frac{\partial q_B}{\partial c_B} \right) \frac{dc_A}{dc_B} - \frac{\partial q_A}{\partial c_B} \right] \frac{\partial q_B}{\partial c_A} = 0 \tag{2.116}$$

Either, $\frac{\partial q_B}{\partial c_A} = 0$, or the differential equation inside the bracket must be fulfilled. Since a dependency between the concentrations is required, only the ODE needs to be considered.

2.3.4 Concept of Coherency

As shown in the two previous sections, a static functional relationship may exist between the concentrations. The functional relationship may be presented in the following general form.

$$c_A = c_A \left(c_B \right), \quad \text{for } i = A, B \tag{2.117}$$

This undetermined expression can be inserted into the partial differential equations, Eq. (2.96) and Eq. (2.97) on page 25. Thus, the PDE can be written using the notation style of complete differentials.

$$\frac{\partial c_i}{\partial t} + F \frac{dq_i}{dc_i} \frac{\partial c_i}{\partial t} = -v_l \frac{\partial c_i}{\partial z} \tag{2.118}$$

In this presentation, the propagation velocity of an arbitrary concentration value is determined by the negated ratio of partial differentials.

$$v_{c_i} = -\frac{\frac{\partial c_i}{\partial t}}{\frac{\partial c_i}{\partial z}} = \frac{v_l}{1 + F \frac{dq_i}{dc_i}}, \quad \text{for } i = A, B \tag{2.119}$$

Because of the static relationship between the two concentrations, the velocities must be the same for a specific concentration composition for both components. This is called coherence condition, [42], [43], [44], [45].

$$v_{c_A} = v_{c_B} \tag{2.120}$$

By inspection of the velocity equations for the concentrations, Eq. (2.119), it is immediately obvious that the equality of the velocities leads to the equality of the complete differentials of the two isotherms.

$$\frac{dq_A}{dc_A} = \frac{dq_B}{dc_B} \tag{2.121}$$

If the complete differentials are replaced by the partial differentials, then a differential equation for the determination of the functional relationship between the two concentrations is formed. It is the same differential equation as derived by the Riemann analysis, Eq. (2.116) on page 28.

$$-\frac{\partial q_B}{\partial c_A} \left(\frac{dc_A}{dc_B}\right)^2 + \left(\frac{\partial q_A}{\partial c_A} - \frac{\partial q_B}{\partial c_B}\right) \frac{dc_A}{dc_B} + \frac{\partial q_A}{\partial c_B} = 0 \tag{2.122}$$

2.3.5 Solving Clairauts Differential Equation

Before the ODE can be solved, the partial derivatives of the isotherm relationships needs to be specified, Eq. (2.123) and Eq. (2.124). In case of Langmuir isotherms, Eq. (2.40) and Eq. (2.41) on page 14, one ends up with Eq. (2.125).

$$\frac{\partial q_A}{\partial c_A} = \frac{H_A \left(1 + K_B c_B\right)}{\left(1 + K_A c_A + K_B c_B\right)^2}, \quad \frac{\partial q_A}{\partial c_B} = -\frac{H_A K_B c_A}{\left(1 + K_A c_A + K_B c_B\right)^2} \tag{2.123}$$

$$\frac{\partial q_B}{\partial c_A} = -\frac{H_B K_A c_B}{\left(1 + K_A c_A + K_B c_B\right)^2}, \quad \frac{\partial q_B}{\partial c_B} = \frac{H_B \left(1 + K_A c_A\right)}{\left(1 + K_A c_A + K_B c_B\right)^2} \tag{2.124}$$

$$c_B \left(\frac{dc_A}{dc_B}\right)^2 + \frac{H_A \left(1 + K_B c_B\right) - H_B \left(1 + K_A c_A\right)}{H_B K_A} \left(\frac{dc_A}{dc_B}\right) - \frac{H_A K_B}{H_B K_A} c_A = 0 \tag{2.125}$$

This differential equation is of Clairauts type. For solving Clairauts equation, it is useful to make some substitution to cast the equation in standard form, [46].

$$c_B \left(\frac{dc_A}{dc_B}\right)^2 - \left(\frac{H_B - H_A}{H_B K_A} + c_A - \frac{H_A K_B}{H_B K_A} c_B\right) \left(\frac{dc_A}{dc_B}\right) - \frac{H_A K_B}{H_B K_A} c_A = 0 \tag{2.126}$$

$$\alpha = \frac{H_B - H_A}{H_B \, K_A}, \quad \beta = \frac{H_A \, K_B}{H_B \, K_A}, \quad H_B > H_A \tag{2.127}$$

$$c_B \left(\frac{dc_A}{dc_B}\right)^2 - (\alpha + c_A - \beta \, c_B) \left(\frac{dc_A}{dc_B}\right) - \beta \, c_A = 0 \tag{2.128}$$

This equation is solved by differentiating with respect to c_B. Notice that this is a non-equivalent transformation. Therefore, one needs to check the result afterward.

$$\begin{aligned}
\left(\frac{dc_A}{dc_B}\right)^2 + 2\,c_B \, \frac{dc_A}{dc_B} \frac{d^2c_A}{dc_B^2} - \left(\frac{dc_A}{dc_B} - \beta\right) \frac{dc_A}{dc_B} \\
- (\alpha + c_A - \beta \, c_B) \frac{d^2c_A}{dc_B^2} - \beta \frac{dc_A}{dc_B} = 0
\end{aligned} \tag{2.129}$$

$$\left(2\,c_B \frac{dc_A}{dc_B} - (\alpha + c_A - \beta \, c_B)\right) \frac{d^2c_A}{dc_B^2} = 0 \tag{2.130}$$

This equation has two solutions. One if the bracket is zero and one if the second derivative is zero. The latter solution gives a linear relationship between the concentrations.

$$\frac{d^2c_A}{dc_B^2} = 0 \quad \rightarrow \quad c_A = C \, c_B + D \tag{2.131}$$

Since the original ODE was of first order, there must be a dependency between the integration constants. To determine this, the linear relationship is plugged into the original equation.

$$c_B \, C^2 - (\alpha + C \, c_B + D - \beta \, c_B) \, C - \beta \, (C \, c_B + D) = 0 \tag{2.132}$$

$$D = -\frac{\alpha \, C}{\beta + C} \tag{2.133}$$

Therefore the first general solution is:

$$c_A = C \, c_B - \frac{\alpha \, C}{\beta + C}. \tag{2.134}$$

The second solution is defined by an ordinary differential equation.

$$2\,c_B\,\frac{dc_A}{dc_B} - (\alpha + c_A - \beta\,c_B) = 0 \tag{2.135}$$

$$\frac{dc_A}{dc_B} = \frac{\alpha + c_A - \beta\,c_B}{2\,c_B} \tag{2.136}$$

This ODE cannot be solved by separating the variables, but one can plug it into the original equation and an algebraic equation is obtained.

$$c_B\left(\frac{\alpha + c_A - \beta\,c_B}{2\,c_B}\right)^2 - (\alpha + c_A - \beta\,c_B)\left(\frac{\alpha + c_A - \beta\,c_B}{2\,c_B}\right) - \beta\,c_A = 0 \tag{2.137}$$

$$(\alpha + c_A - \beta\,c_B)^2 + 4\,\beta\,c_A\,c_B = 0 \tag{2.138}$$

It is not possible to solve this equation for positive concentrations. It is therefore not a physical solution. As result of this analysis, two Riemann invariants are obtained. Instead of using the traditional Riemann invariants, $\tilde{R}_i = D_i\,(c_A, c_B)$, [38], one uses, $R_i = C_i\,(c_A, c_B)$, since it is also a constant. Given a composition, (c_A, c_B), in the composition space, the slopes, C_i, can be calculated from a quadratic equation.

$$c_B\,C_{1,2}^2 + \frac{H_A\,(1 + K_B\,c_B) - H_B\,(1 + K_A\,c_A)}{H_B\,K_A}\,C_{1,2} - \frac{H_A\,K_B}{H_B\,K_A}\,c_A = 0, \quad H_B > H_A \tag{2.139}$$

The Riemann invariant relationship determines the characteristics, where the Riemann invariant stays constant.

$$c_A = C_{1,2}\,c_B - \frac{(H_B - H_A)\,C_{1,2}}{H_A\,K_B + H_B\,K_A\,C_{1,2}} \tag{2.140}$$

Furthermore, the speed of propagation can be computed with help of the associated eigenvalue.

$$\frac{dC_i}{dt} = 0, \quad \frac{dz}{dt} = \frac{v_l}{\lambda_i}, \quad \lambda_i \neq 0 \tag{2.141}$$

$$\lambda_{1,2} = 1 + \frac{F}{2\left(1 + K_A\, c_A + K_B\, c_B\right)^2} \left[\begin{array}{c} \left(H_A\,(1 + K_B\, c_B) + H_B\,(1 + K_A\, c_A)\right) \\ \pm \sqrt{\begin{array}{c} (H_A\,(1 + K_B\, c_B) - H_B\,(1 + K_A\, c_A))^2 \\ + 4\, K_A\, K_B\, H_A\, H_B\, c_A\, c_B \end{array}} \end{array} \right]$$

(2.142)

2.3.6 Hodograph Plane

The static relationship between the concentrations can be represented in the hodograph plane. Their name originates from the hodograph transformation, which interchanges the role of dependent and independent variables. Eq. (2.140) is used to construct this plane as shown in Fig. 2.4. For the construction of these paths one provides arbitrary concentration values at the coordinate axises. The slopes at these points are computed by the quadratic equation, Eq. (2.139). Eq. (2.143) determines the intersections with the coordinate axis:
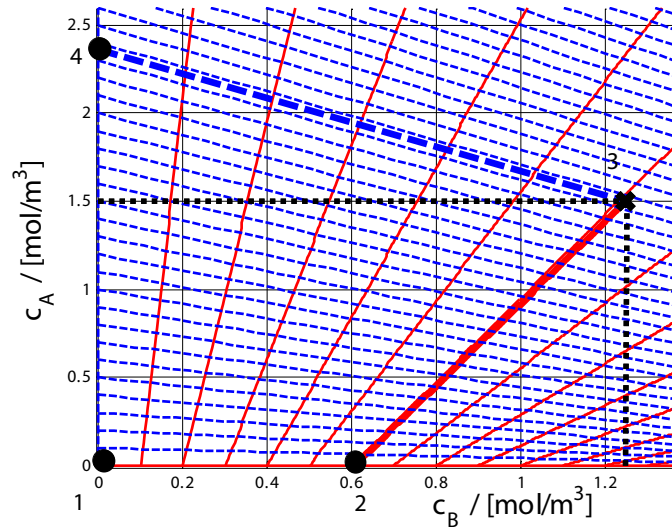

Figure 2.4: Hodograph plane.

$$c_A\,(C_i; c_B = 0) = -\frac{(H_B - H_A)\,C_i}{K_B\, H_A + K_A\, H_B\, C_i}, \quad i = 1, 2\,,$$

(2.143)

$$c_B\,(C_i; c_A = 0) = \frac{(H_B - H_A)}{K_B\, H_A + K_A\, H_B\, C_i}.$$

The ranges of the slopes are immediately obtained from the range of concentrations.

$$C_1 \in [0, \infty), \quad C_2 \in \left(-\frac{H_A\,K_B}{H_B\,K_A}, 0 \right] \tag{2.144}$$

2.3.7 Constructing Solutions Using Riemann Invariants

Given a dispersion-free model, Eq. (2.96) and Eq. (2.97) on page 25, of a chromatographic column with Langmuir isotherms, it is now possible to construct a solution for a given piecewise constant boundary and initial conditions with help of the Riemann invariants. Fig. 2.5 shows at three different time points, how an initially equally distributed concentration profile, with $c_{A,0}(z) = 1.5$ and $c_{B,0}(z) = 1.25$, is rinsed out by a pure solvent stream, e.g. $c_{A,in}(t) = 0$ and $c_{B,in}(t) = 0$ for all $t > 0$. It is clearly seen that a rarefaction is formed. The velocity increases with the magnitude of concentration. Thus, the head moves faster than the tail. Further, one can notice a formation of an intermediate plateau value of the component c_B which has a concentration value of approximately 0.6. To
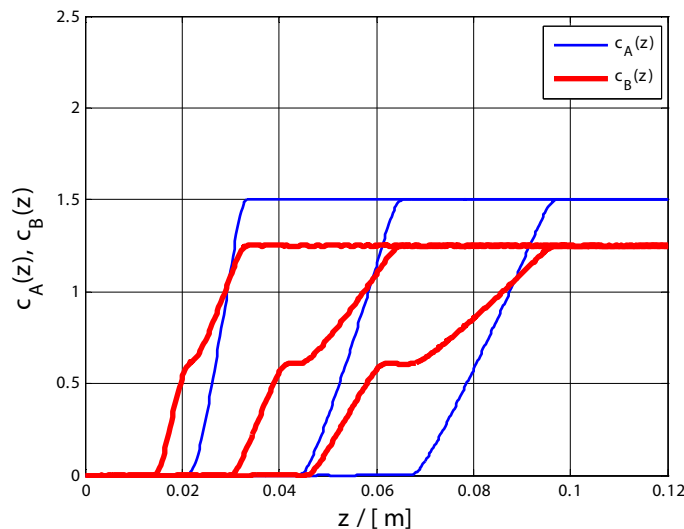

Figure 2.5: Propagation of a rarefaction within a chromatographic column at three different time points.

investigate the solution it is useful to look at the hodograph plane, Fig. 2.4. A cross marks the initial state. The final state will be in the origin. If a simple wave condition is assumed, the Riemann invariant relationship, Eq. (2.140) on

page 31, will hold and both points are connected via a Riemann path. Using the additional knowledge that component B is slower than component A the only possible path in Fig. 2.4 goes from point **3** through point **2** to point **1**. In point **2** the concentration value of component A becomes zero and the concentration value of component B is approximately 0.6. It is just the intermediate plateau value of the concentration profile. The plateau value is bounded by two corners that run with two different velocities corresponding to their eigenvalues and just widens itself. The concentration velocities of the components are determined by Eq. (2.145) and Eq. (2.146).

$$
\begin{aligned}
v_{c_A}(c_A, c_B) &= \frac{v_l}{1+F\frac{dq_A(c_A,c_B)}{dc_A}} \\
&= \frac{v_l}{1+F\left(\frac{\partial q_A}{\partial c_A}+\frac{\partial q_A}{\partial c_B}\frac{dc_B}{dc_A}\right)} \\
&= \frac{v_l}{1+F\frac{H_A(1+K_B c_B)-H_A K_B c_A \frac{dc_B}{dc_A}}{(1+K_A c_A+K_B c_B)^2}}
\end{aligned}
\tag{2.145}
$$

$$
\begin{aligned}
v_{c_B}(c_A, c_B) &= \frac{v_l}{1+F\frac{dq_B(c_A,c_B)}{dc_B}} \\
&= \frac{v_l}{1+F\left(\frac{\partial q_B}{\partial c_A}\frac{dc_A}{dc_B}+\frac{\partial q_B}{\partial c_B}\right)} \\
&= \frac{v_l}{1+F\frac{H_B(1+K_A c_A)-H_B K_A c_B \frac{dc_A}{dc_B}}{(1+K_A c_A+K_B c_B)^2}}
\end{aligned}
\tag{2.146}
$$

The velocities can be evaluated only if the slopes between the concentrations are known. These are determined from the quadratic equation, Eq. (2.139) on page 31.

2.3.8 Shock Paths

The differential description is invalid if a discontinuity in the concentration profile occurs, as already has been shown in section 2.2.3 on page 18. In this case, an integral description is necessary that leads to the Rankine- Huginot- condition, Eq. (2.67) on page 20. If this equation is applied to the system, Eq. (2.147), a relation between the concentrations across the shock is obtained. The shock velocities for both components are equal, thus the coherence condition is still valid

also for shocks.

$$\frac{\partial}{\partial t}\left(c_i + F\,q_i\left(c_A, c_B\right)\right) + v_l\,\frac{\partial c_i}{\partial z} = 0, \quad i = A, B \tag{2.147}$$

$$\dot{s}\left(t\right) = \frac{v_l}{1 + F\,\frac{q_A(c_{A,L}, c_{B,L}) - q_A(c_{A,R}, c_{B,R})}{c_{A,L} - c_{A,R}}} = \frac{v_l}{1 + F\,\frac{q_B(c_{A,L}, c_{B,L}) - q_B(c_{A,R}, c_{B,R})}{c_{B,L} - c_{B,R}}} \tag{2.148}$$

The Eq. (2.148) may be rearranged to give Eq. (2.149).

$$\frac{q_A\left(c_{A,L}, c_{B,L}\right) - q_A\left(c_{A,R}, c_{B,R}\right)}{c_{A,L} - c_{A,R}} = \frac{q_B\left(c_{A,L}, c_{B,L}\right) - q_B\left(c_{A,R}, c_{B,R}\right)}{c_{B,L} - c_{B,R}} \tag{2.149}$$

This algebraic equation can be used to construct possible shock paths in the hodograph plane. Because component B is considered to be slower than component A, the plateau value on the right, $c_{B,R}$, is set to zero. For Langmuir isotherms following relationship across the shock are obtained.

$$c_{A,L}\left(c_{B,L}\right) = -\frac{K_B\,c_{A,R}}{\frac{H_B}{H_A}\left(1 + K_A\,c_{A,R}\right) - 1}\,c_{B,L} + c_{A,R}, \quad c_{B,R} = 0 \tag{2.150}$$

It is easily provable that the possible shock paths are identical with the possible rarefaction paths for Langmuir isotherms, [34], [29]. For this, one can use the rule of L'Hospital to show that the slope of the algebraic equation is identical to the negative slope defined by the Riemann invariant. Eq. (2.151) show this for C_2.

$$\lim_{c_B \to 0} C_{2-}\left(c_A, c_B\right) = -\frac{K_B\,c_A}{\frac{H_B}{H_A}\left(1 + K_A\,c_A\right) - 1} \tag{2.151}$$

The traditional Riemann invariant, $\tilde{R}$, is in this case also identically with the concentration value, $c_{A,R}$, of the component A on the ordinate axis, which can be seen from Eq. (2.140) on page 31. Now, consider following example that presents how shocks are propagated through a column. Fig. 2.6 shows, how an initially purged chromatographic column, $c_{A,0}(z) = 0$ and $c_{B,0}(z) = 0$, is filled from the left side with a binary feed, with $c_{A,in}(t) = 1.5$ and $c_{B,in}(t) = 1.25$ for all $t > 0$. The figure shows at three different time points the formation of a shock. Component B has a plateau value equally to its feed value, which one would expect. Component A has an intermediate plateau value that is higher than its
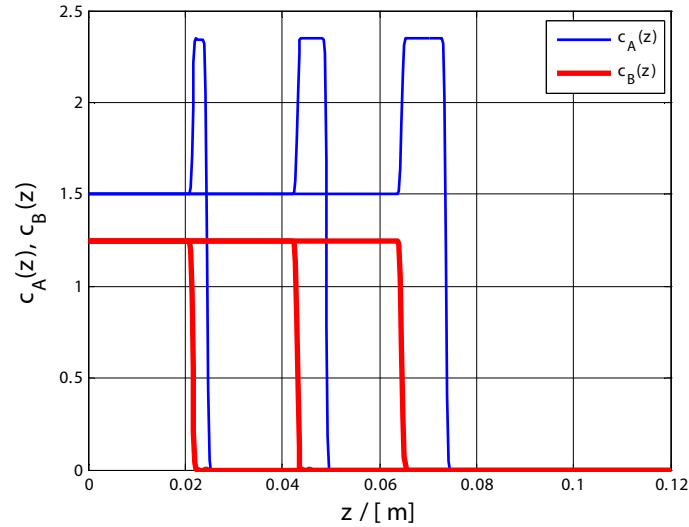
Figure 2.6: Propagation of a shock within a chromatographic column at three different time points.

feed value. A look at the hodograph plane, Fig. 2.4 on page 32, is now helpful. The feed composition is the cross marked point in the associated hodograph plane. This will be the final state for the whole chromatographic column after the transients. At beginning, the column is completely purged. Therefore, this state lies in the origin. With the knowledge that the component A is faster than the component B the only possible path must be from **1** to **4** and finally to **3**. The upper plateau value is immediately found at point **4** and is around 2.4.

A great many people think they are thinking
when they are merely rearranging their prejudices.

$\sim$ William James $\sim$

3 Design of SMB Plants

The design of SMB plants starts with a suitable choice of chromatographic columns according to the desired feed mixture and the desired throughput. This choice also defines the adsorption properties, which may be described mathematically with the aid of an isotherm relationship. For a faultless operation, an exact adjustment of the four volumetric flow rates and switching time is necessary. These, together with the feeding concentrations, define the operating point of the process. Nowadays, there are two methods available to find operating points for SMB plants under idealized conditions. The first method is called *triangle theory*, [2], [3], and the second method is called *standing wave design*, [4], [5]. Both methods rely on the TMB model. Similar to a countercurrent heat exchanger, a TMB model assumes a real countercurrent motion between liquid and adsorbed phase. This leads to a mathematical advantage since stationary concentration profiles exist for a correct setting. Unfortunately, the TMB process and thus both mentioned methods are not able to describe the cyclic concentration fluctuations at the drains. For this reason a new method to determine operating points for SMB plants is developed, which is also capable to predict the cyclic steady state concentration pattern at the drains. The advantage of this method lies in the fact that this method leads for dispersion-free SMB model at cyclic steady state to almost exact solutions and is especially attractive to design SMB plants for reduced purity. Further, this method can be used to a simple and robust adaptive control design. In this chapter, this method is used to derive equations to determine operating conditions of SMB plants for Henry, noncompetitive and competitive Langmuir isotherms for complete regeneration.

3.1 The Dispersion-free SMB Model

Throughout this thesis, a four-zone SMB process is considered as shown in Fig. 3.1. To be able to simulate such a device one must use the model equations for one
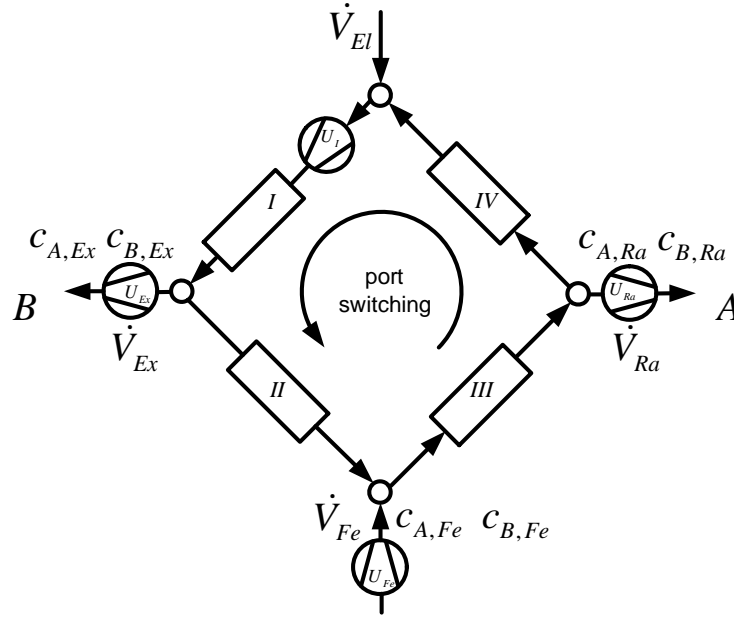
Figure 3.1: SMB process with four zones.

chromatographic column together with the equations that describe the coupling of the columns. These equations can be entered in a suitable simulation package, like COMSOL, [48].

3.1.1 Governing Equations for One Column

For convenience, the model equations of a chromatographic column are repeated here. In this case, mass transfer resistances and axial dispersion are neglected. A detailed derivation can be found in chapter 2 on page 7 or in [29], [32].

$$\frac{\partial c_A}{\partial t} + F \frac{\partial q_A\left(c_A, c_B\right)}{\partial t} = -v_l \frac{\partial c_A}{\partial z} \tag{3.1}$$

$$\frac{\partial c_B}{\partial t} + F \frac{\partial q_B\left(c_A, c_B\right)}{\partial t} = -v_l \frac{\partial c_B}{\partial z} \tag{3.2}$$

$$F = \frac{1-\varepsilon}{\varepsilon}, \quad v_l = \frac{\dot{V}}{\varepsilon A}, \quad z \in (0, L], \quad t \in (0, \infty)$$

The boundary and initial conditions are similar for both components:

$$c_i\left(t, 0\right) = c_{i,in}\left(t\right), \quad i = A, B,$$

$$c_i\left(0,z\right) = c_{i,0}\left(z\right), \quad i = A, B.$$

For the completion of the model, a static relationship between adsorbed and liquid phase is necessary using an adsorption isotherm.

$$q_i = q_i\left(c_A, c_B\right), \quad i = A, B \tag{3.3}$$

3.1.2 Couplings of Columns

The couplings for chromatographic columns are derived in accordance with Fig. 3.1. Under the assumption of equal and constant densities, the overall mass balance reduces to a flow rate balance as given by the Eqs. (3.4)-(3.9).

External flow rates:

$$0 = \dot{V}_{El} + \dot{V}_{Fe} - \dot{V}_{Ex} - \dot{V}_{Ra}, \tag{3.4}$$

$$0 = c_{i,Fe}\,\dot{V}_{Fe} - c_{i,Ex}\,\dot{V}_{Ex} - c_{i,Ra}\,\dot{V}_{Ra}, \quad i = A, B. \tag{3.5}$$

Eluent feed:

$$\dot{V}_I = \dot{V}_{IV} + \dot{V}_{El}, \quad c_{i,in,I}\,\dot{V}_I = c_{i,out,IV}\,\dot{V}_{IV}, \quad i = A, B. \tag{3.6}$$

Extract drain:

$$\dot{V}_{II} = \dot{V}_I - \dot{V}_{Ex}, \quad c_{i,in,II} = c_{i,out,I} = c_{i,Ex}, \quad i = A, B. \tag{3.7}$$

Feed:

$$\dot{V}_{III} = \dot{V}_{II} + \dot{V}_{Fe}, \quad c_{i,in,III}\,\dot{V}_{III} = c_{i,out,II}\,\dot{V}_{II} + c_{i,Fe}\,\dot{V}_{Fe}, \quad i = A, B. \tag{3.8}$$

Raffinate drain:

$$\dot{V}_{IV} = \dot{V}_{III} - \dot{V}_{Ra}, \quad c_{i,Ra} = c_{i,in,IV} = c_{i,out,III}, \quad i = A, B. \tag{3.9}$$

3.2 Operating Points for Henry Isotherms

In this subsection, Henry isotherms are considered to derive design equations for SMB plants for reduced purities and complete regeneration, [47], [52]. Henry isotherms, Eq. (3.10), are the simplest isotherm relationship and may, in general, be insufficient to describe the real adsorption behavior. However, for very low feed concentrations, they often provide a good approximation and, therefore, they are a good starting point to analyze SMB plants.

$$q_i \left(c_A, c_B\right) = H_i c_i, \quad i = A, B \tag{3.10}$$

In Fig. 3.2, the idealized concentration profiles of a SMB plant at cyclic steady state and complete regeneration in the outer zones are indicated. Four concentration fronts can be identified, where each has its own concentration velocity. In this way, one can set up four velocity equations dependent on the control variables. The objective is to choose the control variables such that the desired velocity is assigned to every concentration front.
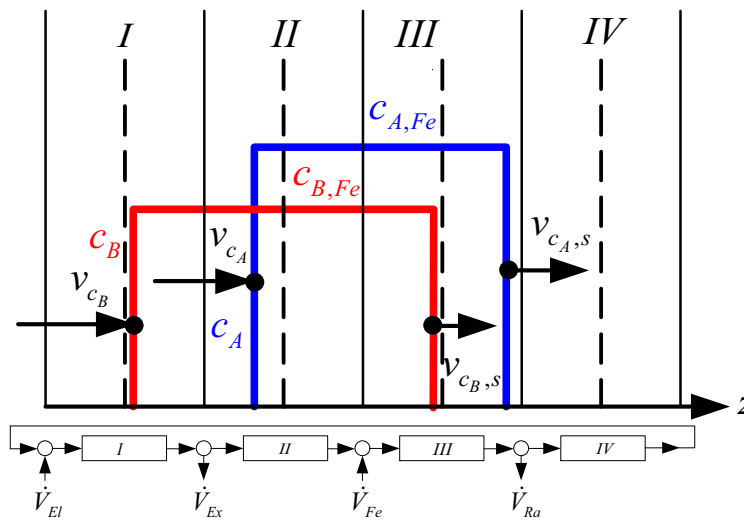

Figure 3.2: Idealized concentration profiles of a SMB plant at the beginning of a time interval for Henry isotherms and for complete regeneration.

3.2.1 Concept of the Characteristic Velocities

Since there is no coupling between the concentrations if one is using Henry isotherms, the concentration velocity can be determined from the ratio of the

partial differentials directly; see Eq. (3.11):

$$v_{c_i} = -\frac{\frac{\partial c_i}{\partial t}}{\frac{\partial c_i}{\partial z}} = \frac{v_l}{1 + F H_i} = \frac{(1 + F)}{A} \frac{\dot{V}}{1 + F H_i}, \quad i = A, B. \tag{3.11}$$

If one considers a characteristic point of the concentration front, the traveled distance of this point is calculated with the aid of the concentration velocity. For robust operations of SMB plants, it is necessary that the outer concentration fronts travel between two zones with different zone velocities. The mean velocity can be calculated with the help of the time integral and is equated to the port shift velocity. In cyclic steady state, the following velocity equation can be found for the concentration front of the component B at the extract side; Eq. (3.12):

$$\frac{L}{T_S} = \frac{1}{T_S} \int_0^{\tau_{B,I} T_S} v_{c_B,I} dt + \frac{1}{T_S} \int_{\tau_{B,I} T_S}^{T_S} v_{c_B,II} dt = \tau_{B,I} v_{c_B,I} + (1 - \tau_{B,I}) v_{c_B,II}. \tag{3.12}$$

The introduced normalized residence times, $\tau_{B,I}$, determines how long the concentration front stays within zone I. This parameter is an ideal measure in order to set the time-stamp at which the concentration front will appear at the drain at cyclic steady state to the desired value. If this concept is used for all four concentration fronts, the following four velocity equations are derived.

$$\frac{L}{T_S} = \tau_{B,I} \frac{(1 + F)}{A} \frac{\dot{V}_I}{1 + F H_B} + (1 - \tau_{B,I}) \frac{(1 + F)}{A} \frac{\dot{V}_I - \dot{V}_{Ex}}{1 + F H_B} \tag{3.13}$$

$$\frac{L}{T_S} = (1 - \tau_{A,II}) \frac{(1 + F)}{A} \frac{\dot{V}_I}{1 + F H_A} + \tau_{A,II} \frac{(1 + F)}{A} \frac{\dot{V}_I - \dot{V}_{Ex}}{1 + F H_A} \tag{3.14}$$

$$\frac{L}{T_S} = \tau_{B,III} \frac{(1 + F)}{A} \frac{\dot{V}_I - \dot{V}_{Ex} + \dot{V}_{Fe}}{1 + F H_B} + (1 - \tau_{B,III}) \frac{(1 + F)}{A} \frac{\dot{V}_I - \dot{V}_{Ex} + \dot{V}_{Fe} - \dot{V}_{Ra}}{1 + F H_B}$$
$$\tag{3.15}$$

$$\frac{L}{T_S} = (1 - \tau_{A,IV}) \frac{(1 + F)}{A} \frac{\dot{V}_I - \dot{V}_{Ex} + \dot{V}_{Fe}}{1 + F H_A} + \tau_{A,IV} \frac{(1 + F)}{A} \frac{\dot{V}_I - \dot{V}_{Ex} + \dot{V}_{Fe} - \dot{V}_{Ra}}{1 + F H_A}$$
$$\tag{3.16}$$

If one sets the positions of the four concentration fronts with aid of the normalized residence times, the equations can be solved for the four control variables. However, it is desired to express the positions of the inner concentration fronts by the purities.

3.2.2 Additional Equations

The purities at the drains are defined by the following equations:

$$P_{Ex} = \frac{\bar{c}_{B,Ex}}{\bar{c}_{A,Ex} + \bar{c}_{B,Ex}}, \quad P_{Ra} = \frac{\bar{c}_{A,Ra}}{\bar{c}_{A,Ra} + \bar{c}_{B,Ra}}. \tag{3.17}$$

For their calculation, the knowledge of the mean concentrations for both components at the extract and raffinate for one switching interval is necessary. The time trajectories of the concentrations at the extract drain, see also Fig. 3.4, are determined with aid of the normalized residence times and the plateau values, Eqs. (3.18)-(3.19):

$$\bar{c}_{A,Ex} = (1 - \tau_{A,II}) \, c_{A,Fe}, \tag{3.18}$$

$$\bar{c}_{B,Ex} = \tau_{B,I} \, c_{B,Fe}. \tag{3.19}$$

The ideal trajectory of the concentrations at the raffinate drain, see also Fig. 3.5, can be determined in a similar way, Eqs. (3.20)-(3.21):

$$\bar{c}_{A,Ra} = \tau_{A,IV} \, c_{A,Fe}, \tag{3.20}$$

$$\bar{c}_{B,Ra} = (1 - \tau_{B,III}) \, c_{B,Fe}. \tag{3.21}$$

The four mean concentrations may now be inserted in the equations for the drain purities. After this, these equations are solved for the inner normalized residence times, $\tau_{A,II}$ and $\tau_{B,III}$, by Eqs. (3.22)-(3.23), respectively:

$$\tau_{A,II} = 1 - \frac{1 - P_{Ex}}{P_{Ex}} \frac{c_{B,Fe}}{c_{A,Fe}} \tau_{B,I}, \tag{3.22}$$

$$\tau_{B,III} = 1 - \frac{1 - P_{Ra}}{P_{Ra}} \frac{c_{A,Fe}}{c_{B,Fe}} \tau_{A,IV}. \tag{3.23}$$

3.2.3 Explicit Equations for Henry Isotherms

The velocity equations, Eqs. (3.13)-(3.16), can be solved explicitly. In this case, it is useful to define the following intermediate variables:

$$\gamma_{Ex} = \frac{1 - P_{Ex}}{P_{Ex}} \frac{c_{B,Fe}}{c_{A,Fe}}, \quad \gamma_{Ra} = \frac{1 - P_{Ra}}{P_{Ra}} \frac{c_{A,Fe}}{c_{B,Fe}}. \tag{3.24}$$

Given the feed concentrations, $c_{A,Fe}$ and $c_{B,Fe}$, the feed flow rate, $\dot{V}_{Fe}$, the desired purities, P_{Ex} and P_{Ra}, and the outer normalized residence times, $0 \ll \tau_{B,I} \leqslant 1$ and $0 \ll \tau_{A,IV} \leqslant 1$, one can compute the necessary volumetric flow rates, $\dot{V}_I$, $\dot{V}_{Ex}$, $\dot{V}_{Ra}$, and the switching time, T_S, for $H_A < H_B$ and complete regeneration in the following way.

$$\dot{V}_I = \frac{(1 - \gamma_{Ra})}{(1 - \gamma_{Ex}\,\gamma_{Ra})\,\tau_{B,I}} \left(\frac{(1 - \gamma_{Ex}) - F\,(\gamma_{Ex}\,H_B - H_A)}{F\,(H_B - H_A)} \tau_{B,I} + 1 \right) \dot{V}_{Fe} \tag{3.25}$$

$$\dot{V}_{Ex} = \frac{(1 - \gamma_{Ra})}{(1 - \gamma_{Ex}\,\gamma_{Ra})\,\tau_{B,I}} \dot{V}_{Fe} \tag{3.26}$$

$$\dot{V}_{Ra} = \frac{(1 - \gamma_{Ex})}{(1 - \gamma_{Ex}\,\gamma_{Ra})\,\tau_{A,IV}} \dot{V}_{Fe} \tag{3.27}$$

$$T_S = \frac{F\,A\,L}{(1 + F)\,\dot{V}_{Fe}} \frac{(1 - \gamma_{Ex}\,\gamma_{Ra})}{(1 - \gamma_{Ex})\,(1 - \gamma_{Ra})} (H_B - H_A) \tag{3.28}$$

If incomplete regeneration in the zones I and IV is desired a similar procedure leads to the design equations as given in the appendix.

3.2.4 Simulation Results

To check the validity of the equations derived, a dynamic simulation was carried out with the help of finite element software called COMSOL, [48], [49].
In this case, Lagrange polynomials of third order as well as 384 elements per column were used. In order to stabilize the numerics, streamline diffusion was switched on. In Fig. 3.3 the concentration profiles for the cyclic steady state are given. The operating point is given in Tab. 3.1 and the simulation parameters are indicated in the appendix. The broader lines are the concentration profiles in the middle of the switching interval, whereas the thin lines are the profiles to the beginning and end of the switching interval. The typical moving box pro-

file is formed with concentration plateaus identical to the feed concentrations, as pointed out in [50]. The time trajectories of the concentrations at the drains are
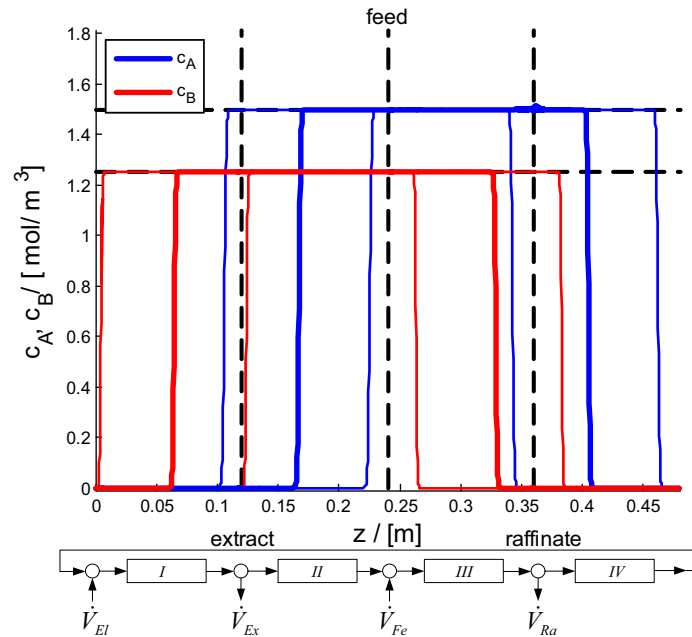

Figure 3.3: Concentration profiles for SMB process with $\tau_{B,I} = 0.95$, $\tau_{A,IV} = 0.9$, $P_{Ex} = 0.9$, $P_{Ra} = 0.8$, cfg $= [1,1,1,1]$ and model parameters taken from table A-2 on page 128.

represented in Fig. 3.4 and Fig. 3.5. The dotted trajectories are calculated theoretically, while the solid lines are the results of the dynamic simulation. They are in good agreement with the predicted values. The influence of the purities on the solvent consumption can be studied in a simple way with the aid of these equations. This is highlighted graphically through a contour plot in which the ratio of solvent flow rate to feed flow rate is represented. It is immediately obvious from Fig. 3.6 that an increase of the purities leads to an increase of the solvent flow rate. On a similar way, the dependence of the switching time from the purities can be studied. A higher switching time is required for lower purities, as indicated in Fig. 3.7.

3.2.5 Summary

In this section, simple explicit equations for Henry isotherms were derived to determine the control variables of a dispersion-free SMB model. The positions of the concentration fronts as well as the desired purities can be provided directly,
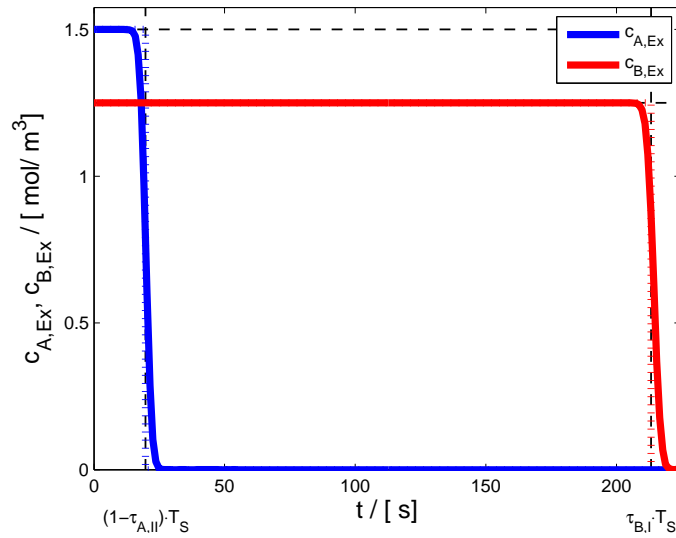
Figure 3.4: Time trajectories of the concentrations at the extract drain within one switching interval to Fig. 3.3.
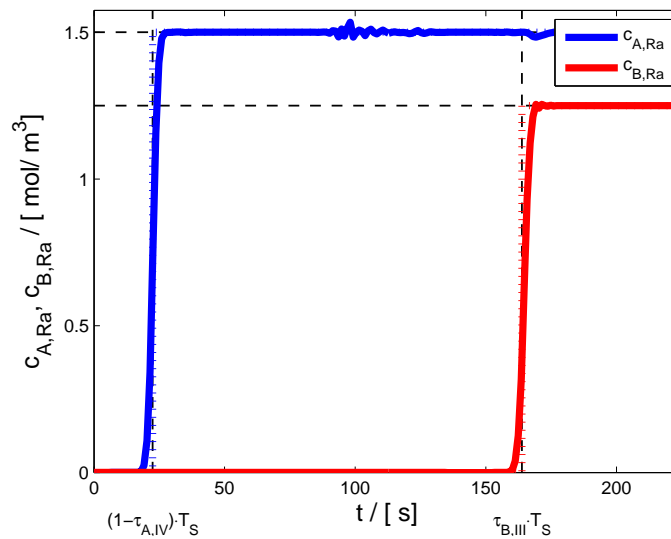

Figure 3.5: Time trajectories of the concentrations at the raffinate drain within one switching interval to Fig. 3.3.

Table 3.1: Operating points.

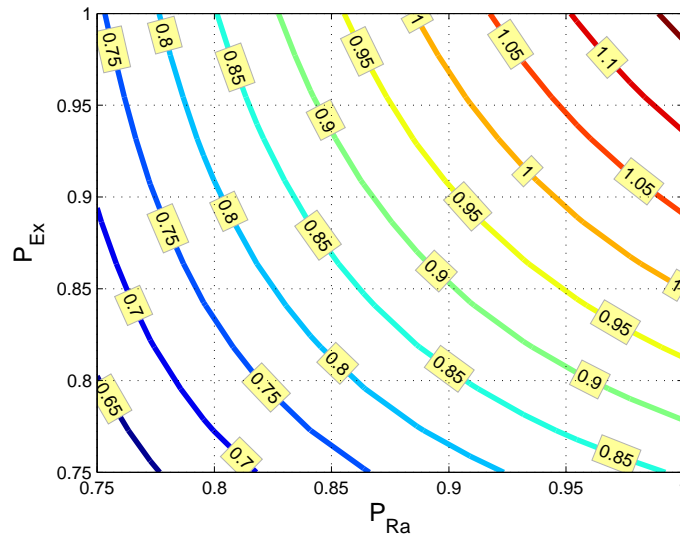|	$\dot{V}_I /$ $\left[\frac{ml}{min}\right]$	$\dot{V}_{Ex} /$ $\left[\frac{ml}{min}\right]$	$\dot{V}_{Ra} /$ $\left[\frac{ml}{min}\right]$	$T_S /$ $[s]$
Fig. 3.3	27.44	7.58	10.37	224.43

Figure 3.6: On the influence of the purities to the ratio of solvent to feed flow rate, $\dot{V}_{El}/\dot{V}_{Fe}$, with $\tau_{B,I} = 0.95$ and $\tau_{A,IV} = 0.9$ and model parameters taken from table A-2.
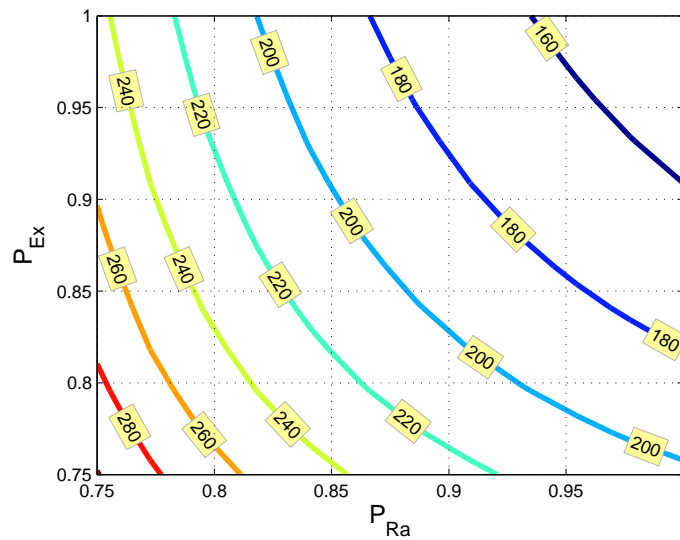

Figure 3.7: On the influence of the purities to the switching time, T_S, with $\tau_{B,I} = 0.95$ and $\tau_{A,IV} = 0.9$ and model parameters taken from table A-2.

which is not possible either by the *triangle theory*, [2], or the *standing wave design*, [4]. Furthermore, the time trajectories of the concentrations at the drains can be predicted exactly, which opens new fields of application, such as an intelligent optimization.

3.3 Operating Points for Noncompetitive Langmuir Isotherms

Since Henry isotherms are often insufficient to describe the adsorption behavior at high concentrations, it is natural to extend the proposed method to nonlinear isotherms. In this section, noncompetitive Langmuir isotherms are used to derive design equations for complete separation and complete regeneration, [51].

$$q_i\left(c_i\right) = \frac{H_i\,c_i}{1 + K_i\,c_i}, \quad i = A, B \tag{3.29}$$

Fig. 3.8 shows an idealized concentration profile of a dispersion-free SMB model at cyclic steady state for complete regeneration by using noncompetitive Langmuir isotherms at the beginning of a time interval. There are four concentration fronts, each having its own propagation velocity. Furthermore, two plateau concentrations are formed with values depending on the feed concentrations and the isotherm parameters. In zones I and II there are smooth transitions to the plateau concentrations. These transitions are called expansion waves. In zones III and IV discontinuous transitions occur, called shock waves. The objective is to set up four velocity equations in dependence on the volumetric flow rates and the time interval which are the control variables. The control variables are chosen in a way that each concentration front moves exactly one column length during one time interval at cyclic steady state.

3.3.1 Concept of Characteristic Velocities

If one assumes that the foot point of the expansion wave of component B above the extract drain runs between zones I and II, then the following velocity equa-
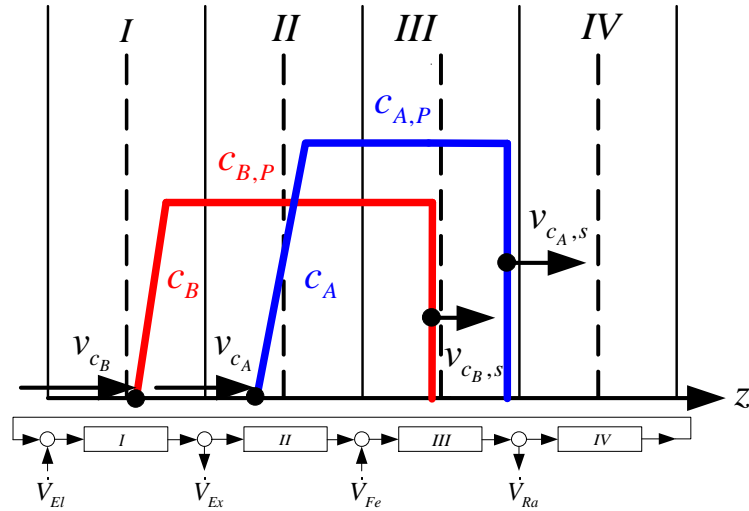
Figure 3.8: Idealized concentration profile of SMB plant at the beginning of a time interval for noncompetitive Langmuir isotherms.

tion holds for one time interval.

$$\frac{L}{T_S} = \frac{1}{T_S} \int_0^{\tau_{B,I} T_S} v_{c_B,I} \, dt + \frac{1}{T_S} \int_{\tau_{B,I} T_S}^{T_S} v_{c_B,II} \, dt = \tau_{B,I} \, v_{c_B,I} + (1 - \tau_{B,I}) \, v_{c_B,II} \quad (3.30)$$

The normalized residence time, $\tau_{B,I}$, introduced here, gives the time in percent during which the foot point stays in zone I. This parameter is an ideal quantity to adjust the position of the concentration front to the desired value at the time trajectory. See also Fig. 3.10 on page 54. In the same way, it is possible to determine a velocity equation for each concentration front. For further analysis, it is necessary to examine the velocities of the concentration fronts and their dependence on the control variables.

3.3.2 Foot Point Velocities

Since the isotherms considered in this study do not interact, the concentration velocity is simply determined through the negative ratio of the partial differentials:

$$v_{c_i} = -\frac{\frac{\partial c_i}{\partial t}}{\frac{\partial c_i}{\partial z}} = \frac{v_l}{1 + F \frac{dq_i(c_i)}{dc_i}} = \frac{v_l}{1 + F \frac{H_i}{(1+K_i \, c_i)^2}}, \quad i = A, B. \quad (3.31)$$

To determine the foot point velocities of the expansion waves, the concentration to be considered is set to zero, since complete regeneration in the outer zones is assumed. In this way, the following expressions for the foot point velocities in zones I and II are obtained:

$$v_{c_B,I} = \frac{v_l}{1 + F\,H_B}, \tag{3.32}$$

$$v_{c_A,II} = \frac{v_l}{1 + F\,H_A}. \tag{3.33}$$

3.3.3 Shock Velocities

If there is a discontinuity in the concentration profile, the differential description of this discontinuity by the partial differential equation is invalid. In this case, an integral description must be used. From this, one obtains the Rankine-Huginot condition, [29], for the description of shocks. The shock speed is calculated using the ratio of differences between adsorbed and liquid concentration across the shock, [32]:

$$v_{c_i,s}(t) = \frac{v_l}{1 + F\,\frac{q_i(c_{i,L}) - q_i(c_{i,R})}{c_{i,L} - c_{i,R}}}, \quad i = A, B. \tag{3.34}$$

For complete regeneration in the outer zones, the following velocities for the shock fronts of zones III and IV are determined:

$$v_{c_B,s,III} = \frac{v_l}{1 + F\,\frac{H_B}{1 + K_B\,c_{B,P}}}, \tag{3.35}$$

$$v_{c_A,s,IV} = \frac{v_l}{1 + F\,\frac{H_A}{1 + K_A\,c_{A,P}}}. \tag{3.36}$$

3.3.4 Velocity Equations

Using the foot point and shock velocities, the following four velocity equations in dependence of the control variables for the case of complete separation, i.e. $\tau_{A,II} = 1$ and $\tau_{B,III} = 1$, can be found.

$$\frac{A\,L}{(1 + F)\,T_S} = \frac{1}{1 + F\,H_B}\left[\tau_{B,I}\,\dot{V}_I + (1 - \tau_{B,I})\left(\dot{V}_I - \dot{V}_{Ex}\right)\right] \tag{3.37}$$

$$\frac{A\,L}{(1+F)\,T_S} = \frac{1}{1+F\,H_A}\,\left(\dot{V}_I - \dot{V}_{Ex}\right) \tag{3.38}$$

$$\frac{A\,L}{(1+F)\,T_S} = \frac{1}{1+\frac{F\,H_B}{1+K_B\,c_{B,P}}}\,\left(\dot{V}_I - \dot{V}_{Ex} + \dot{V}_{Fe}\right) \tag{3.39}$$

$$\frac{A\,L}{(1+F)\,T_S} = \frac{1}{1+\frac{F\,H_A}{1+K_A\,c_{A,P}}}\,\left[\begin{array}{l}(1-\tau_{A,IV})\,\left(\dot{V}_I - \dot{V}_{Ex} + \dot{V}_{Fe}\right) \\ +\tau_{A,IV}\,\left(\dot{V}_I - \dot{V}_{Ex} + \dot{V}_{Fe} - \dot{V}_{Ra}\right)\end{array}\right] \tag{3.40}$$

For the determination of the control variables, the plateau values must still be determined. For this, two further equations are required.

3.3.5 Component Balances

To determine the plateau values, $c_{A,P}$ and $c_{B,P}$, the component balances of the overall system are used. It is assumed that at cyclic steady state the stored mass is constant during one time interval. Further, complete separation is assumed. For components A and B the following equations hold:

$$0 = c_{A,Fe}\,\dot{V}_{Fe} - \bar{c}_{A,Ra}\,\dot{V}_{Ra}, \tag{3.41}$$

$$0 = c_{B,Fe}\,\dot{V}_{Fe} - \bar{c}_{B,Ex}\,\dot{V}_{Ex}. \tag{3.42}$$

To evaluate the equations, the mean concentration values must be determined with respect to one time interval. The time trajectory of the concentrations at the raffinate drain can be described for one time interval by Eq. (3.43), as can be seen from Fig. 3.9.

$$c_{A,Ra}\,(t) = \begin{cases} 0 & 0 \leqslant t < (1-\tau_{A,IV})\,T_S \\ c_{A,P} & (1-\tau_{A,IV})\,T_S \leqslant t \leqslant T_S \end{cases} \tag{3.43}$$

The mean concentration of component A at the raffinate drain is expressed by the normalized residence time, $\tau_{A,IV}$, and the plateau value, $c_{A,P}$, of this component:

$$\bar{c}_{A,Ra} = \frac{1}{T_S}\int_0^{T_S} c_{A,Ra}\,(t)\,dt = \tau_{A,IV}\,c_{A,P}. \tag{3.44}$$
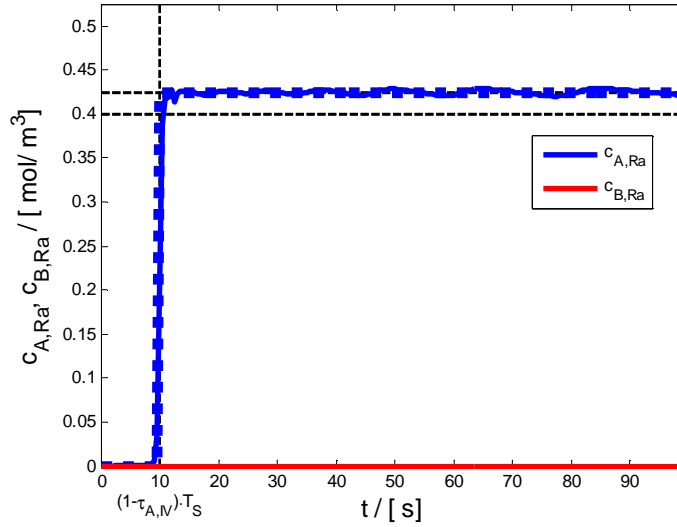
Figure 3.9: Estimated and simulated time trajectories of concentrations at the raffinate drain within one switching interval to Fig. 3.12 on page 59.

The time trajectory of the concentration at the extract drain is mainly determined by the shape of the expansion wave, see Fig. 3.10. The course can be exactly determined from the partial differential equation, [29]. The transition between the two states is between two time points, which are expressed by the normalized residence times of the foot and head point. For one time interval, the course at the extract can be described by Eq. (3.45).

$$
c_{B,Ex}\left(t\right) = \begin{cases} c_{B,P} & 0 \leqslant t \leqslant \tau\, T_S \\ \dfrac{1}{K_B}\left[\sqrt{\dfrac{(1+K_B\, c_{B,P})^2\, (\tau_{B,I}-\tau)\, T_S}{(2+K_B\, c_{B,P})\, K_B\, c_{B,P}\, (t-\tau\, T_S)+(\tau_{B,I}-\tau)\, T_S}} - 1\right] & \tau\, T_S < t < \tau_{B,I}\, T_S \\ 0 & \tau_{B,I}\, T_S \leqslant t \leqslant T_S \end{cases}
$$
$$(3.45)$$

The mean concentration value with respect to one time interval is now calculated using the integral:

$$
\bar{c}_{B,Ex} = \frac{1}{T_S}\int_0^{T_S} c_{B,Ex}\left(t\right) dt = \tau\, c_{B,P} + (\tau_{B,I} - \tau)\, \frac{c_{B,P}}{2 + K_B\, c_{B,P}}. \tag{3.46}
$$

The normalized residence time, τ, of the head point is determined with the aid of the concentration velocity, Eq. (3.31) on page 50. It is assumed that the head point runs between zones I and II. This assumption can be checked afterwards and is valid for low feed concentrations. Thus, the following velocity equation can be derived:

$$\frac{L}{T_S} = \frac{1+F}{A} \frac{1}{1 + \frac{F\,H_B}{(1+K_B\,c_{B,P})^2}} \left[\tau\,\dot{V}_I + (1-\tau)\,\left(\dot{V}_I - \dot{V}_{Ex}\right)\right]. \tag{3.47}$$

This equation is solved for the normalized residence time, τ, of the head point:

$$\tau = \left(1 + \frac{F\,H_B}{(1+K_B\,c_{B,P})^2}\right) \frac{A\,L}{(1+F)\,\dot{V}_{Ex}\,T_S} - \frac{\dot{V}_I - \dot{V}_{Ex}}{\dot{V}_{Ex}}. \tag{3.48}$$

Now, four velocity equations and two component balances are available for the determination of the four control variables and the two plateau values.

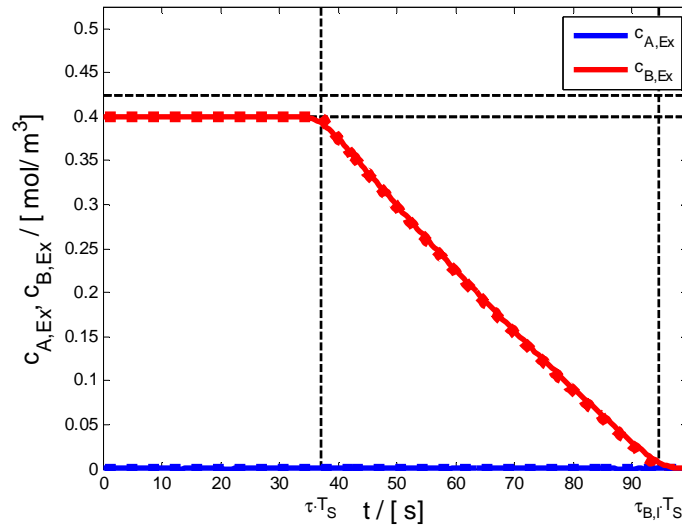

Figure 3.10: Estimated and simulated time trajectories of concentrations at the extract drain within one switching interval to Fig. 3.12 on page 59.

3.3.6 Solution for Low Feed Concentration

The system of equations consisting of Eqs. (3.37)-(3.40), (3.41), (3.42) and the auxiliary Eqs. (3.44), (3.46), (3.48) can be solved explicitly. As stated above, for low

feed concentrations the head point of the expansion wave travels between zones I and II. The validity of this solution structure for low feed concentration of component B can be checked with Eqs. (3.49) and (3.50). Thus, given the feed concentrations, $c_{A,Fe}$, $c_{B,Fe}$, the feed flow rate, $\dot{V}_{Fe}$, and the normalized residence times, $0 \ll \tau_{B,I} \leqslant 1$ and $0 \ll \tau_{A,IV} \leqslant 1$, the necessary flow rates $\dot{V}_I$, $\dot{V}_{Ex}$, $\dot{V}_{Ra}$ and switching time, T_S, for $H_A < H_B$ can be computed for complete separation and complete regeneration in the following way.

$$c_{B,0} = \frac{1}{K_B} \frac{H_B - H_A}{\sqrt{H_A\,H_B} + H_A} \tag{3.49}$$

$$c_{B,Fe} < c_{B,0} \tag{3.50}$$

$$c_{A,P} = \frac{2\,c_{A,Fe}}{(1 - K_A\,c_{A,Fe}) + \sqrt{(1 + K_A\,c_{A,Fe})^2 + \frac{4\,H_A\,(\,1 + K_B\,c_{B,Fe}\,)}{H_B - H_A\,(1 + K_B\,c_{B,Fe})}\,K_A\,c_{A,Fe}}} \tag{3.51}$$

$$c_{B,P} = c_{B,Fe} \tag{3.52}$$

$$\dot{V}_I = \frac{[F\,H_B + \tau_{B,I} - F\,H_A\,(1 - \tau_{B,I})]}{F\,\tau_{B,I}\,[H_B - H_A\,(1 + K_B\,c_{B,Fe})]}\,(1 + K_B\,c_{B,Fe})\,\dot{V}_{Fe} \tag{3.53}$$

$$\dot{V}_{Ex} = \frac{(H_B - H_A)\,(1 + K_B\,c_{B,Fe})}{\tau_{B,I}\,[H_B - H_A\,(1 + K_B\,c_{B,Fe})]}\,\dot{V}_{Fe} \tag{3.54}$$

$$\dot{V}_{Ra} = \frac{c_{A,Fe}}{\tau_{A,IV}\,c_{A,P}}\,\dot{V}_{Fe} \tag{3.55}$$

$$T_S = \frac{F}{1 + F}\,\frac{A\,L}{\dot{V}_{Fe}}\,\frac{H_B - H_A\,(1 + K_B\,c_{B,Fe})}{1 + K_B\,c_{B,Fe}} \tag{3.56}$$

$$\tau = \frac{H_B - H_A\,(1 + (2 + K_B\,c_{B,Fe})\,K_B\,c_{B,Fe})}{(H_B - H_A)\,(1 + K_B\,c_{B,Fe})^2}\,\tau_{B,I} \tag{3.57}$$

The time trajectories of the concentrations at the extract and raffinate can be constructed with Eqs. (3.43) and (3.45) on page 52 for the cyclic steady state. Note

that Eq. (3.56) for the time interval may also be solved for the feed flow rate if the time interval is fixed in advance. If one likes to restrict the pressure drop in zone I, it is also possible to preselect the volumetric flow rate of zone I and solve Eq. (3.53) for the feed flow rate instead.

3.3.7 Extension to High Feed Concentration

For high concentrations, the head point of the expansion wave only runs in zone II. Therefore, the assumption made before is invalid so that the components balance for component B in the form of Eq. (3.42) on page 52 and Eq. (3.46) on page 53 is incorrect. The maximum concentration, $c_{B,0}$, that appears at the extract drain can again be determined with the aid of the concentration velocity, Eq. (3.31) on page 50. This concentration value moves exactly one column length in zone I during one time interval so that the following equation holds:

$$\frac{L}{T_S} = \frac{(1+F)}{A} \frac{\dot{V}_I - \dot{V}_{Ex}}{1 + \frac{F\,H_B}{(1+K_B\,c_{B,0})^2}}. \tag{3.58}$$

This equation is solved for the concentration value:

$$c_{B,0} = \frac{1}{K_B} \left(\frac{F\,H_B}{\sqrt{\frac{(1+F)\,(\dot{V}_I - \dot{V}_{Ex})\,T_S}{A\,L}} - 1} - 1 \right). \tag{3.59}$$

The time trajectory of the concentration at the extract can be described for one time interval by Eq. (3.60).

$$c_{B,Ex}(t) = \begin{cases} \frac{1}{K_B} \left[\sqrt{\frac{(1+K_B\,c_{B,0})^2\,\tau_{B,I}\,T_S}{(2+K_B\,c_{B,0})\,K_B\,c_{B,0}\,t + \tau_{B,I}\,T_S}} - 1 \right] & 0 \leqslant t \leqslant \tau_{B,I}\,T_S \\ 0 & \tau_{B,I}\,T_S < t \leqslant T_S \end{cases} \tag{3.60}$$

The mean concentration value can be calculated using the integral.

$$\bar{c}_{B,Ex} = \frac{1}{T_S} \int_0^{T_S} c_{B,Ex}(t)\,dt = \tau_{B,I} \frac{c_{B,0}}{2 + K_B\,c_{B,0}} \tag{3.61}$$
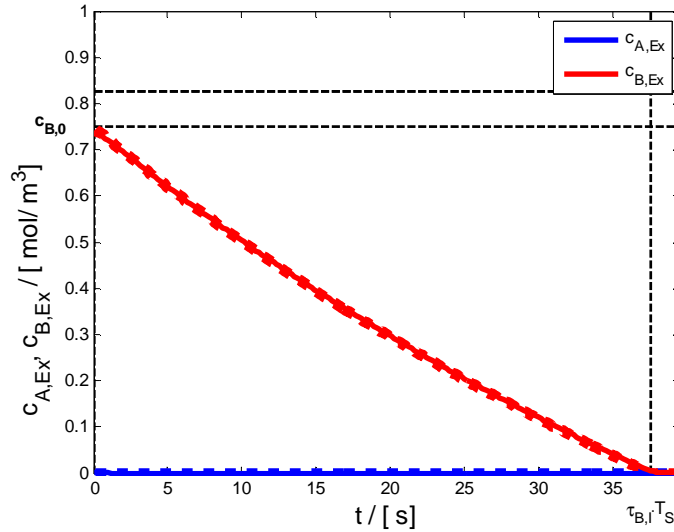
Figure 3.11: Estimated and simulated time trajectories of concentrations at the extract drain within one switching interval to Fig. 3.13 on page 60.

Thus, the correct component balance for component B for high feed concentration is described by Eq. (3.62):

$$0 = c_{B,Fe} \, \dot{V}_{Fe} - \tau_{B,I} \, \frac{c_{B,0}}{2 + K_B \, c_{B,0}} \, \dot{V}_{Ex}. \tag{3.62}$$

3.3.8 Solution for High Feed Concentration

The system of equations consisting of the Eqs. (3.37)-(3.40), (3.41), (3.42) and the auxiliary Eqs. (3.59), (3.61) can be again solved explicitly. Eq. (3.63) indicates the concentration value at which the solution structure will change.

$$c_{B,0} = \frac{1}{K_B} \frac{H_B - H_A}{\sqrt{H_A \, H_B} + H_A} \tag{3.63}$$

$$c_{B,Fe} > c_{B,0} \tag{3.64}$$

$$c_{A,P} = \frac{H_B - H_A}{2} \frac{\left(\sqrt{ \begin{array}{c} (H_B - H_A)^2 \, (1 + K_A \, c_{A,Fe})^2 \\ + 4 \, H_A \, \left(\sqrt{H_B} + \sqrt{H_A} \right)^2 K_A \, K_B \, c_{A,Fe} \, c_{B,Fe} \end{array} } - (H_B - H_A) \, (1 - K_A \, c_{A,Fe}) \right)}{K_A \, \left(H_A \, \left(\sqrt{H_B} + \sqrt{H_A} \right)^2 K_B \, c_{B,Fe} + (H_B - H_A)^2 \right)} \tag{3.65}$$

$$c_{B,P} = \frac{H_B - H_A}{K_B} \frac{\left(\sqrt{H_B} + \sqrt{H_A}\right)^2 K_B c_{B,Fe} - (H_B - H_A)}{H_A \left(\sqrt{H_B} + \sqrt{H_A}\right)^2 K_B c_{B,Fe} + (H_B - H_A)^2} \tag{3.66}$$

$$\dot{V}_I = \frac{\left(\sqrt{H_B} + \sqrt{H_A}\right)^2 \left[F \left(H_B - H_A \left(1 - \tau_{B,I}\right)\right) + \tau_{B,I}\right]}{F \tau_{B,I} \left(H_B - H_A\right)^2} K_B c_{B,Fe} \dot{V}_{Fe} \tag{3.67}$$

$$\dot{V}_{Ex} = \frac{\left(\sqrt{H_B} + \sqrt{H_A}\right)^2}{\tau_{B,I} \left(H_B - H_A\right)} K_B c_{B,Fe} \dot{V}_{Fe} \tag{3.68}$$

$$\dot{V}_{Ra} = \frac{c_{A,Fe}}{\tau_{A,IV} c_{A,P}} \dot{V}_{Fe} \tag{3.69}$$

$$T_S = \frac{F}{1 + F} \frac{A\,L}{\dot{V}_{Fe}} \frac{(H_B - H_A)^2}{\left(\sqrt{H_B} + \sqrt{H_A}\right)^2 K_B c_{B,Fe}} \tag{3.70}$$

Again, a rearrangement can be carried out between the predefined and the quantities to be calculated if required.

3.3.9 Simulation Results

A dynamic simulation was performed to validate the derived equations. This was done using the finite element software COMSOL, [48], [49]. Third-order Lagrange polynomials as well as 384 elements per column were used. To stabilize the numerics, streamline diffusion was switched on. For the feeding concentrations, $c_{A,Fe} = 0.5$ and $c_{B,Fe} = 0.4$, and the parameters given in the Appendix, one obtains the cyclic steady state concentration profile shown in Fig. 3.12. The broader lines correspond to the concentration profile in the middle of a time interval whereas the thin lines are the profiles at the beginning and the end of a time interval. The corresponding time trajectories of the concentrations at the drains were already shown in Fig. 3.10 on page 54 and Fig. 3.9 on page 53. The dotted trajectories are calculated theoretically while the solid lines are the results of the dynamic simulation. There is a very good agreement with the predicted values.

A second simulation was performed with increased feed concentrations, $c_{A,Fe} = 1.50$ and $c_{B,Fe} = 1.25$. These results are shown in Fig. 3.13, Fig. 3.11 and Fig. 3.14. Again, a very good agreement between predicted and the simulated concentration trajectories can be observed with only one difference at the raffinate side.
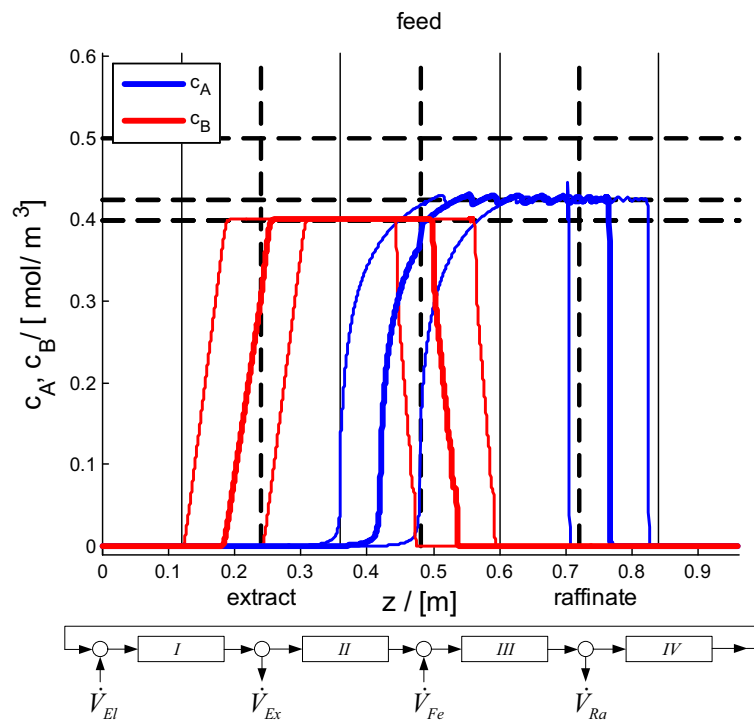
Figure 3.12: Concentration profile for SMB plant with $\tau_{B,I} = 0.95$, $\tau_{A,IV} = 0.9$, $c_{A,Fe} = 0.5$, $c_{B,Fe} = 0.4$, cfg $= [2, 2, 2, 2]$ und model parameters from table A-2.

Around the predicted plateau value, an oscillating behavior can be observed which is caused by the periodic switching.
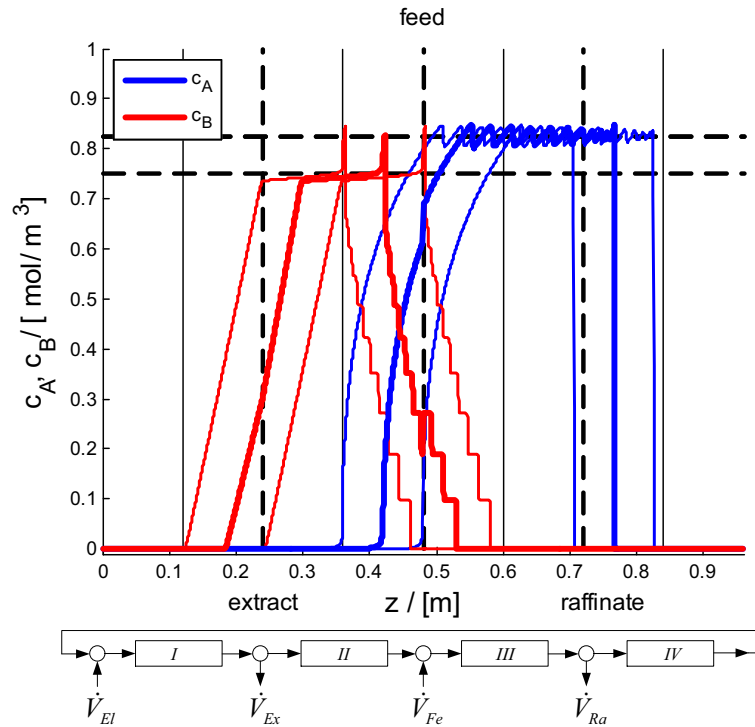

Figure 3.13: Concentration profiles for SMB plant with $\tau_{B,I} = 0.95$, $\tau_{A,IV} = 0.9$, $c_{A,Fe} = 1.50$, $c_{B,Fe} = 1.25$, cfg $= [2, 2, 2, 2]$ and model parameters from table A-2.

3.3.10 Summary

In this section, simple explicit equations were derived to determine the control variables of a dispersion-free SMB model for noncompetitive Langmuir isotherms. To account for model inaccuracies and non-modeled dispersion, the positions of the outer concentration fronts and thus the distance to the outer zone boundaries can be set by the normalized residence times. Furthermore, the periodical time trajectories of the concentrations at the drains can be predicted very well. This opens up new fields of application, such as an intelligent optimization or control of SMB plants. The designer can use these equations to quickly calculate the desired control variables and may take them as an ideal starting point to optimize SMB plants that are more complex. Thus, a great reduction in computation time can be achieved. In addition, the equations may be used to study the influence
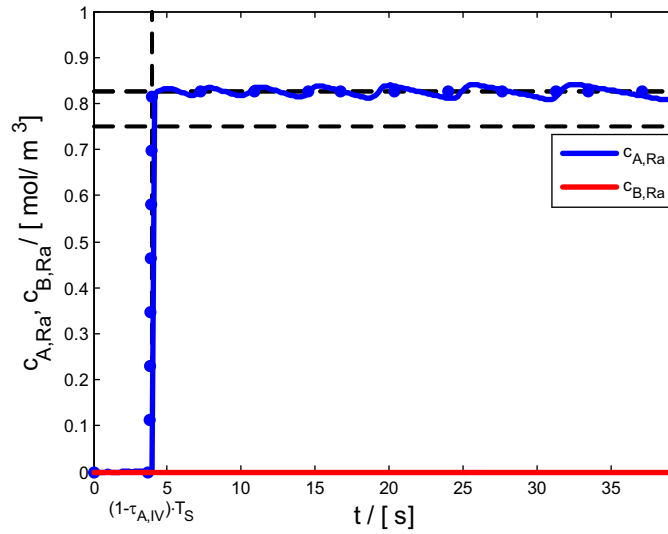
Figure 3.14: Estimated and simulated time trajectories of concentrations at the raffinate drain within one switching interval to Fig. 3.13.

Table 3.2: Operating points.

	Fig. 3.12	Fig. 3.13
$c_{A,Fe}/\left[\frac{mol}{m^3}\right]$	0.50	1.5
$c_{B,Fe}/\left[\frac{mol}{m^3}\right]$	0.40	1.25
$\dot{V}_I/\left[\frac{ml}{min}\right]$	61.82	155.73
$\dot{V}_{Ex}/\left[\frac{ml}{min}\right]$	15.51	39.07
$\dot{V}_{Ra}/\left[\frac{ml}{min}\right]$	13.07	20.20
$T_S/\left[s\right]$	99.50	39.50
$c_{A,P}/\left[\frac{mol}{m^3}\right]$	0.42	0.83
$c_{B,P}/\left[\frac{mol}{m^3}\right]$	0.40	1.07

of the model parameters on the trajectories of the concentrations at the drains in a simple way. Finally, the equations are also very useful to validate software for simulation and optimization of SMB plants. The concept of the characteristic velocities can also be transferred to other isotherms. Applied to competitive Langmuir isotherms, it leads to the equations indicated in [49]. This method can also be extended to compute operating points for reduced purities.

3.4 Operating Points for Langmuir Isotherms

The adsorption affinity of a substance often depends on the composition of the substance mixture. To describe the interactions, one can use a competitive Langmuir isotherm. Thus, the method will now be extended to derive design equations for complete and incomplete separation and complete regeneration, [52], [53], by using competitive Langmuir isotherms, as described by Eq. (3.71):

$$q_i\left(c_A, c_B\right) = \frac{H_i\, c_i}{1 + K_A\, c_A + K_B\, c_B}, \quad \text{for } i = A, B. \tag{3.71}$$

Now, the velocities of the concentration fronts cannot be adjusted independently for each component and an extended mathematical analysis is necessary. To analyze a coupled system of hyperbolic differential equations, one needs to solve a left eigenvalue problem to decouple the system differentially. This leads to a set of ordinary differential equations, which describes the Riemann invariants along the characteristic lines. For a homogenous 2x2 system, the differential equations in time can be converted to the phase plane, which gives a differential relationship between both dependent variables. For Langmuir isotherms, this differential equation is of Clairauts type and can be solved. The physically relevant solutions lead to a linear Riemann invariant relationship, which determines the characteristics where the Riemann invariants stay constant. Graphically, these relations are best represented in the hodograph plane, Fig. 3.16. Furthermore, the speed of propagation can be computed with help of the associated eigenvalue. For a complete treatment, the reader is referred to [29], [32] and for the basic concept to [38]. In chapter 2.3, the reader will find an introduction to this theory. The sequel will build up on these known results.

In Fig. 3.15, the idealized concentration profiles of a SMB plant at cyclic steady state with zero axial dispersion and complete regeneration in zones I and IV are

given. It is possible to define some characteristic points at this profile for which the velocity can be determined and, therefore, the propagation can be evaluated. It is also helpful to have a look at the track of the associated hodograph plane for this profile as shown in Fig. 3.16. One can identify four characteristic plateau
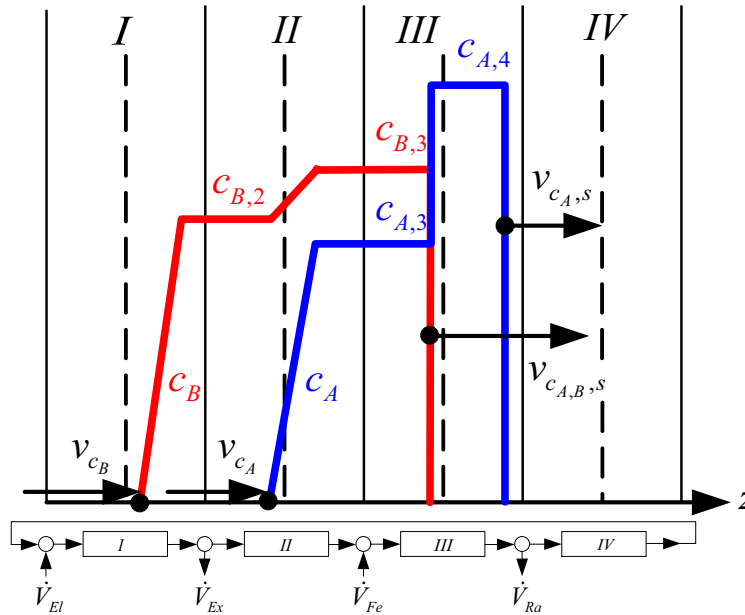

Figure 3.15: Idealized concentration profiles of a SMB plant at the beginning of a time interval for Langmuir isotherms.

values that represent just the corners of the track within the hodograph plane. These corners are indicated with Arabic numbers. If the track follows the Riemann invariants sufficiently well, the simple wave condition is established and can be used as basic tool for constructing the desired startup formula.

3.4.1 Concept of Characteristic Velocities

It is assumed that the foot point of the expansion wave of the component, B, above the extract drain runs between zone I and II. Therefore, the velocity equation, Eq. (3.72), holds for one time interval.

$$\frac{L}{T_S} = \frac{1}{T_S} \int_0^{\tau_{B,I} T_S} v_{c_B,I} \, dt + \frac{1}{T_S} \int_{\tau_{B,I} T_S}^{T_S} v_{c_B,II} \, dt = \tau_{B,I} \, v_{c_B,I} + (1 - \tau_{B,I}) \, v_{c_B,II} \quad (3.72)$$
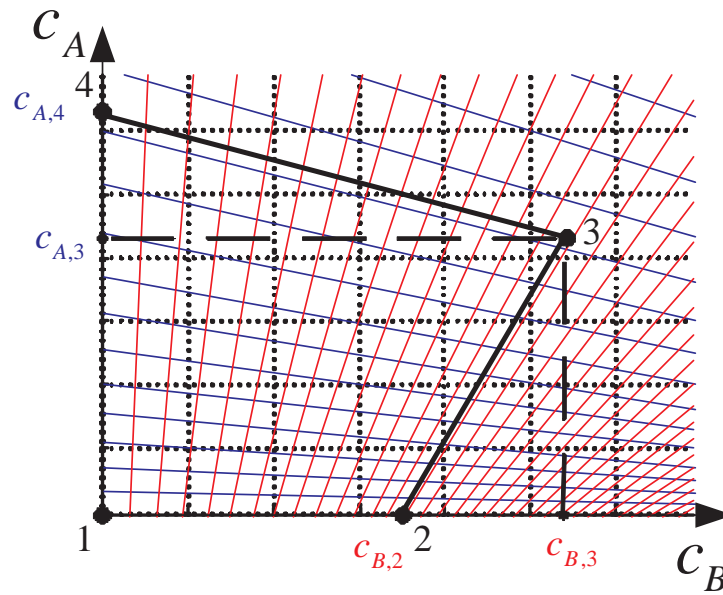
Figure 3.16: Associated hodograph plane to Fig. 3.15.

The introduced normalized residence time, $\tau_{B,I}$, gives the time in percentage for which the foot point stays in zone I. This parameter is a suitable measure to adjust the position of the concentration front to the desired value at the time trajectory. See also Fig. 3.18 on page 69. Thus, for each concentration front, a velocity equation can be determined again. Now, the velocity of the concentration fronts and their dependence on the control variables need to be analyzed.

3.4.2 Foot Point Velocities

Within the first and second zone, an expansion wave is established. The velocities of the foot points are determined as special cases of concentration velocities, where the concentration under investigation is zero, since complete regeneration is required. In general, the concentration velocity is computed with Eq. (3.73):

$$v_{c_i} = \frac{v_l}{1 + F \frac{dq_i(c_A, c_B)}{dc_i}}, \quad \text{for } i = A, B. \tag{3.73}$$

From the hodograph plane, it becomes immediately clear that the plateau value, $c_{B,2}$, is maintained when c_A becomes nonzero. In the case of Langmuir isotherms,

these velocities are identified as:

$$v_{c_B,I} = \frac{v_l}{1 + F\,H_B},\tag{3.74}$$

$$v_{c_A,II} = \frac{v_l}{1 + F\,\frac{H_A}{1 + K_B\,c_{B,2}}}.\tag{3.75}$$

3.4.3 Shock Velocities

Within the third and fourth zone, a shock wave is established. The shock velocities can be determined using the Rankine- Huginot condition, which for this model can be stated as:

$$v_s = \frac{v_l}{1 + F\,\frac{q_i(c_{A,L},c_{B,L}) - q_i(c_{A,R},c_{B,R})}{c_{i,L} - c_{i,R}}}, \quad \text{for } i = A, B.\tag{3.76}$$

Notice that the indices, L and R, are the left and right values across the shock, respectively. Therefore, the shock velocities depend on the plateau values. Considering Langmuir isotherms and complete regeneration, following velocities, Eq. (3.77) and Eq. (3.78), are determined:

$$v_{c_{A,B},III} = \frac{v_l}{1 + F\,\frac{H_B}{1 + K_A\,c_{A,3} + K_B\,c_{B,3}}},\tag{3.77}$$

$$v_{c_A,IV} = \frac{v_l}{1 + F\,\frac{H_A}{1 + K_A\,c_{A,4}}}.\tag{3.78}$$

3.4.4 Velocity Equations for Complete Separation

If a cyclic steady state is achieved, the chosen characteristic points will travel one column length within a switching interval. That means they travel with averaged velocity, L/T_S. One can now set up the system of equations to find the unknown liquid velocities. For complete separation, the inner concentration fronts are forced to stay only within the inner zones. To get a formula that is capable of incorporating some safety margin due to model uncertainty, the outer concentration fronts are allowed to travel within two zones. The safety margins, $0 \ll \tau_{B,I} \leqslant 1$ and $0 \ll \tau_{A,IV} \leqslant 1$, are defined to be the normalized residence time. With them, this concentration fronts stays within the outer zones. Expressing the

liquid velocities by the appropriate volumetric flow rates leads to the following four basic velocity equations for complete separation and complete regeneration, Eqs. (3.79-3.82).

$$\frac{A}{(1+F)}\frac{L}{T_S} = \frac{1}{1+F\,H_B}\left[\tau_{B,I}\,\dot{V}_I + (1-\tau_{B,I})\,(\dot{V}_I - \dot{V}_{Ex})\right] \tag{3.79}$$

$$\frac{A}{(1+F)}\frac{L}{T_S} = \frac{1}{1+\frac{F\,H_A}{1+K_B\,c_{B,2}}}\,(\dot{V}_I - \dot{V}_{Ex}) \tag{3.80}$$

$$\frac{A}{(1+F)}\frac{L}{T_S} = \frac{1}{1+\frac{F\,H_B}{1+K_A\,c_{A,3}+K_B\,c_{B,3}}}\,(\dot{V}_I - \dot{V}_{Ex} + \dot{V}_{Fe}) \tag{3.81}$$

$$\frac{A}{(1+F)}\frac{L}{T_S} = \frac{1}{1+\frac{F\,H_A}{1+K_A\,c_{A,4}}}\left[\begin{array}{c}(1-\tau_{A,IV})\,(\dot{V}_I - \dot{V}_{Ex} + \dot{V}_{Fe})\\ +\tau_{A,IV}\,(\dot{V}_I - \dot{V}_{Ex} + \dot{V}_{Fe} - \dot{V}_{Ra})\end{array}\right] \tag{3.82}$$

3.4.5 Simple Wave Condition

If the simple wave condition is satisfied, the concentration profile of the SMB plant will track along the Riemann invariants and the linear relationship, Eq. (3.83), between the concentrations is maintained, [29], [53]. Notice that for Langmuir isotherms, one needs not to distinguish between shock path and expansion path, since both go on the same curves in the hodograph plane, [34], [53].

$$c_A = C_i\,c_B - \frac{(H_B - H_A)\,C_i}{H_A\,K_B + H_B\,K_A\,C_i}, \quad C_i = \left(\frac{dc_A}{dc_B}\right)_i, \quad \text{for } i = 1,2 \tag{3.83}$$

By investigating the hodograph plane, Fig. 3.16 on page 64, it is immediate clear that if $c_{B,2}$ and $c_{A,4}$ are known, the inner plateaus, $c_{A,3}$ and $c_{B,3}$, are determined from the intersection point of two Riemann invariants. The Riemann invariants are obtained from the equations that determine the intersection with the coordinate axis, Eqs. (3.84) and (3.85):

$$c_{B,2} = \frac{(H_B - H_A)}{K_B\,H_A + K_A\,H_B\,C_1}, \tag{3.84}$$

$$c_{A,4} = -\frac{(H_B - H_A)\,C_2}{K_B\,H_A + K_A\,H_B\,C_2}. \tag{3.85}$$

The intersection point 3 of both invariants is found with help of the Riemann invariant relationship, Eq. (3.86).

$$c_{A,3} = C_i\, c_{B,3} - \frac{(H_B - H_A)\, C_i}{H_A\, K_B + H_B\, K_A\, C_i}, \quad \text{for } i = 1, 2 \tag{3.86}$$

Solving Eq. (3.84) and Eq. (3.85) for the Riemann invariants and using them in the Eqs. of (3.86), the concentrations of intersection point 3 yields:

$$c_{A,3} = \frac{(H_B - H_A - K_B\, H_A\, c_{B,2})\, c_{A,4}}{H_B - H_A}, \tag{3.87}$$

$$c_{B,3} = \frac{(H_B - H_A + K_A\, H_B\, c_{A,4})\, c_{B,2}}{H_B - H_A}. \tag{3.88}$$

3.4.6 Component Balances for Complete Separation

To get a solution for the system of equations, Eqs. (3.79) to (3.82) on page 66, the outer plateau values, $c_{B,2}$ and $c_{A,4}$, must be determined. This can be done with the aid of the component balances of the complete system. It is assumed that in cyclic steady state, the stored amount of substance is constant during one cycle. For the components, A and B, the following equations will hold for complete separation:

$$0 = c_{A,Fe}\, \dot{V}_{Fe} - \bar{c}_{A,Ra}\, \dot{V}_{Ra}, \tag{3.89}$$

$$0 = c_{B,Fe}\, \dot{V}_{Fe} - \bar{c}_{B,Ex}\, \dot{V}_{Ex}. \tag{3.90}$$

To evaluate the equations, the mean concentrations must be determined for one switching time. The concentration course at the raffinate for one cycle is very simply parameterized, Eq. (3.91), because of the shock wave.

$$c_{A,Ra}(t) = \begin{cases} 0 & 0 \leqslant t < (1 - \tau_{A,IV})\, T_S \\ c_{A,4} & (1 - \tau_{A,IV})\, T_S \leqslant t \leqslant T_S \end{cases} \tag{3.91}$$
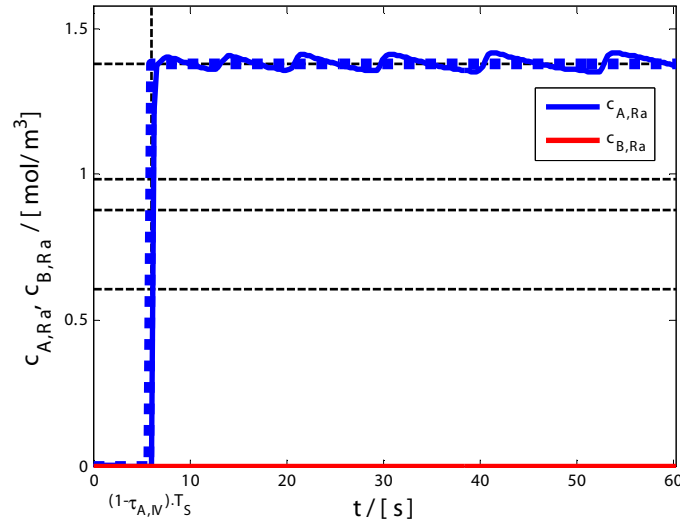
Figure 3.17: Estimated and simulated time trajectories of concentrations at the raffinate drain within one switching interval to Fig. 3.19 on page 71.

Thus, the mean concentration at the raffinate drain can be represented with the aid of the normalized residence time and the plateau value by Eq. (3.92):

$$\bar{c}_{A,Ra} = \frac{1}{T_S} \int\limits_0^{T_S} c_{A,Ra}(t)\, dt = \tau_{A,IV}\, c_{A,4}.$$

(3.92)

The concentration course at the extract depends on the shape of the expansion wave (see Fig. 3.18). This course is exactly determined from the PDEs, Eq. (3.1) and (3.2) on page 40, by the self-similarity solution, Eq. (2.95) on page 24. The transition between the two states is expressed by the normalized residence times of the foot and head point.

$$c_{B,Ex}(t) = \begin{cases} c_{B,2} & 0 \leqslant t \leqslant \tau\, T_S \\[2mm] \frac{1}{K_B} \left[\sqrt{\frac{(1+K_B\, c_{B,2})^2\, (\tau_{B,I}-\tau)\, T_S}{(2+K_B\, c_{B,2})\, K_B\, c_{B,2}\, (t-\tau\, T_S)+(\tau_{B,I}-\tau)\, T_S}} - 1 \right] & \tau\, T_S < t < \tau_{B,I}\, T_S \\[2mm] 0 & \tau_{B,I}\, T_S \leqslant t \leqslant T_S \end{cases}$$
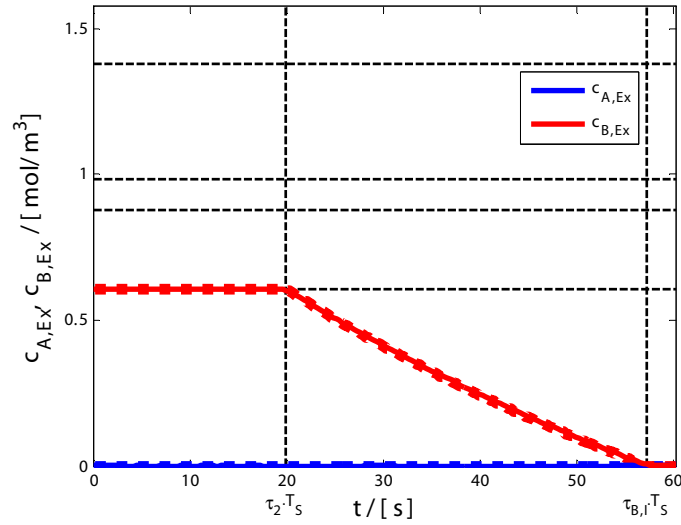
(3.93)

Figure 3.18: Estimated and simulated time trajectories of concentrations at the extract drain within one switching interval to Fig. 3.19 on page 71.

Now the mean concentration is computed by the time integral:

$$\bar{c}_{B,Ex} = \frac{1}{T_S} \int_0^{T_S} c_{B,Ex}(t) \, dt = \tau \, c_{B,2} + (\tau_{B,I} - \tau) \, \frac{c_{B,2}}{2 + K_B \, c_{B,2}}. \tag{3.94}$$

For the determination of the normalized residence time of the head point, τ, the concentration velocity, Eq. (3.73) on page 64, of this point can be used. It is assumed that the head point runs between zone I and II. The validity of this assumption can be checked afterwards.

$$\frac{A}{(1+F)} \frac{L}{T_S} = \frac{1}{1 + \frac{F H_B}{(1+K_B c_{B,2})^2}} \left[\tau \dot{V}_I + (1-\tau) \left(\dot{V}_I - \dot{V}_{Ex} \right) \right] \tag{3.95}$$

Solving Eq. (3.95) for τ leads to Eq. (3.96).

$$\tau = \left(1 + \frac{F H_B}{(1 + K_B c_{B,2})^2} \right) \frac{A L}{(1+F) \dot{V}_{Ex} T_S} - \frac{\dot{V}_I - \dot{V}_{Ex}}{\dot{V}_{Ex}} \tag{3.96}$$

Finally, there are four velocity equations, Eq. (3.79) to Eq. (3.82) on page 66, and two component mass balances, Eq. (3.89) and Eq. (3.90) on page 67, to determine the four control variables, $\dot{V}_I$, $\dot{V}_{Ex}$, $\dot{V}_{Ra}$ and T_S, and the two outer plateau values,

$c_{B,2}$ and $c_{A,4}$.

3.4.7 Explicit Equations for Langmuir Isotherms

Given a specific feed composition, $c_{A,Fe}$ and $c_{B,Fe}$ and feed flow rate, $\dot{V}_{Fe}$, Eqs. (3.79)-(3.82), Eq. (3.89) and Eq. (3.90) can be solved for the unknown volumetric flow rates, $\dot{V}_I$, $\dot{V}_{Ex}$, and $\dot{V}_{Ra}$, and switching time, T_S, where some arbitrary normalized residence times, $0 \ll \tau_{B,I} \leqslant 1$ and $0 \ll \tau_{A,IV} \leqslant 1$, can be chosen to increase robustness. Thus, for $H_B > H_A$, $K_A > 0$, and $K_B > 0$, the following result, Eqs. (3.97)-(3.103), is obtained for complete separation and complete regeneration.

$$\alpha = H_B \left(1 + K_A\, c_{A,Fe}\right) - H_A \left(1 + K_B\, c_{B,Fe}\right)$$

$$C_1 = \frac{\alpha + \sqrt{\alpha^2 + 4\, H_A\, H_B\, K_A\, K_B\, c_{A,Fe}\, c_{B,Fe}}}{2\, H_B\, K_A\, c_{B,Fe}} \tag{3.97}$$

$$c_{B,2} = \frac{H_B - H_A}{H_B\, K_A\, C_1 + H_A\, K_B} \tag{3.98}$$

$$c_{A,4} = \frac{H_B - H_A}{H_B - H_A\, \left[1 - K_A\, c_{A,Fe} + K_B\, c_{B,2}\right]}\, c_{A,Fe} \tag{3.99}$$

$$\dot{V}_I = \frac{1}{\tau_{B,I}}\, \frac{\left(\tau_{B,I} + F\, H_B\right)\left(1 + K_B\, c_{B,2}\right) - F\, H_A\, \left(1 - \tau_{B,I}\right)}{F\, \left[H_B - H_A\, \left(1 + K_A\, c_{A,4}\right)\right]}\, \left(1 + K_A\, c_{A,4}\right)\, \dot{V}_{Fe} \tag{3.100}$$

$$\dot{V}_{Ex} = \frac{1}{\tau_{B,I}}\, \frac{H_B\, \left(1 + K_B\, c_{B,2}\right) - H_A}{H_B - H_A\, \left(1 + K_A\, c_{A,4}\right)}\, \left(1 + K_A\, c_{A,4}\right)\, \dot{V}_{Fe} \tag{3.101}$$

$$\dot{V}_{Ra} = \frac{1}{\tau_{A,IV}}\, \frac{H_B - H_A\, \left(1 + K_B\, c_{B,2}\right)}{H_B - H_A\, \left(1 + K_A\, c_{A,4}\right)}\, \dot{V}_{Fe} \tag{3.102}$$

$$T_S = \frac{F}{1 + F}\, \frac{A\, L}{\dot{V}_{Fe}}\, \frac{H_B - H_A\, \left(1 + K_A\, c_{A,4}\right)}{\left(1 + K_B\, c_{B,2}\right)\left(1 + K_A\, c_{A,4}\right)} \tag{3.103}$$

The time trajectories of the concentrations at the raffinate and extract can be constructed with Eqs. (3.91) and (3.93) for the cyclic steady state. Notice that

Eq. (3.103), for the switching time, may also be solved for the feed flow rate, if the time interval is fixed in advance. If one likes to restrict the pressure drop in zone I, it is also possible to pre-select the volumetric flow rate of zone I and solve Eq. (3.100) for the feed flow rate instead. In a similar way, the solution for Anti-Langmuir isotherms may also be derived as indicated in [53] and stated in the appendix.

3.4.8 Simulation Results for Complete Separation

Using the operating points from Tab. 3.3 and the parameters from the appendix, table A-2, the profile plot of Fig. 3.19 is obtained for an eight-column SMB assuming zero dispersion. The normalized residence times are chosen as $\tau_{B,I} = 0.95$ and $\tau_{A,IV} = 0.90$. The plateau values, $c_{B,2}$ and $c_{A,4}$, are very well predicted as
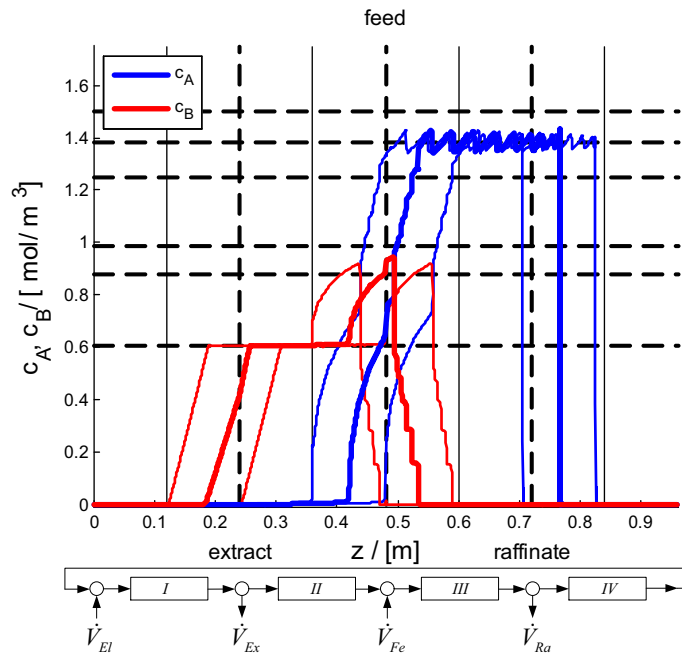

Figure 3.19: Concentration profiles for SMB plant with $\tau_{B,I} = 0.95$, $\tau_{A,IV} = 0.90$, cfg $= [2, 2, 2, 2]$ and model parameters taken from table A-2.

indicated in Fig. 3.19. More interesting are the time trajectories at the drains for one switching interval at cyclic steady state; see Figs. 3.17 and 3.18. The rarefaction at the extract is well described by the self-similarity solution, Eq. (3.92) and Eq. (3.93) on page 68, as shown in Fig. 3.18 on page 69. The dotted lines are the predicted concentrations, which are equal to the solid lines obtained by dynamic

simulation. In Fig. 3.17 on page 68, the typical saw tooth effect due to zero dispersion is observed around the plateau value, $c_{A,4}$. This was not considered in the mass balance, but the discrepancies between the predicted, Eq. (3.91) on page 67, and the simulated trajectory is small.

In a simple way, the design formulas may also be used to study the influence of the outer normalized residence times on the eluent consumption using a contour plot, as given in Fig. 3.20. It immediately shows that the ratio of eluent to feed flow rate increases from 3.6 to 5 as the normalized residence times decreases. Therefore, robustness leads to higher eluent consumption.
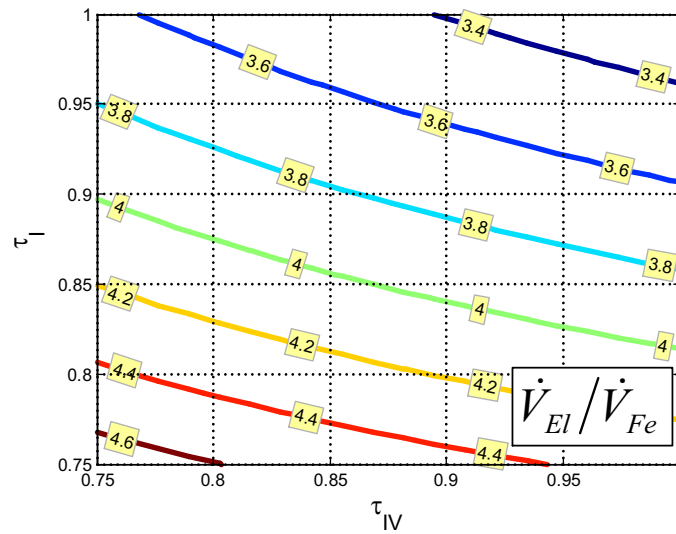

Figure 3.20: On the influence of normalized residence times on the ratio of eluent to feed flow rate, $\dot{V}_{El}/\dot{V}_{Fe}$, for complete separation with model parameters taken from table A-2.

Additionally, the question may be answered, which values should be chosen for the feeding concentrations in order to allow a low solvent consumption. To this, an often-used definition of the solvent consumption, Eq. (3.104) from [13], may be used together with the derived design equations to produce the contour plot of Fig. 3.21.

$$sc = \frac{\dot{V}_{El} + \dot{V}_{Fe}}{\dot{V}_{Fe}\left(c_{A,Fe} + c_{B,Fe}\right)} \tag{3.104}$$

From the picture, it is immediately clear that the feeding concentrations should be chosen as highly as possible. However, there may be some technical restric-
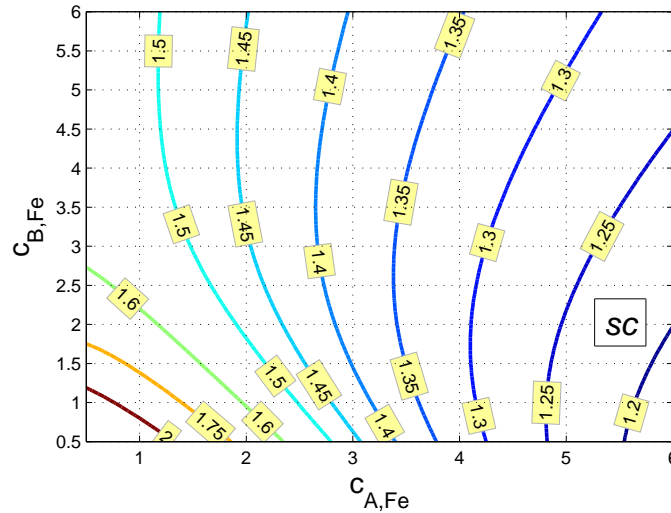
Figure 3.21: On the influence of feeding concentrations on the eluent consumption for complete separation with $\tau_{B,I} = 0.95$, $\tau_{A,IV} = 0.90$ and model parameters taken from table A-2.

tions. In addition, there are asymmetrical contours recognizable, which suggest to choose the feeding concentration of component A higher than those of component B at high concentrations.

In the same way the influences of different design parameters on specific performance measures can be studied quickly with the help of the design equations.

3.4.9 Extension to Reduced Purities

The previous results have shown that the positions of the outer concentration fronts can be adjusted very well by the normalized residence times. If incomplete separation is requested, the inner concentration fronts are allowed to move in the outer zones. Again, they can be adjusted by introducing normalized residence times. Using this approach, the main velocity equations, Eq. (3.80) and Eq. (3.81) on page 66, changes to Eq. (3.105) and Eq. (3.106).

$$\frac{A}{1+F}\frac{L}{T_S} = \frac{1}{1 + \frac{F H_A}{1 + K_B c_{B,2}}} \left[(1 - \tau_{A,II})\, \dot{V}_I + \tau_{A,II}\, \left(\dot{V}_I - \dot{V}_{Ex} \right) \right] \qquad (3.105)$$

$$\frac{A}{1+F}\frac{L}{T_S} = \frac{1}{1+\frac{F\,H_B}{1+K_A\,c_{A,3}+K_B\,c_{B,3}}} \left[\begin{array}{l} \tau_{B,III}\left(\dot{V}_I - \dot{V}_{Ex} + \dot{V}_{Fe}\right) \\ + \left(1 - \tau_{B,III}\right)\left(\dot{V}_I - \dot{V}_{Ex} + \dot{V}_{Fe} - \dot{V}_{Ra}\right) \end{array} \right]$$
(3.106)

The inner plateau values are entirely determined by the outer plateau values using Eq. (3.87) and Eq. (3.88) on page 67. The outer plateau values, $c_{B,2}$ and $c_{A,4}$, must be determined from the overall component balances which, for reduced purities, are given by Eq. (3.107) and Eq. (3.108).

$$0 = c_{A,Fe}\,\dot{V}_{Fe} - \bar{c}_{A,Ex}\,\dot{V}_{Ex} - \bar{c}_{A,Ra}\,\dot{V}_{Ra}$$
(3.107)

$$0 = c_{B,Fe}\,\dot{V}_{Fe} - \bar{c}_{B,Ex}\,\dot{V}_{Ex} - \bar{c}_{B,Ra}\,\dot{V}_{Ra}$$
(3.108)

One needs to express the mean values at the drains in terms of the plateau values and the normalized residence times. The inner normalized residence times should be expressed in terms of the drain purities, which are defined by Eq. (3.109) and Eq. (3.110).

$$P_{Ex} = \frac{\bar{c}_{B,Ex}}{\bar{c}_{A,Ex} + \bar{c}_{B,Ex}}$$
(3.109)

$$P_{Ra} = \frac{\bar{c}_{A,Ra}}{\bar{c}_{A,Ra} + \bar{c}_{B,Ra}}$$
(3.110)

Mean Concentrations at Raffinate

According to Fig. 3.22, the ideal time trajectories of the concentrations at the raffinate drain are expressed mathematically for one switching interval by Eq. (3.111) and Eq. (3.112).

$$c_{A,Ra}\left(t\right) = \begin{cases} 0 & 0 \leq t < \left(1 - \tau_{A,IV}\right)T_S \\ c_{A,4} & \left(1 - \tau_{A,IV}\right)T_S \leq t \leq \tau_{A,B,III}\,T_S \\ c_{A,3} & \tau_{A,B,III}\,T_S < t \leq T_S \end{cases}$$
(3.111)

$$c_{B,Ra}\left(t\right) = \begin{cases} 0 & 0 \leq t < \tau_{A,B,III}\,T_S \\ c_{B,3} & \tau_{A,B,III}\,T_S \leq t \leq T_S \end{cases}$$
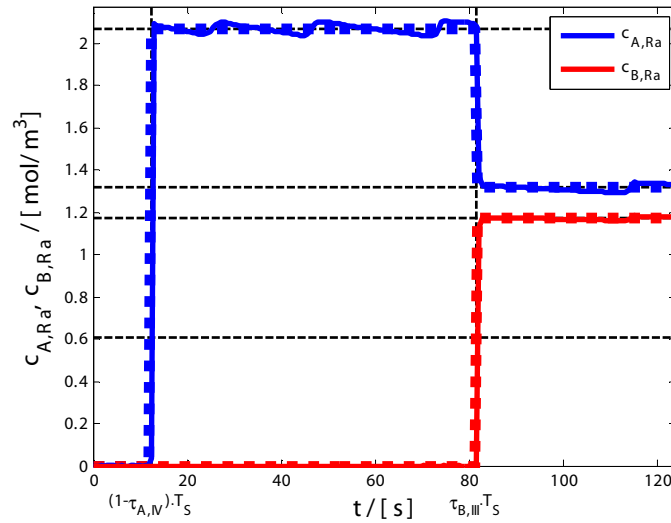(3.112)

Figure 3.22: Estimated and simulated time trajectories of concentrations at the raffinate drain within one switching interval to Fig. 3.25 on page 81.

The mean concentrations for one switching interval are computed using the time integral, Eqs. (3.113) and (3.114).

$$
\begin{aligned}
\bar{c}_{A,Ra} &= \frac{1}{T_S} \int_0^{T_S} c_{A,Ra}(t)\, dt \\
&= c_{A,4} \left(\tau_{A,B,III} - (1 - \tau_{A,IV}) \right) + c_{A,3} \left(1 - \tau_{A,B,III} \right)
\end{aligned}
\tag{3.113}
$$

$$
\begin{aligned}
\bar{c}_{B,Ra} &= \frac{1}{T_S} \int_0^{T_S} c_{B,Ra}(t)\, dt \\
&= c_{B,3} \left(1 - \tau_{A,B,III} \right)
\end{aligned}
\tag{3.114}
$$

Now, the definition of the raffinate purity, Eq. (3.110), is used to express the inner normalized residence time, $\tau_{A,B,III}$, by the raffinate purity, P_{Ra}.

$$
\tau_{A,B,III} = 1 - \frac{1 - P_{Ra}}{P_{Ra}} \frac{c_{A,4}}{c_{B,3} + \frac{1-P_{Ra}}{P_{Ra}} \left(c_{A,4} - c_{A,3} \right)} \tau_{A,IV}
\tag{3.115}
$$

Mean Concentrations at Extract for High Extract Purity

In Fig. 3.23, the time trajectories of the concentrations at the extract drain for one switching time is given. To express this course mathematically, the concentrations, $c_{A,0}$ and $c_{B,0}$, at $t = 0$ must be determined. These concentration values
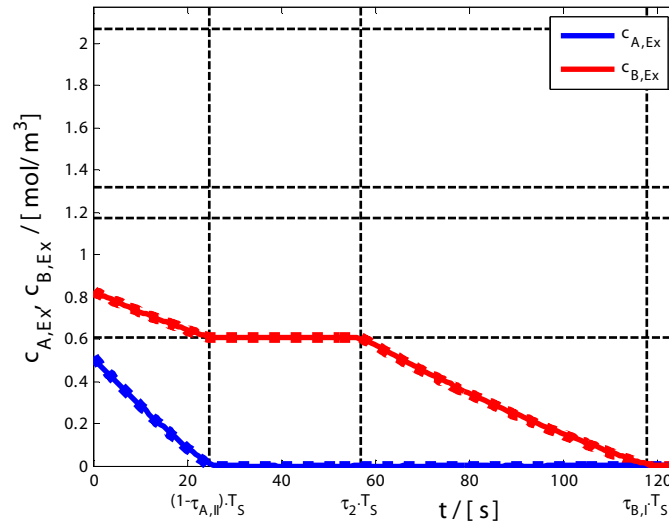
Figure 3.23: Estimated and simulated time trajectories of concentrations at the extract drain within one switching interval to Fig. 3.25 on page 81.

are determined with aid of the concentration velocity, since both corner concentrations cover exactly one column length in zone II during a switching interval.

$$\frac{A}{(1+F)}\,\frac{L}{T_S} = \frac{1}{1 + F\,\frac{dq_A}{dc_A}\Big|_{\substack{c_{A,0}\\c_{B,0}}}}\,\left(\dot{V}_I - \dot{V}_{Ex}\right) \tag{3.116}$$

Using the simple wave condition, these values are determined by Eq. (3.117) and (3.118).

$$c_{A,0} = \frac{H_B - H_A\,(1 + K_B\,c_{B,2})}{K_A\,(H_B - H_A)}\left(\sqrt{\frac{F\,H_A}{1 + K_B\,c_{B,2}}\,\frac{1}{\frac{(1+F)\,\left(\dot{V}_I - \dot{V}_{Ex}\right)\,T_S}{A\,L} - 1}} - 1\right) \tag{3.117}$$

$$c_{B,0} = \frac{K_A\,H_B\,c_{B,2}}{H_B - H_A\,(1 + K_B\,c_{B,2})}\,c_{A,0} + c_{B,2} \tag{3.118}$$

Now, the self-similarity solution is used to express both trajectories. To do this, modified Langmuir constants are defined, Eq. (3.119) and Eq. (3.120):

$$\tilde{K}_A = \frac{H_B - H_A}{H_B - H_A\,(1 + K_B\,c_{B,2})}\,K_A, \tag{3.119}$$

$$\tilde{K}_B = \frac{H_B - H_A}{H_B} \frac{1}{c_{B,2}}.$$

(3.120)

This leads to the mathematical description of the concentrations at the extract drain by Eqs. (3.121) and (3.122).

$$c_{A,Ex}(t) = \begin{cases} \frac{1}{\tilde{K}_A} \left[\sqrt{\frac{\left(1+\tilde{K}_A c_{A,0}\right)^2 \left(1-\tau_{A,II}\right) T_S}{\left(2+\tilde{K}_A c_{A,0}\right) \tilde{K}_A c_{A,0} t + \left(1-\tau_{A,II}\right) T_S}} - 1 \right] & 0 \leq t \leq \left(1-\tau_{A,II}\right) T_S \\ 0 & \left(1-\tau_{A,II}\right) T_S < t \leq T_S \end{cases}$$

(3.121)

$$c_{B,Ex}(t) = \begin{cases} c_{B,2} + \frac{1}{\tilde{K}_B} \left[\sqrt{\frac{\left(1+\tilde{K}_B\left(c_{B,0}-c_{B,2}\right)\right)^2 \left(1-\tau_{A,II}\right) T_S}{\left(2+\tilde{K}_B\left(c_{B,0}-c_{B,2}\right)\right) \tilde{K}_B\left(c_{B,0}-c_{B,2}\right) t + \left(1-\tau_{A,II}\right) T_S}} - 1 \right] & 0 \leq t \leq \left(1-\tau_{A,II}\right) T_S \\ c_{B,2} & \left(1-\tau_{A,II}\right) T_S < t \leq \tau T_S \\ \frac{1}{K_B} \left[\sqrt{\frac{\left(1+K_B c_{B,2}\right)^2 \left(\tau_{B,I}-\tau\right) T_S}{\left(2+K_B c_{B,2}\right) K_B c_{B,2} \left(t-\tau T_S\right) + \left(\tau_{B,I}-\tau\right) T_S}} - 1 \right] & \tau T_S < t \leq \tau_{B,I} T_S \\ 0 & \tau_{B,I} T_S < t \leq T_S \end{cases}$$

(3.122)

Again, the mean values are computed using the time integrals, Eq. (3.123) and Eq. (3.124).

$$\begin{aligned} \bar{c}_{A,Ex} &= \frac{1}{T_S} \int_0^{T_S} c_{A,Ex}(t)\, dt \\ &= \left(1-\tau_{A,II}\right) \frac{c_{A,0}}{2+\tilde{K}_A c_{A,0}} \end{aligned}$$

(3.123)

$$\begin{aligned} \bar{c}_{B,Ex} &= \frac{1}{T_S} \int_0^{T_S} c_{B,Ex}(t)\, dt \\ &= \left(1-\tau_{A,II}\right) \frac{c_{B,0}-c_{B,2}}{2+\tilde{K}_B\left(c_{B,0}-c_{B,2}\right)} + \tau c_{B,2} + \left(\tau_{B,I}-\tau\right) \frac{c_{B,2}}{2+K_B c_{B,2}} \end{aligned}$$

(3.124)

Finally, the definition of the extract purity, Eq. (3.109) on page 74, is used to express the inner normalized residence time, $\tau_{A,II}$, by the extract purity, P_{Ex}.

$$\tau_{A,II} = 1 - \frac{1-P_{Ex}}{P_{Ex}} \frac{\tau_{B,I} + \left(1+K_B c_{B,2}\right) \tau}{\frac{c_{A,0}}{2+\tilde{K}_A c_{A,0}} - \frac{1-P_{Ex}}{P_{Ex}} \frac{c_{B,0}-c_{B,2}}{2+\tilde{K}_B\left(c_{B,0}-c_{B,2}\right)}} \frac{c_{B,2}}{2+K_B c_{B,2}}$$

(3.125)

Mean Concentrations at Extract for Low Extract Purity

As shown in Fig. 3.24, the inner plateau values, $c_{A,3}$ and $c_{B,3}$, will now appear at the extract drain for low extract purities. Thus, the solution structure changes and must be treated separately. To express the concentration trajectories at the extract for low purities, it is necessary to find the time point, $\tau_3 T_S$, until these plateau values are detected at the extract. The corner concentrations run be-
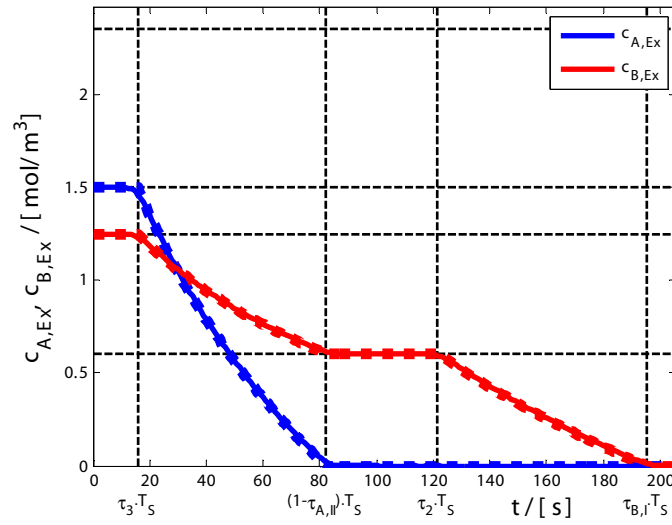
Figure 3.24: Estimated and simulated time trajectories of concentrations at the extract drain within one switching interval to Fig. 3.26 on page 81.

tween zone I and zone II. Therefore, a new normalized residence time, τ_3, is introduced to locate these corner concentrations. Using the concentration velocity and the simple wave condition, the normalized residence time is determined by Eq. (3.127).

$$\frac{L}{T_S} = \frac{1+F}{A} \left(\tau_3 \dot{V}_I + (1-\tau_3)\left(\dot{V}_I - \dot{V}_{Ex}\right) \right) \frac{1}{1 + F \frac{dq_A}{dc_A}\Big|_{c_{B,3}}^{c_{A,3}}} \tag{3.126}$$

$$\tau_3 = \left(1 + \frac{F\,H_A}{\left(1+K_B\,c_{B,2}\right)\left(1+K_A\,c_{A,4}\right)^2} \right) \frac{A\,L}{(1+F)\,\dot{V}_{Ex}\,T_S} - \frac{\dot{V}_I - \dot{V}_{Ex}}{\dot{V}_{Ex}} \tag{3.127}$$

Now, the self-similarity solution of the rarefaction at the extract is used to express both time trajectories of the concentrations at the extract, Eq. (3.128) and Eq. (3.129), respectively.

$$c_{A,Ex}(t) = \begin{cases} c_{A,3} & 0 \le t < \tau_3\,T_S \\[2mm] \frac{1}{\tilde{K}_A}\left[\sqrt{\dfrac{\left(1+\tilde{K}_A\,c_{A,3}\right)^2\left(1-\tau_{A,II}-\tau_3\right)T_S}{\left(2+\tilde{K}_A\,c_{A,3}\right)\tilde{K}_A\,c_{A,3}\,(t-\tau_3\,T_S)+\left(1-\tau_{A,II}-\tau_3\right)T_S}} - 1 \right] & \tau_3\,T_S \le t < \left(1-\tau_{A,II}\right)T_S \\[3mm] 0 & \left(1-\tau_{A,II}\right)T_S \le t < T_S \end{cases} \tag{3.128}$$

$$c_{B,Ex}(t) = \begin{cases} c_{B,3} & 0 \le t < \tau_3 \, T_S \\[2ex] c_{B,2} + \frac{1}{\tilde{K}_B} \left[\sqrt{\frac{\left(1+\tilde{K}_B\left(c_{B,3}-c_{B,2}\right)\right)^2 \left(1-\tau_{A,II}-\tau_3\right) T_S}{\left(2+\tilde{K}_B\left(c_{B,3}-c_{B,2}\right)\right)\tilde{K}_B\left(c_{B,3}-c_{B,2}\right)\left(t-\tau_3\,T_S\right)+\left(1-\tau_{A,II}-\tau_3\right) T_S}} - 1 \right] & \tau_3\,T_S \le t < \left(1-\tau_{A,II}\right) T_S \\[2ex] c_{B,2} & \left(1-\tau_{A,II}\right) T_S \le t < \tau\,T_S \\[2ex] \frac{1}{K_B} \left[\sqrt{\frac{\left(1+K_B\,c_{B,2}\right)^2 \left(\tau_{B,I}-\tau\right) T_S}{\left(2+K_B\,c_{B,2}\right)K_B\,c_{B,2}\left(t-\tau\,T_S\right)+\left(\tau_{B,I}-\tau\right) T_S}} - 1 \right] & \tau\,T_S \le t < \tau_{B,I}\,T_S \\[2ex] 0 & \tau_{B,I}\,T_S \le t \le T_S \end{cases}$$

$$(3.129)$$

The mean concentrations at the extract for low purities are determined by Eq. (3.130) and Eq. (3.131).

$$\begin{aligned} \bar{c}_{A,Ex} &= \frac{1}{T_S} \int_0^{T_S} c_{A,Ex}(t)\, dt \\ &= \tau_3\, c_{A,3} + \left(1 - \tau_{A,II} - \tau_3\right) \frac{c_{A,3}}{2+\tilde{K}_A\, c_{A,3}} \end{aligned} \qquad (3.130)$$

$$\begin{aligned} \bar{c}_{B,Ex} &= \frac{1}{T_S} \int_0^{T_S} c_{B,Ex}(t)\, dt \\ &= \tau_3\, c_{B,3} + \left(1 - \tau_{A,II} - \tau_3\right) \frac{c_{B,3}-c_{B,2}}{2+\tilde{K}_B\,\left(c_{B,3}-c_{B,2}\right)} \\ &\quad + \left(\tau - \tau_3\right) c_{B,2} + \left(\tau_{B,I} - \tau\right) \frac{c_{B,2}}{2+K_B\, c_{B,2}} \end{aligned} \qquad (3.131)$$

Using the definition of the extract purity, the inner normalized residence time is determined by Eq. (3.132).

$$\tau_{A,II} = 1 - \tau_3 - \frac{\frac{1-P_{Ex}}{P_{Ex}}\left(\tau_3\, c_{B,3} + \left(\tau - \tau_3\right) c_{B,2} + \left(\tau_{B,I} - \tau\right)\frac{c_{B,2}}{2+K_B\, c_{B,2}}\right) - \tau_3\, c_{A,3}}{\frac{c_{A,3}}{2+\tilde{K}_A\, c_{A,3}} - \frac{1-P_{Ex}}{P_{Ex}}\frac{c_{B,3}-c_{B,2}}{2+\tilde{K}_B\,\left(c_{B,3}-c_{B,2}\right)}} \qquad (3.132)$$

The System of Equations for Reduced Purities

Now, all required equations are found to compute the flow rates and switching time for the desired purities. The Eqs. (3.79), (3.105), (3.106), (3.82), (3.107), and (3.108) are the main equations that have to be solved for the desired flow rates, $\dot{V}_I$, $\dot{V}_{Ex}$, $\dot{V}_{Ra}$, the switching time, T_S, and the plateau values, $c_{B,2}$ and $c_{A,4}$. This system of equations can be solved numerically using the explicit formula for complete separation as a starting guess.

At every iteration step, the inner plateau values are computed by Eqs. (3.87) and (3.88). The mean concentrations at the raffinate are determined by Eqs. (3.115),

(3.113), (3.114). To compute the mean concentrations at the extract, Eqs. (3.96), (3.119) and (3.120) are solved first. After this, the residence time, τ_3, is computed by Eq. (3.127) to discriminate between the two solution structures at the extract. If $\tau_3 \leq 0$, the equations for high purity at the extract are used. This means Eqs. (3.117), (3.118), (3.125), (3.123), and (3.124) are evaluated. If $\tau_3 > 0$, the equations for low purity at the extract are used, which means that Eqs. (3.132), (3.130), and (3.131) are evaluated. Finally, the equation errors of the four velocities, Eqs. (3.79), (3.105), (3.106), and (3.82), and the equation errors of the two component balances, Eqs. (3.107) and (3.108), are determined.

After the numerical solution is found, the normalized residence times and the plateau values can be computed afterwards to construct the time trajectories of the concentrations at the drains for one switching time.

3.4.10 Simulation Results for Reduced Purities

To show the practical usefulness of this method, a simulation result is introduced here. It is assumed that the feed flow rate and the feed concentrations are given. The goal is to design a SMB plant that will separate a given feed stream. This task is natural since one like to achieve a desired throughput. One can now use the proposed approach to determine the corresponding flow rates and switching time. If there are some constraints on the flow rates due to pressure drops, one just needs to reduce the requested feed flow rate. The simulation is carried out with $\tau_{B,I} = 0.95$, $\tau_{A,IV} = 0.90$, $P_{Ex} = 90\%$ and $P_{Ra} = 80\%$. The concentration profiles are given by Fig. 3.25. The time trajectories at the drains are well predicted as given in Fig. 3.23 on page 76 and Fig. 3.22 on page 75. The dotted lines are the predicted concentrations, whereas the solid lines obtained by simulation. A second simulation is carried out with reduced extract purity, $P_{Ex} = 65\%$. The concentration profiles are given by Fig. 3.26 and the associated trajectories at the extract are given in Fig. 3.24 on page 78. To show that the self-similarity solution will produce exact results, an additional simulation is carried out with feeding concentrations considerably increased. The concentration course at the extract drain is represented in Fig. 3.27. It shows that the proposed approach is able to predict the time trajectory sufficiently well. Finally, one can study with this approach the influence of the purities on the eluent consumption and switching time using contour plots given in Fig. 3.28 and Fig. 3.29. To prove the results by dynamic simulation, a high number of base points per column are necessary.
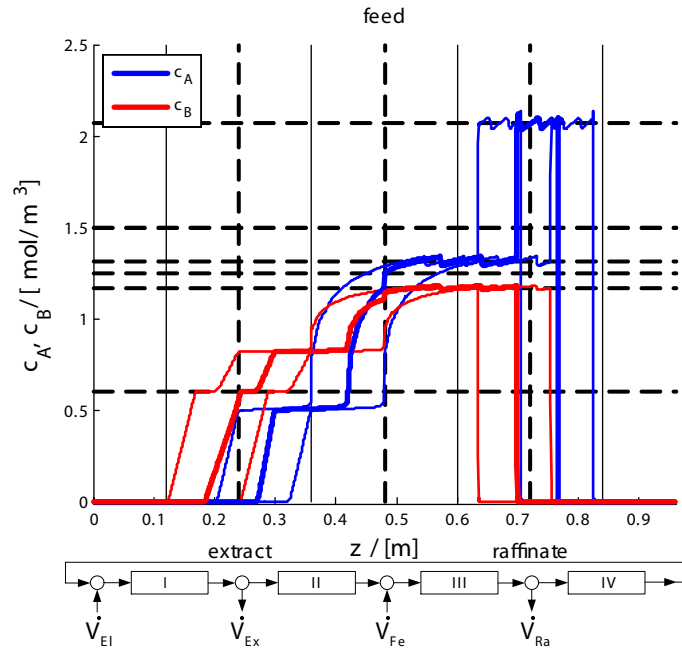
Figure 3.25: Concentration profiles for SMB plant with $\tau_{B,I} = 0.95$, $\tau_{A,IV} = 0.90$, $P_{Ex} = 0.90$, $P_{Ra} = 0.80$, cfg $= [2, 2, 2, 2]$ and model parameters taken from table A-2.
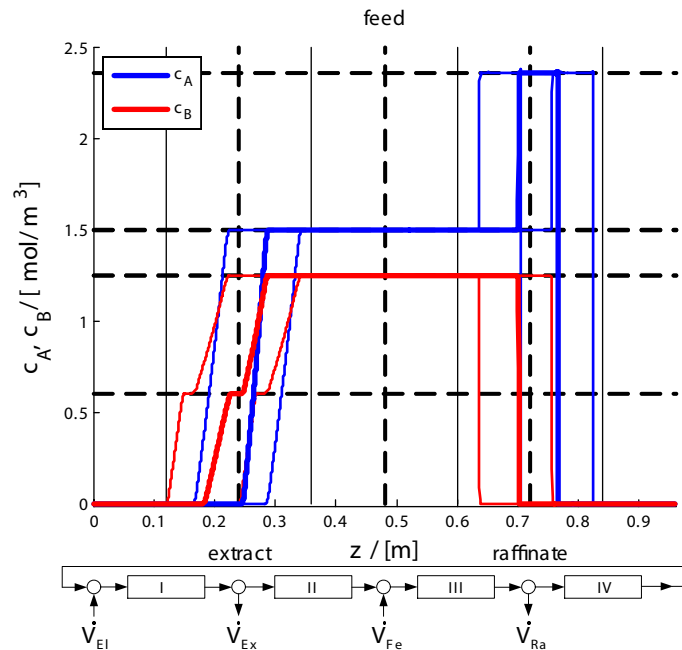

Figure 3.26: Concentration profiles for SMB plant with $\tau_{B,I} = 0.95$, $\tau_{A,IV} = 0.90$, $P_{Ex} = 0.65$, $P_{Ra} = 0.80$, cfg $= [2, 2, 2, 2]$ and model parameters taken from table A-2.
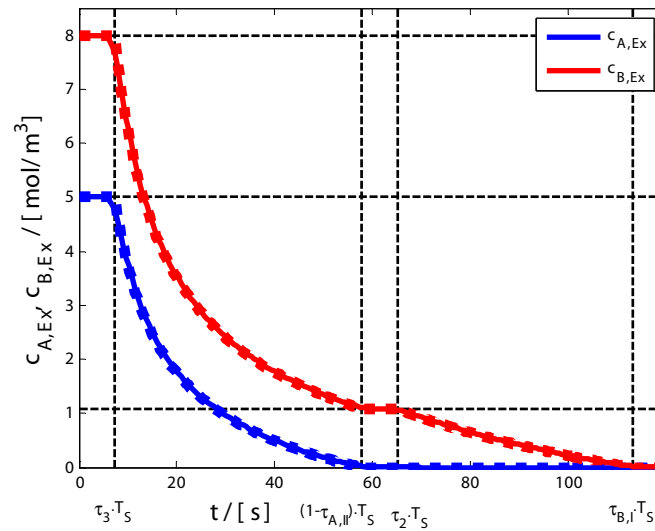
Figure 3.27: Estimated and simulated time trajectories of concentrations at the extract drain within one switching interval with $\tau_{B,I} = 0.95$, $\tau_{A,IV} = 0.90$, $P_{Ex} = 0.70$, $P_{Ra} = 0.80$, $c_{A,Fe} = 5.0$, $c_{B,Fe} = 8.0$, cfg $= [2, 2, 2, 2]$ and the remaining parameters taken from table A-2.
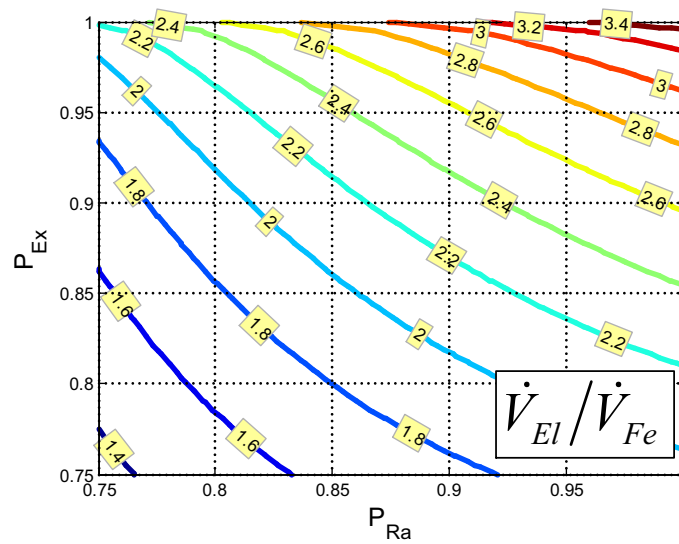

Figure 3.28: On the influence of purities on the ratio of eluent to feed flow rate, $\dot{V}_{El}/\dot{V}_{Fe}$, with $\tau_{B,I} = 0.95$ and $\tau_{A,IV} = 0.9$ and model parameters taken from table A-2.
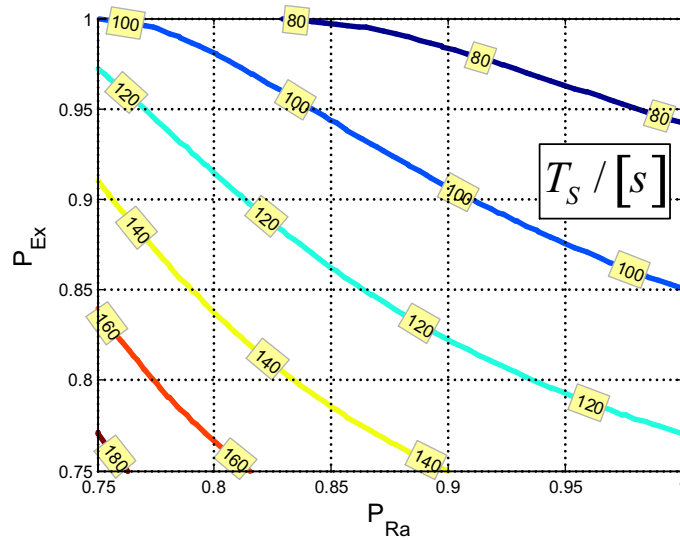
Figure 3.29: On the influence of purities on the switching time, T_S, with $\tau_{B,I} = 0.95$ and $\tau_{A,IV} = 0.9$ and model parameters taken from table A-2.

Further, the simulation time should be chosen as sufficiently large, so that the raffinate trajectory converges to the predicted trajectory. In this contribution, all simulations were carried out with a commercially available finite element package called COMSOL, [48], using third-order Lagrange polynomials and 192 elements per column. Streamline diffusion was used to stabilize the numerics. However, the same results are obtained if using a traditional method of lines algorithm, [54], with flux limiter.

Table 3.3: Operating points.

	$\dot{V}_I /\left[\frac{ml}{min}\right]$	$\dot{V}_{Ex} /\left[\frac{ml}{min}\right]$	$\dot{V}_{Ra} /\left[\frac{ml}{min}\right]$	$T_S / [s]$
Fig. 3.19	102.60	33.54	12.07	60.19
Fig. 3.25	50.10	20.63	8.73	123.80
Fig. 3.26	30.40	16.96	5.28	205.51
Fig. 3.27	50.03	39.49	1.77	118.97

3.4.11 Summary

A new explicit startup formula for SMB plants using Langmuir isotherms for complete separation was derived. The advantage is that the outer concentration

fronts can be very well adjusted by the normalized residence times introduced, $\tau_{B,I}$ and $\tau_{A,IV}$, that are essential for robustness. An extension of the proposed method to incomplete separation was made, which enables the designer to do a quick study of the necessary eluent consumption in terms of the required purities or other parameters. If implementing these equations, appropriate scaling should be made to find numerical reliable solutions.

3.5 Conclusion

In this chapter, a new method to analyze SMB plants was proposed. It leads to design equations for dispersion-free SMB models for the most practical isotherms. The formulas give the designers more insight into the process and, thus, they can use this information for further optimizations. With the aid of these formulas, the influences of the parameters on the operating conditions can be examined very well. The numeric solution methods to simulate SMB plants may also be judged. Although, the equations derived are only valid for zero dispersion. This is in practice an unrealistic assumption. To derive design equations that also consider dispersion, one can make use of the traveling wave solution. For Langmuir isotherms it was derived in chapter 2.2.4, Eq. (2.87) on page 23. The thickness of the shock layer may also indicate the zone length necessary. However, it is unlikely to find solutions with low computational effort. For this reason, one may use the operating point determined for a dispersion-free SMB model as a starting guess for a rigorous dynamic optimization. Such possibilities are pointed out in chapter 4. As shown in Fig. 3.30, dispersion will have a negative effect on the eluent consumption. Therefore, methods should be developed to avoid or counter act dispersion.

$$\dot{n}_B = \dot{V}_l \cdot c_B - D \cdot \varepsilon \cdot A \cdot \frac{\partial c_B}{\partial z} < \dot{V}_l \cdot c_B \quad \therefore \dot{V}_l \uparrow \qquad \dot{n}_A = \dot{V}_l \cdot c_A - D \cdot \varepsilon \cdot A \cdot \frac{\partial c_A}{\partial z} > \dot{V}_l \cdot c_A \quad \therefore \dot{V}_l \downarrow$$

The liquid flow rate must be increased to keep the assigned component flow.

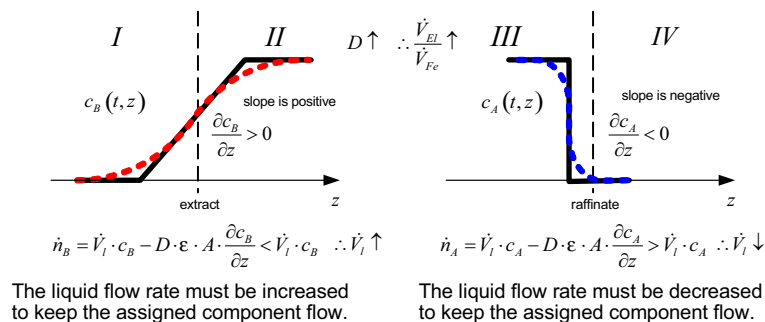The liquid flow rate must be decreased to keep the assigned component flow.

Figure 3.30: On the effect of dispersion.

Little people discuss other people.
Average people discuss events.
Big people discuss ideas.

~ Rudolf Emil Kálmán ~

4 Adaptive Control of SMB Plants

The SMB technology is an attractive separation process for binary mixtures and has its applications in the fine chemical and pharmaceutical industry. Nowadays, most plants operate in open loop far away from their optimum to increase robustness. Since this process is very sensitive to disturbances and parameter changes, it is natural to design an automatic controller which is capable of always driving the system near the optimum.

In this chapter, two control concepts for complete and incomplete separation and for complete regeneration are suggested. These are capable, to find a suitable operating point automatically and independently of the adsorption behavior. For this purpose, the specific properties of the process will be exploited in order to derive simple models of low order. Based on these models a classical control design will be carried out.

4.1 Control of SMB Plants for Complete Separation

This section proposes an adaptive control concept for SMB plants for complete separation and complete regeneration, [56]. First, a reduced model is derived to predict the location of the foot points of the concentration fronts. Then a simple control design is carried out using this model. At the end of this section, a simulation is used to underline the potential of this proposed control concept.

4.1.1 Simplified Modeling

A symmetric SMB configuration with eight columns is represented in Fig. 4.1. The zone velocities are adjusted by four pumps as indicated. In the middle of

each section, a UV- sensor is mounted to measure a concentration dependent signal. The associated concentration profiles of a SMB plant at cyclic steady state
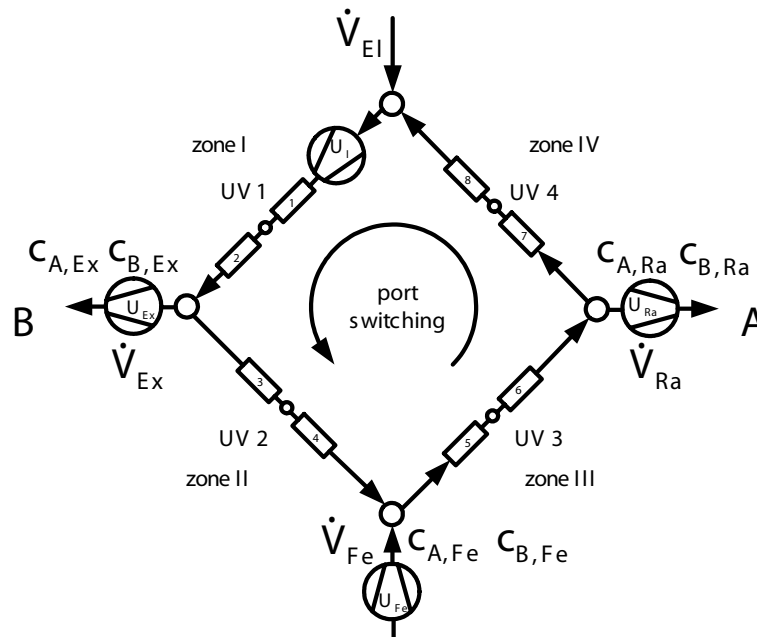

Figure 4.1: SMB configuration with eight chromatographic columns.

are indicated in Fig. 4.2. The thin lines are the profiles at the beginning and the end of a switching period, whereas the broader lines correspond to profiles at the middle of the switching time. In addition to the single concentrations, the sum of both concentrations is indicated by black lines. This is because UV- sensors often cannot detect the concentrations separately, but provide a weighted sum of both.

Derivation of the Concentration Front Model

Four concentration fronts of the concentration profiles can be identified. In Fig. 4.3, an idealized concentration front that travels between two connected columns, where a UV-detector is located in the middle, is represented. It is assumed that the velocity of the foot point of the concentration front is constant for one switching period. This opens a simple and advantageous discrete description of the movement of the foot point of the concentration front. The distance traveled by the foot point of the concentration front on the left side of the UV- sensor is calculated by using the velocity and time. The time is a fraction of the switch-
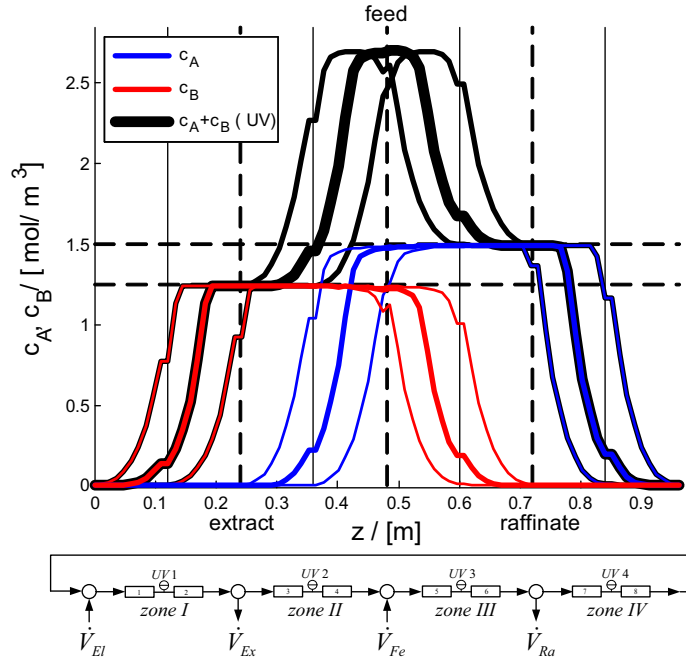
Figure 4.2: Concentration profiles at cyclic steady state for Henry isotherms and model parameters taken from table A-2.

ing time, which may be expressed by introducing a normalized residence time, τ. The dependency of distance traveled on the right side of the UV- sensor on normalized residence time is also expressed, Eq. (4.1) and Eq. (4.2):

$$\Delta z_L (k) = v (k) \ \tau (k) \ T_S (k), \quad \tau \in [0, 1], \tag{4.1}$$

$$\Delta z_R (k) = v (k) \ (1 - \tau (k)) \ T_S (k). \tag{4.2}$$

As indicated in Fig. 4.3, the left and right distances are related to Eq. (4.3):

$$\Delta z_L (k + 1) = L - \Delta z_R (k). \tag{4.3}$$

The distances are substituted by their velocities and times. The resulting equation is solved for the future normalized residence time, Eq. (4.4) and Eq. (4.5).

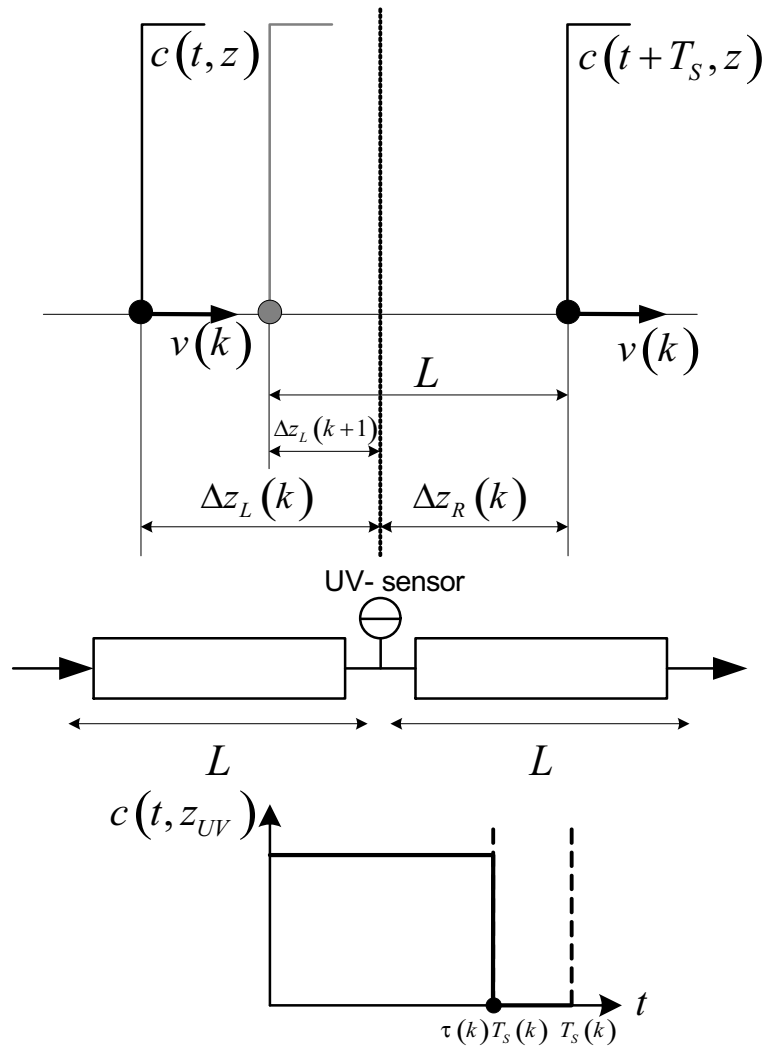$$v (k + 1) \ \tau (k + 1) \ T_S (k + 1) = L - v (k) \ (1 - \tau (k)) \ T_S (k) \tag{4.4}$$

Figure 4.3: On the derivation of the foot point movement.

$$\tau(k+1) = \frac{L - v(k)(1 - \tau(k)) T_S(k)}{v(k+1) T_S(k+1)} \tag{4.5}$$

It is now assumed that the velocity of the foot point of the concentration front is linearly dependent on the volumetric flow rate, which will be the case under idealized conditions.

$$v(k) = \frac{L}{\theta} \dot{V}(k) \tag{4.6}$$

This leads to following equation:

$$\tau(k+1) = \frac{\theta - \dot{V}(k)(1 - \tau(k)) T_S(k)}{\dot{V}(k+1) T_S(k+1)}. \tag{4.7}$$

Model Equations

The model is now stated using the traditional notation style of the control community. Before this is done, it should be noted that the normalized residence times can be measured only after a delay of one sample. Therefore, one must add an additional delay of one sample to the outputs. In order to avoid redundancy, the volumetric flow rates are concatenated with the switching time, Eq. (4.8) to Eq. (4.10).

$$u_i(k) = \dot{V}_i(k), \quad u_5(k) = T_S(k), \quad i = 1, 2, 3, 4 \tag{4.8}$$

$$\widehat{u}_i(k) = u_i(k) u_5(k), \quad y_i(k) = \tau_i(k-1) \tag{4.9}$$

$$y_i(k+1) = \frac{\theta_i - \widehat{u}_i(k-1)(1 - y_i(k))}{\widehat{u}_i(k)} \tag{4.10}$$

At cyclic steady state, the input, $\widehat{u}_i$, will be equal to the parameter, θ_i. This presents a simple way to compute the parameters from existing design rules, as given in the previous chapter, for complete separations directly from the parameters of the full model.

$$\theta_i = \widehat{u}_i = \dot{V}_i T_S \tag{4.11}$$

In case of Henry isotherms, the parameters are determined explicitly as follows, [47].

$$\theta_1 = \theta_3 = \frac{1 + F H_B}{1 + F} A L \tag{4.12}$$

$$\theta_2 = \theta_4 = \frac{1 + F H_A}{1 + F} A L \tag{4.13}$$

4.1.2 Control Design

Based on the reduced model an arbitrary controller design can be carried out. For the evaluation of the control concept, only a simple controller shall be introduced here. To improve the control performance, the order of the controller can be increased easily, e.g. [57], [61].

Proportional Feedback Design

The plant has integral behavior near the optimum, and therefore, is very sensitive to disturbances. Every small disturbance step leads to a running away of the concentration fronts from the optimal operating point. For this reason, a controller should be used to adjust the flow rates in order to keep the foot points of the concentration fronts at the desired locations. The following simple control law is suggested, which consists of an ideal open loop control and a proportional feedback.

$$\widehat{u}_i(k) = \theta_i - a\left(y_{i,ref} - y_i(k)\right)\theta_i, \quad i = 1, 2, 3, 4 \tag{4.14}$$

This control law is inserted to the model equation to obtain the closed loop dynamics, Eq. (4.15).

$$y_i(k) = \frac{1 - \left(1 - a\left(y_{i,ref} - y_i(k-2)\right)\right)\left[1 - y_i(k-1)\right]}{1 - a\left(y_{i,ref} - y_i(k-1)\right)} \tag{4.15}$$

If a stationary solution exists, one concludes that the output will approach the reference value.

$$\lim_{k \to \infty} y_i(k) = y_{i,\infty} = y_{i,ref} \tag{4.16}$$

A linearization around the stationary value is performed to analyze local stability. This leads to the following linear difference equation:

$$\Delta y_i(k) - \left(1 - a\, y_{i,ref}\right) \Delta y_i(k-1) + a\left(1 - y_{i,ref}\right) \Delta y_i(k-2) = 0, \qquad (4.17)$$

with $\Delta y_i(k) = y_i(k) - y_{i,ref}$. One can derive the following associated characteristic equation.

$$\lambda^2 - \left(1 - a\, y_{i,ref}\right)\lambda + a\left(1 - y_{i,ref}\right) = 0, \quad y_{i,ref} \in [0,1] \qquad (4.18)$$

The polynomial depends on the actual reference value. However, for $a = 0.25$ the two real roots are inside the unit disc, as seen in Fig. 4.4. Therefore, local stability is at least guaranteed for this value.

$$\lambda_{1,2} = \frac{\left(1 - a\, y_{i,ref}\right)}{2} \pm \frac{1}{2}\sqrt{\left(1 + a\, y_{i,ref}\right)^2 - 4\, a} \qquad (4.19)$$
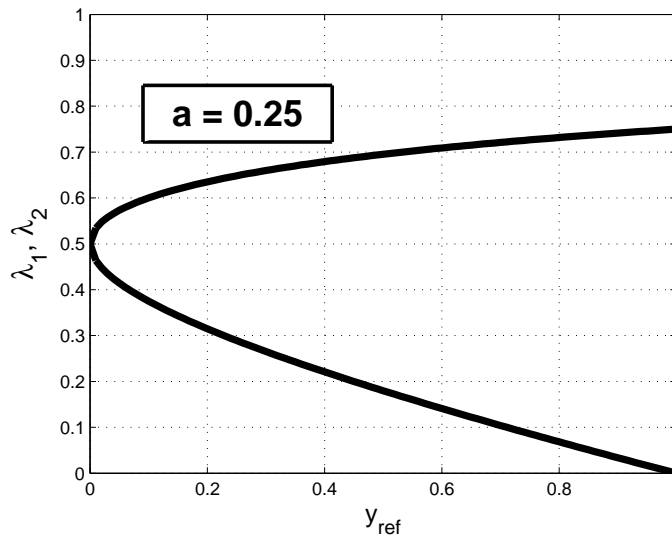

Figure 4.4: Dependency of the roots from the set point.

Computing the Optimal Switching Time

The SMB process is usually designed for a fixed throughput of the binary feed. To achieve this even in presence of disturbances, the feed flow rate cannot be

used as control input. However, the switching time can be used instead. The optimal switching time for a fixed feed flow rate is computed from the normalized control inputs by the following equation:

$$T_S(k) = \frac{\widehat{u}_3(k) - \widehat{u}_2(k)}{\dot{V}_{Fe}}.$$ (4.20)

The flow rates for each section can be computed with the aid of the optimal switching time, Eq. (4.21).

$$u_i(k) = \frac{\widehat{u}_i(k)}{T_S(k)}, \quad i = 1, 2, 3, 4$$ (4.21)

It should be noted that the scaling property of the switching time may also be used to satisfy upper constraints on the volumetric flow rates. With other words, the switching time is chosen such that following constraints are satisfied.

$$T_S \geq \frac{\widehat{u}_1}{\dot{V}_{I,\max}}, \quad T_S \geq \frac{\widehat{u}_1 - \widehat{u}_2}{\dot{V}_{Ex,\max}}, \quad T_S \geq \frac{\widehat{u}_3 - \widehat{u}_2}{\dot{V}_{Fe,\max}}, \quad T_S \geq \frac{\widehat{u}_3 - \widehat{u}_4}{\dot{V}_{Ra,\max}}$$ (4.22)

Computing Parameter Errors

It is likely that the parameters will change with time due to thermal processes, see Eq. (2.38) on page 13, or aging. Therefore, it is necessary to estimate the parameters online from measurements. The parameter errors are defined as the difference between the true parameters and their estimates.

$$\tilde{\theta}_i(k) = \theta_i - \hat{\theta}_i(k), \quad i = 1, 2, 3, 4$$ (4.23)

The difference between the measured and one-step ahead forecasted output is used to compute the previous parameter errors.

$$\tilde{\theta}_i(k-1) = u_i(k-1)(y_i(k) - \hat{y}_i(k))$$ (4.24)

Estimator Design

The following parameter estimator is suggested to determine the parameters, Eq. (4.25):

$$\hat{\theta}_i(k) = \hat{\theta}_i(k-1) + (1 - a_\theta)\tilde{\theta}_i(k-1), \quad |a_\theta| < 1, \quad i = 1, 2, 3, 4.$$ (4.25)

The resulting error equation reduces to a first-order homogenous difference equation.

$$\tilde{\theta}_i(k) = \tilde{\theta}_i(k-1) - (1 - a_\theta)\, \tilde{\theta}_i(k-1) = a_\theta\, \tilde{\theta}_i(k-1) \tag{4.26}$$

This means that the estimation error will vanish as $k \to \infty$.

Determination of the Normalized Residence Times

The normalized residence times of the foot points can be determined with the aid of a correlation technique. In order to achieve this, one may define the following intermediate signals.

$$x(t) = sign\,(c(t) - c_0), \tag{4.27}$$

$$x_{ref}(t) = \alpha\, sign\,(t - \tau_{ref}\, T_S), \tag{4.28}$$

$$\alpha = \begin{cases} -1 & \text{extract side} \\ +1 & \text{raffinate side} \end{cases} \tag{4.29}$$

The offset, c_0, defines the concentration value at which propagation will be investigated. For robustness, this value should lie above the expected sensor noise level. The sign of α takes into account the different qualitative course of the concentrations between the extract and raffinate side. The intermediate signal, x, can be interpreted as actual trajectory, whereas x_{ref} can be thought of as a reference signal. The cross-correlation of both signals will result in a maximum at the shift, $\Delta\tau_{\max}$, as shown in Fig. 4.5. This is a measure of the control error.

$$R_{x_{ref}x}(\Delta\tau) = \lim_{T \to \infty} \frac{1}{2\,T} \int_{-T}^{T} x_{ref}(t)\, x(t + \Delta\tau\, T_S)\, dt \tag{4.30}$$

$$\Delta\tau \in [-1, 1] \tag{4.31}$$

$$\max R_{x_{ref}x} = R_{x_{ref}x}(\Delta\tau_{\max}) \tag{4.32}$$

The maximum value of $\Delta\tau$ may then be determined by a simple one-dimensional search. The sum of the shift, $\Delta\tau_{\max}$, and reference, τ_{ref}, results in the actual value τ.
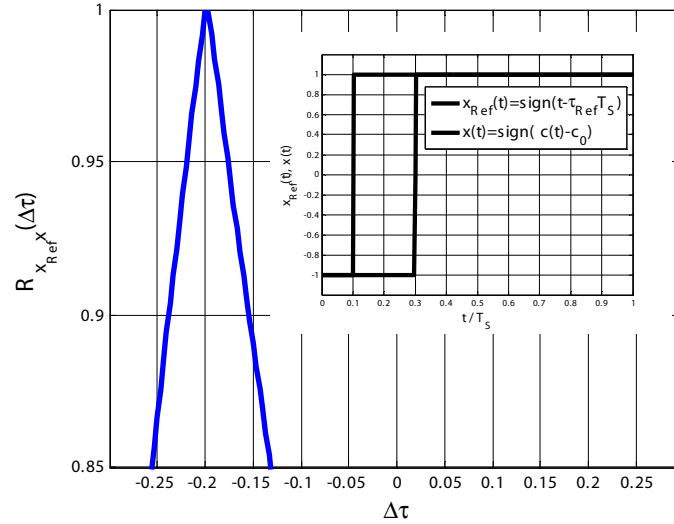

Figure 4.5: On cross correlation of two phase shifted sign signals.

A Note on Concentration Measurements

In practice, one cannot measure the concentration directly. A simple and cheap possibility to determine a concentration dependent signal is the usage of UV-sensors. These optical sensors exploit differences in the optical property of the two components. However, only a weighted sum of the concentrations can be determined. The weighting factors depend on the components and the wavelength used.

$$c_{UV} = k_1\, c_A + k_2\, c_B, \quad k_1 = k_2 = 1 \tag{4.33}$$

One way to determine the single concentrations is to use sensors with two different wavelengths. If the linear factors are independent, the set of two equations can be solved for the concentrations. In this contribution, the measured weighted sum is used directly. For simplicity, it shall be assumed that the weighting factors are equal to one. If the offset values for the intermediate signals are set correctly, the control concept can be used with simple UV- sensors. The fol-

lowing intermediate signals are constructed, Eq. (4.34) to Eq. (4.37).

$$x_1(t) = sign\left(c_{UV1}(t) - 0.03\,c_{B,Fe}\right) \tag{4.34}$$

$$x_2(t) = sign\left(c_{UV2}(t) - (c_{B,Fe} + 0.03\,c_{A,Fe})\right) \tag{4.35}$$

$$x_3(t) = sign\left(c_{UV3}(t) - (c_{A,Fe} + 0.03\,c_{B,Fe})\right) \tag{4.36}$$

$$x_4(t) = sign\left(c_{UV4}(t) - 0.03\,c_{A,Fe}\right) \tag{4.37}$$

4.1.3 Simulation Results

A simulation using the detailed model is carried out to validate the control concept. The model parameters are taken from [47]. The discretization of the partial differential equation is performed using finite differences, [54], where 51 base points per column were used. The modeling of the dispersion was neglected, since the numerical dispersion was considered as sufficient. The initial flow rates, the switching time, and therefore, the initial parameters were computed using the formulas for complete separation as given by Eqs. (3.25)-(3.28) on page 45 or in [47]. The controller parameter was selected as $a = 0.25$ and the estimator pole as $a_\theta = 0.40$. The set points were chosen to $\tau_I = \tau_{II} = 0.75$ and $\tau_{III} = \tau_{IV} = 0.25$. It should be noticed that the proposed adaptive control concept makes use of the *certainty equivalence* principle, [58]. This means that both the controller and estimator are stable if they are used separately, but stability is not guaranteed if they are used together. However, a simulation study has shown that for a proper selection of the controller parameters, the control loop can always be stabilized. The resulting concentration profiles at cyclic steady state are shown in Fig. 4.2 on page 89. At the second UV- sensor location, one can record the time trajectories of the concentrations as given in Fig. 4.6. At cyclic steady state, the concentration of the component B is nearly constant and equal to the feed concentration. To detect the foot point of component A from the sum of both concentrations, the offset value is chosen slightly higher than the feed concentration of component B. The time trajectories of the normalized residence times are represented in Fig. 4.7. It can be seen that after a transient time, the
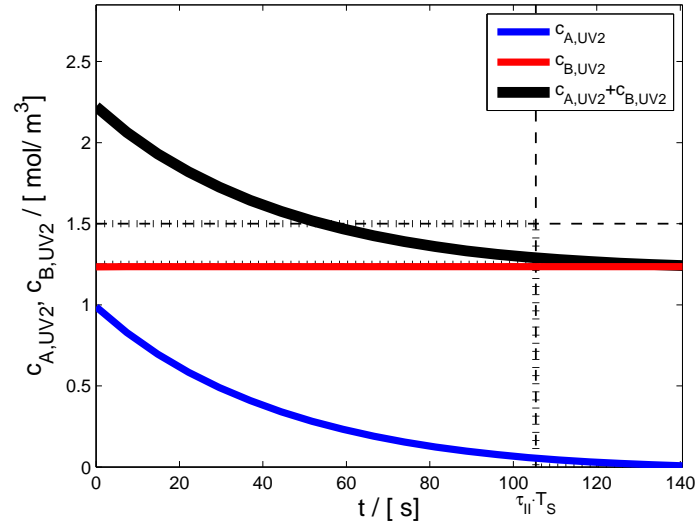
Figure 4.6: Time trajectories of the concentrations at the second UV- sensor within one switching interval to Fig. 4.2 on page 89.

controller is capable of setting the locations of the concentration fronts as desired. The parameters are adjusted as soon as the concentration fronts appear at the associated UV- sensor locations, as seen in Fig. 4.8. They depart slightly from their initial conditions, which is due to the dispersion. The switching time is initially high, which is desired since the concentration fronts should appear at the UV- locations as fast as possible. After a transient time, the switching time approaches a constant value, as indicated in Fig. 4.9. Finally, a portion of the time trajectory of the concentrations at the extract is given in Fig. 4.10. In cyclic steady state only component B is drained off at the extract. The controller ensures the positioning of the concentration fronts, and therefore, the complete separation of the binary feed.

Table 4.1: Operating points for $\tau_1 = \tau_2 = 0.75$, $\tau_3 = \tau_4 = 0.25$, $a = 0.25$, $a_\theta = 0.40$.

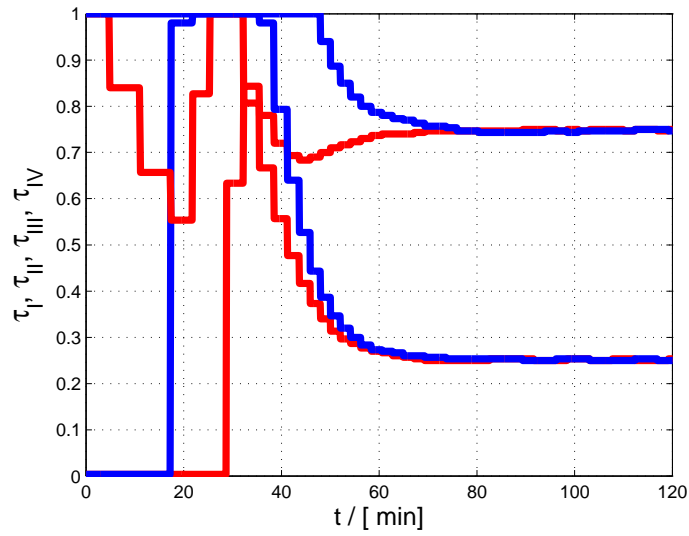|	$\dot{V}_I / \left[\frac{ml}{min}\right]$	$\dot{V}_{Ex} / \left[\frac{ml}{min}\right]$	$\dot{V}_{Fe} / \left[\frac{ml}{min}\right]$	$\dot{V}_{Ra} / \left[\frac{ml}{min}\right]$	$T_S / [s]$
$t = 0$	41.43	10.00	10.00	10.00	146.63
$t = t_{end}$	42.42	10.25	10.00	10.20	140.80

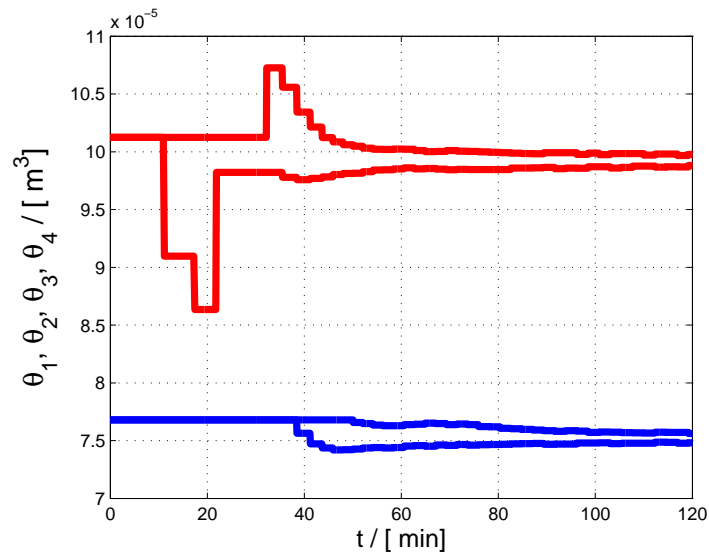Figure 4.7: Time trajectories of the normalized residence times during startup phase.

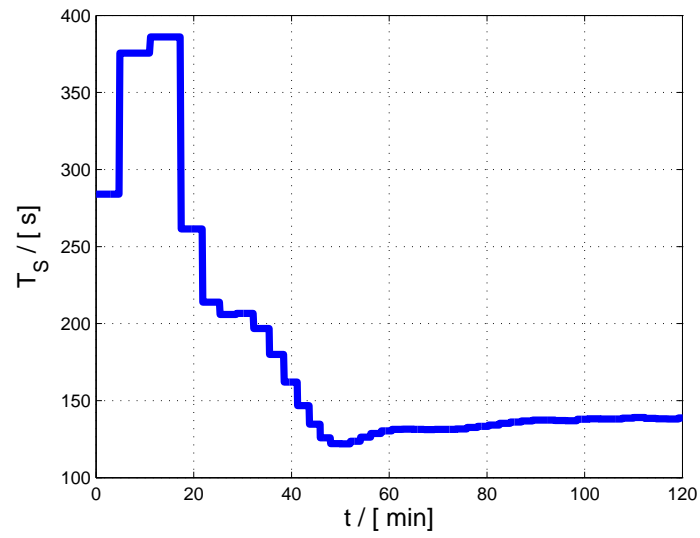Figure 4.8: Time trajectories of the parameter estimates during startup phase.

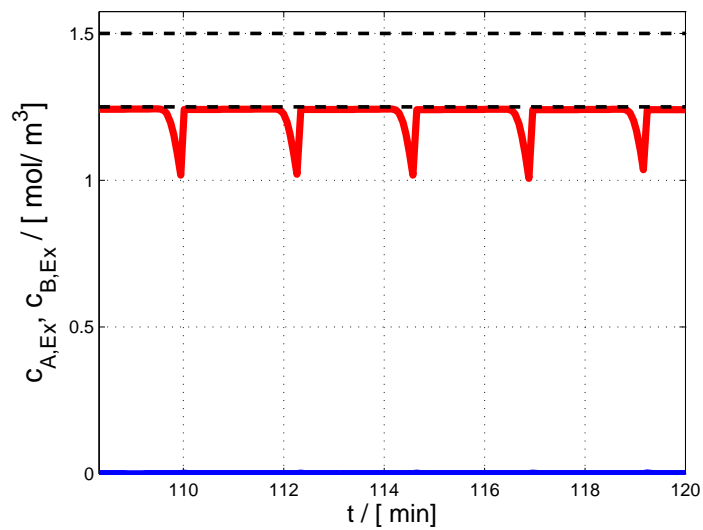Figure 4.9: Time trajectories of the switching time during startup phase.

Figure 4.10: Time trajectories of the concentrations at the extract.

4.1.4 Summary

A simple control concept for SMB plants is introduced for the case of complete separation. It is based on a simple nonlinear model for the movements of the foot points of the concentration fronts. If the concentrations can be measured separately, the proposed control concept leads to a reliable and robust adjustment of the volumetric flow rates and switching time. However, even if one cannot measure the concentrations separately it is possible to apply this method, as shown in the simulation results. The only crucial selection is the choice of correct offset values for the inner intermediate signals. The placement of the sensors in the middle of each section has an advantage in that the presence of small displacements of the concentration fronts from their set points do not result in significant impurities occurring at the drains. Sensor offset will be unaffected as long as these are smaller than the offset value, c_0. The controller drives the process to the optimal point for a dispersion-free system. This leads to lower eluent consumption compared to an open loop operating SMB plant, which must be run with some safety margins. One may assume that this will also be the case in presence of dispersion. This proposed concept is quite versatile and works independently of the adsorption behavior, see also [59]. It can be extended to SMB plants with multi-component separation and reactive SMBs. Furthermore, this concept can be used as a special optimization technique. In this way, it is possible to compute optimal operating conditions for more complex SMB plants where no analytical solution is known.

4.2 Control of SMB Plants under Reduced Purity Requirements

The basic idea of the previous section to construct an adaptive controller for SMB plants is now extended to the case of incomplete separation and complete regeneration, [60]. This time a symmetric four-column SMB will be considered, as shown in Fig. 4.11. Again, a simple model is derived to predict the locations of the foot points of the concentration fronts for each switching interval. Based on this model, an adaptive controller is constructed to fix the concentration fronts in such a way that the purity requirements are fulfilled. Finally, some simulation results are given to show the potential of this control concept for industrial
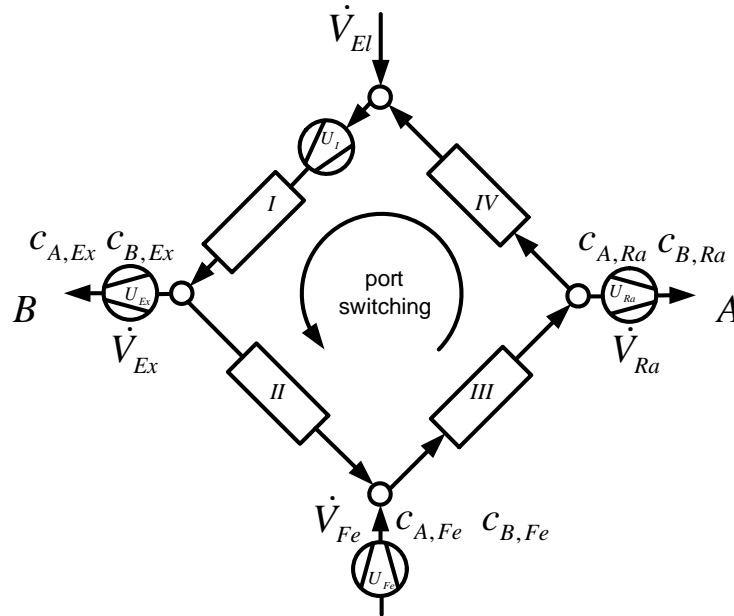
Figure 4.11: Configuration of the SMB installation.

application.

4.2.1 Simplified Modeling

The full model, Eq. (3.1) to Eq. (3.9) on page 40, is able to describe the plant sufficiently well, but it is less suited for control design. For this reason, a simple model for the movements of the foot points of the concentration fronts is derived. In Fig. 4.12, a typical concentration profile at cyclic steady state is shown. The concentration fronts move from the left to the right side. The narrow lines are the profiles at the beginning and the end of a switching interval, whereas the thick lines correspond to profiles at the middle of the switching interval. In Fig. 4.13 and Fig. 4.14, the time trajectories of the concentrations at the drains for one switching interval are presented. They are the measured quantities. The goal of the control device is to place the concentration fronts within the measured time trajectories for one switching interval in such a way that the purity requirements are fulfilled. To find a simple low-order model, it is sufficient to only describe the positions of the foot points of the concentration fronts. It is useful to fix the volumetric flow rates for one period, which opens an advantageous, discrete description.
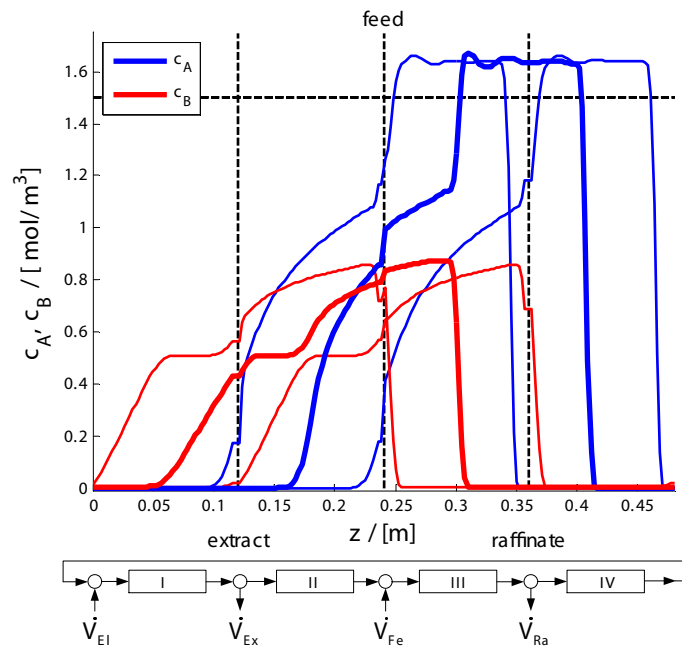
Figure 4.12: Concentration profiles at cyclic steady state for Langmuir isotherms and model parameters taken from table A-2.
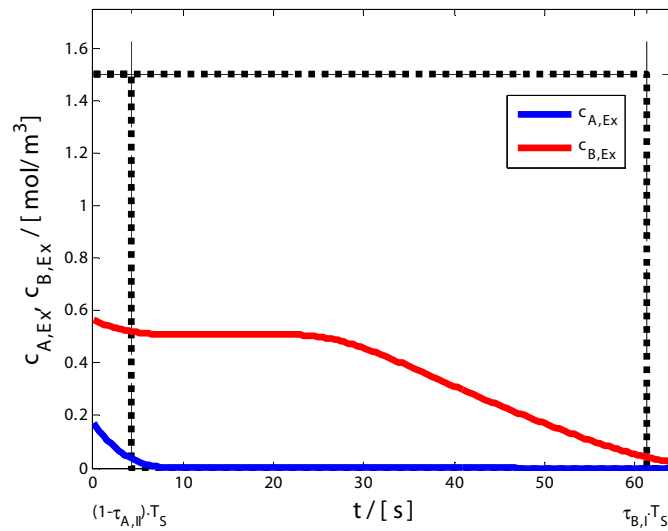
Figure 4.13: Time trajectories of the concentrations at the extract drain within one switching interval to Fig. 4.12.
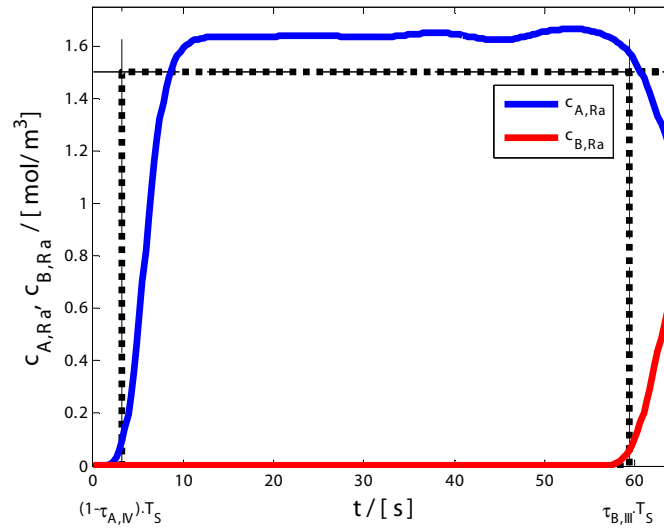
Figure 4.14: Time trajectories of the concentrations at the raffinate drain within one switching interval to Fig. 4.12.

Outer Concentration Front of the Extract

In Fig. 4.15, the movement of the foot points of the outer concentration front at the extract side is given. This point moves now in contrast to the previous section between two zones with different velocities. The distance traveled by the foot point can be computed through velocity and time. For this purpose, it is advantageous to define a normalized residence time, $\tau_{B,I}$. This time determines how long the foot point stays within zone I, and is normalized to the actual switching time. Later, this value is simply computed from the concentration measurements at the drain. The distances traveled in each zone are computed as follows.

$$\Delta z_{B,I}(k) = v_{B,I}(k)\, \tau_{B,I}(k)\, T_S(k)\,, \quad \tau_{B,I} \in [0,1] \tag{4.38}$$

$$\Delta z_{B,II}(k) = v_{B,II}(k)\, (1 - \tau_{B,I}(k))\, T_S(k) \tag{4.39}$$

If the end of the switching time is reached, the foot point is shifted back by one column length, therefore Eq. (4.40) holds.

$$\Delta z_{B,I}(k+1) = L - \Delta z_{B,II}(k) \tag{4.40}$$

Figure 4.15: On the derivation of the foot point movement.

The distances are substituted through their velocities and times, Eq. (4.38) and Eq. (4.39). Thereafter, Eq. (4.40) is solved for the future normalized residence time.

$$\tau_{B,I}(k+1) = \frac{L - v_{B,II}(k)\,(1 - \tau_{B,I}(k))\,T_S(k)}{v_{B,I}(k+1)\,T_S(k+1)} \tag{4.41}$$
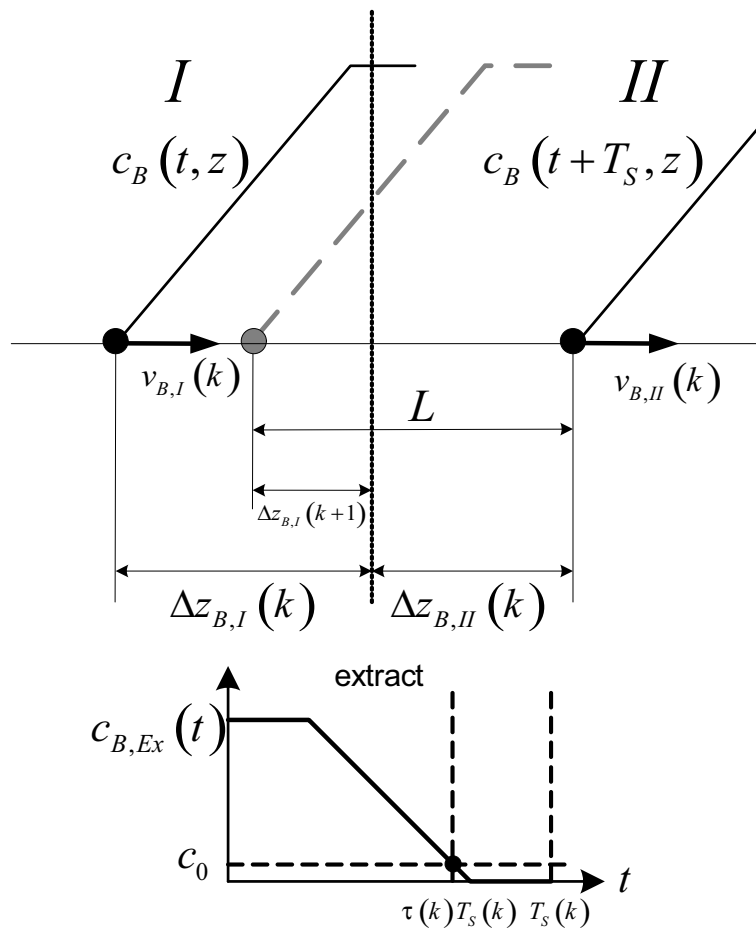
Inner Concentration Front of the Extract

The same method is now applied to the inner concentration front of the extract. The distances are expressed in the normalized residence time of the inner foot point of zone II.

$$\Delta z_{A,I}(k) = v_{A,I}(k)\,(1 - \tau_{A,II}(k))\,T_S(k), \quad \tau_{A,II} \in [0,1] \tag{4.42}$$

$$\Delta z_{A,II}(k) = v_{A,II}(k)\,\tau_{A,II}(k)\,T_S(k) \tag{4.43}$$

The back shifting of the foot point by one column length and the elimination of the distances leads to the future normalized residence time for the inner concentration front.

$$\tau_{A,II}(k+1) = 1 - \frac{L - v_{A,II}(k)\,\tau_{A,II}(k)\,T_S(k)}{v_{A,I}(k+1)\,T_S(k+1)} \tag{4.44}$$

Now the assumption is made again that the velocities of the foot points depend linearly on the volumetric flow rates of the zones.

$$v_{B,I}(k) = \frac{L}{\theta_1}\,\dot{V}_I(k), \quad v_{B,II}(k) = \frac{L}{\theta_1}\,\dot{V}_{II}(k) \tag{4.45}$$

$$v_{A,I}(k) = \frac{L}{\theta_2}\,\dot{V}_I(k), \quad v_{A,II}(k) = \frac{L}{\theta_2}\,\dot{V}_{II}(k) \tag{4.46}$$

This leads to the following model, Eq. (4.47) and Eq. (4.48), for the extract side.

$$\tau_{B,I}(k+1) = \frac{\theta_1 - \dot{V}_{II}(k)\,(1 - \tau_{B,I}(k))\,T_S(k)}{\dot{V}_I(k+1)\,T_S(k+1)} \tag{4.47}$$

$$\tau_{A,II}(k+1) = 1 + \frac{\dot{V}_{II}(k)\,T_S(k)\,\tau_{A,II}(k) - \theta_2}{\dot{V}_I(k+1)\,T_S(k+1)} \tag{4.48}$$

The derivation of the equations for the raffinate side is done in a similar way.

Model Equations

The normalized residence times are first measured after an additional delay of one sample. For this reason, an additional delay must be added to the model equations. Using the traditional notation of the control community for the inputs and outputs, Eq. (4.49), the complete model for the movements of the foot points of the concentration fronts, Eq. (4.51) to Eq. (4.54), can be derived as follows:

$$
\begin{aligned}
y_1(k) &= \tau_{B,I}(k-1), & y_2(k) &= \tau_{A,II}(k-1), \\
y_3(k) &= \tau_{B,III}(k-1), & y_4(k) &= \tau_{A,IV}(k-1),
\end{aligned}
$$

$$
\begin{aligned}
u_1(k) &= \dot{V}_I(k), & u_2(k) &= \dot{V}_{II}(k), \\
u_3(k) &= \dot{V}_{III}(k), & u_4(k) &= \dot{V}_{IV}(k), \\
u_5(k) &= T_S(k).
\end{aligned}
\tag{4.49}
$$

$$
\widehat{u}_i(k) = u_i(k)\, u_5(k), \quad i = 1,2,3,4
\tag{4.50}
$$

Model:

$$
y_1(k+1) = \frac{\theta_1 - \widehat{u}_2(k-1)\left[1 - y_1(k)\right]}{\widehat{u}_1(k)},
\tag{4.51}
$$

$$
y_2(k+1) = 1 + \frac{\widehat{u}_2(k-1)\, y_2(k) - \theta_2}{\widehat{u}_1(k)},
\tag{4.52}
$$

$$
y_3(k+1) = \frac{\theta_3 - \widehat{u}_4(k-1)\left[1 - y_3(k)\right]}{\widehat{u}_3(k)},
\tag{4.53}
$$

$$
y_4(k+1) = 1 + \frac{\widehat{u}_4(k-1)\, y_4(k) - \theta_4}{\widehat{u}_3(k)}.
\tag{4.54}
$$

If one sets all outputs and, consequently, the normalized residence times to unity, it becomes noticeable that every model parameter corresponds to one normalized control input.

$$
\theta_i = \widehat{u}_i, \quad i = 1,2,3,4
\tag{4.55}
$$

This state occurs for the ideal case of complete separation. Design rules already exist to compute this control inputs and thus, the parameters, e.g. in [49] or in chapter 3. From now on, only the extract side will be analyzed because the extract and raffinate sides have the same structure. The results obtained for the extract side are simply transferred to the raffinate side.

4.2.2 Control Design

Based on the simplified model, different controller designs are possible. Again, only a simple, but still powerful, controller is introduced here. An improvement may be obtained as shown in [57], [61].

Derivation of the Inverse Model

To decouple the multivariable system and to allow a simple control design, an inverse model is derived. Setting the outputs, y_i, equal to new virtual inputs, w_i, delayed by two lags, Eq. (4.56) and Eq. (4.57), and solving the resulting system of equations for the inputs with the aid of the system dynamics, gives the inverse model in Eq. (4.58) and Eq. (4.59).

Model:

$$y_1\left(k\right) = w_1\left(k-2\right) = \frac{\theta_1 - \widehat{u}_2\left(k-2\right)\left[1 - y_1\left(k-1\right)\right]}{\widehat{u}_1\left(k-1\right)}, \tag{4.56}$$

$$y_2\left(k\right) = w_2\left(k-2\right) = 1 + \frac{\widehat{u}_2\left(k-2\right)y_2\left(k-1\right) - \theta_2}{\widehat{u}_1\left(k-1\right)}. \tag{4.57}$$

Inverse model:

$$\widehat{u}_1\left(k\right) = \frac{w_2\left(k-2\right)\theta_1 - \left[1 - w_1\left(k-2\right)\right]\theta_2}{w_1\left(k-1\right)w_2\left(k-2\right) - \left[1 - w_1\left(k-2\right)\right]\left[1 - w_2\left(k-1\right)\right]}, \tag{4.58}$$

$$\widehat{u}_2\left(k\right) = \frac{w_1\left(k\right)\theta_2 - \left[1 - w_2\left(k\right)\right]\theta_1}{w_1\left(k\right)w_2\left(k-1\right) - \left[1 - w_1\left(k-1\right)\right]\left[1 - w_2\left(k\right)\right]}. \tag{4.59}$$

Feedback Control

Assuming exact parameter knowledge, the resulting dynamics with respect to the new virtual input is just a delay of two.

$$y_i(k) = w_i(k-2), \quad i = 1,2 \tag{4.60}$$

In order to place the concentration fronts even in the presence of disturbances, following control law is suggested.

$$w_i(k) = a\,w_i(k-1) + (1-a)\,w_i(k-2) + (1-a)\,e_i(k), \quad i = 1,2 \tag{4.61}$$

$$e_i(k) = y_{i,ref}(k) - y_i(k), \quad |a| < 1 \tag{4.62}$$

Using Eq. (4.60), the closed loop dynamics is derived as follows.

$$\begin{aligned} y_i(k) &= a\,y_i(k-1) + (1-a)\,y_i(k-2) + (1-a)\,e_i(k-2) \\ &= a\,y_i(k-1) + (1-a)\,y_{i,ref}(k-2) \end{aligned} \tag{4.63}$$

This is a first-order difference equation with a delay of two. If a is chosen to lie inside the unit disc, the output will converge to the reference as $k \to \infty$.

Tracing the Purity Error back to a Normalized Residence Time Error

To place the inner concentration front in such a way that the purity requirements are fulfilled, one needs to find a static relationship between purity and both concentration fronts. Such a relationship, Eq. (4.64), was derived in [47] for a dispersion-free SMB model under consideration of Henry isotherms, see also Eq. (3.22) at page 44. For Langmuir isotherms this relationship is more complicated as shown by Eq. (3.125) at page 77 or Eq. (3.132) at page 79. However, for the purpose of the controller design it is found that the relationship for Henry isotherms generally represents a sufficient approximation.

$$\tau_{A,II} = 1 - \frac{1-P_{Ex}}{P_{Ex}}\frac{c_{B,Fe}}{c_{A,Fe}}\tau_{B,I} \tag{4.64}$$

It is assumed that the ratio of the feed concentrations remains constant. Furthermore, it is assumed that the outer normalized residence time, $\tau_{B,I}$, is already

fixed to the desired value by the outer control loop. These assumptions allow the following substitutions.

$$p_{Ex} = \frac{1 - P_{Ex}}{P_{Ex}}, \quad \vartheta_{Ex} = \frac{c_{B,Fe}}{c_{A,Fe}} \tau_{B,I} \tag{4.65}$$

The static relationship, (4.64), can be rearranged to give the newly introduced virtual output, p_{Ex}.

$$p_{Ex} = \frac{1 - \tau_{A,II}}{\vartheta_{Ex}} \tag{4.66}$$

The control error, (4.67), in this quantity is proportional to the control error in the normalized residence times. For this reason, one can use the same control design as before. Thus, the transformation has a linearizing effect and a cascaded control design, which would lead to a reduction in the bandwidth of the closed loop is avoided through this.

$$e_p = p_{Ex,ref} - p_{Ex} = -\frac{\tau_{A,II,ref} - \tau_{A,II}}{\vartheta_{Ex}} = -\frac{1}{\vartheta_{Ex}} e_\tau \tag{4.67}$$

Notice that the introduced transformation of the purities is one to one. With other words, if the error in the transformed signals goes to zero, the purity will also converge to its reference. Notice further that if disturbances in the feed concentrations occur, the parameter, ϑ_{Ex}, may be weakly time-varying. Therefore, the closed loop needs a good gain margin, which can be assigned by a proper choice of a.

Computing the Optimal Switching Time

The switching time is an additional, redundant input which may be used to gain additional advantages. It is natural to demand a fixed throughput of the binary feed. Therefore, the feed flow rate is always kept constant and the switching time is changed instead. The optimal switching time is computed from the normalized control inputs for a fixed feed flow rate by following equation.

$$u_5(k) = \frac{\widehat{u}_3(k) - \widehat{u}_2(k)}{\dot{V}_{Fe}} \tag{4.68}$$

Notice that this degree of freedom may also be used to satisfy upper constraints on the volumetric flow rates. In this case, the switching time serves as a proper scaling factor, see Eq. (4.22) on page 94.

After determination of the optimal switching time, the flow rates for each section can be calculated.

$$u_i(k) = \frac{\widehat{u}_i(k)}{u_5(k)}, \quad i = 1, 2, 3, 4 \tag{4.69}$$

Computing Parameter Errors

In general, the parameters of the process may be unknown and subject to changes, e.g. aging, thermal processes; see Eq. (2.38) on page 13. For this reason, an automatic adaptation is desirable in practice. The parameter errors are defined as the difference between the true parameters and their estimates.

$$\tilde{\theta}_i(k) = \theta_i - \hat{\theta}_i(k), \quad i = 1, 2 \tag{4.70}$$

The error between the measured and the one-step-ahead predicted output can now be used to compute the previous parameter errors.

$$\tilde{\theta}_1(k-1) = \widehat{u}_1(k-1) \, \varepsilon_1(k) = \widehat{u}_1(k-1) \, (y_1(k) - \hat{y}_1(k)) \tag{4.71}$$

$$\tilde{\theta}_2(k-1) = -\widehat{u}_1(k-1) \, \varepsilon_2(k) = -\widehat{u}_1(k-1) \, (y_2(k) - \hat{y}_2(k)) \tag{4.72}$$

Estimator Design

For the determination of the parameters, the following parameter estimator is suggested.

$$\hat{\theta}_i(k) = \hat{\theta}_i(k-1) + (1 - a_\theta) \, \tilde{\theta}_i(k-1), \quad |a_\theta| < 1, \quad i = 1, 2 \tag{4.73}$$

If this equation is written as an error equation, a first-order difference equation arises.

$$\tilde{\theta}_i(k) = \tilde{\theta}_i(k-1) - (1 - a_\theta) \, \tilde{\theta}_i(k-1) = a_\theta \, \tilde{\theta}_i(k-1) \tag{4.74}$$

In other words, the estimation error will vanish as $k \to \infty$.

Computing Purities and Normalized Residence Times

To apply this control concept, the purities and the normalized residence times have to be determined for each cycle. The purities are defined as follows.

$$
P_{Ex} = \frac{\bar{c}_{B,Ex}}{\bar{c}_{A,Ex} + \bar{c}_{B,Ex}}, \quad P_{Ra} = \frac{\bar{c}_{A,Ra}}{\bar{c}_{A,Ra} + \bar{c}_{B,Ra}} \tag{4.75}
$$

To compute the purities, one needs to calculate the mean concentrations at the drains.

$$
\bar{c}_{i,j} = \frac{1}{T_S} \int_0^{T_S} c_{i,j}(t)\, dt, \quad i = A, B; \quad j = Ex, Ra \tag{4.76}
$$

With the aid of the correlation technique, it is possible to evaluate the normalized residence times of the foot points from concentration measurements at the drains for each cycle. Using the sign function, the following intermediate signals can be defined.

$$
x_{ref}(t) = \alpha\, sign\left(t - \tau_{ref}\, T_S\right) \tag{4.77}
$$

$$
x(t) = sign\left(c(t) - c_0\right) \tag{4.78}
$$

$$
\alpha = \begin{cases} -1 & \text{extract} \\ +1 & \text{raffinate} \end{cases} \tag{4.79}
$$

The newly introduced quantity, c_0, has a small positive value above the expected sensor noise level. The sign of α takes care of the different qualitative course of the concentrations between extract and raffinate. The intermediate signal, x_{ref}, may be thought of as the reference signal, whereas the signal, x, may be interpreted as actual trajectory. The cross correlation of both signals by Eq. (4.80), also see Fig. 4.16, will reach a maximum at the shift, $\Delta\tau_{max}$, which is a measure of the control error.

$$
R_{x_{ref}x}(\Delta\tau) = \lim_{T\to\infty} \frac{1}{2T} \int_{-T}^{T} x_{ref}(t)\, x(t + \Delta\tau\, T_S)\, dt \tag{4.80}
$$

$$\Delta\tau \in [-1, 1] \tag{4.81}$$

$$\max R_{x_{ref}x} = R_{x_{ref}x}\left(\Delta\tau_{\max}\right) \tag{4.82}$$

The sum of reference, τ_{ref}, and shift, $\Delta\tau_{\max}$, results in the actual value τ. The maximum is found by a simple one-dimensional search. A suitable choice of c_0 and the application of the correlation integral lead to a robust determination of the normalized residence times, even in the presence of sensor noise.
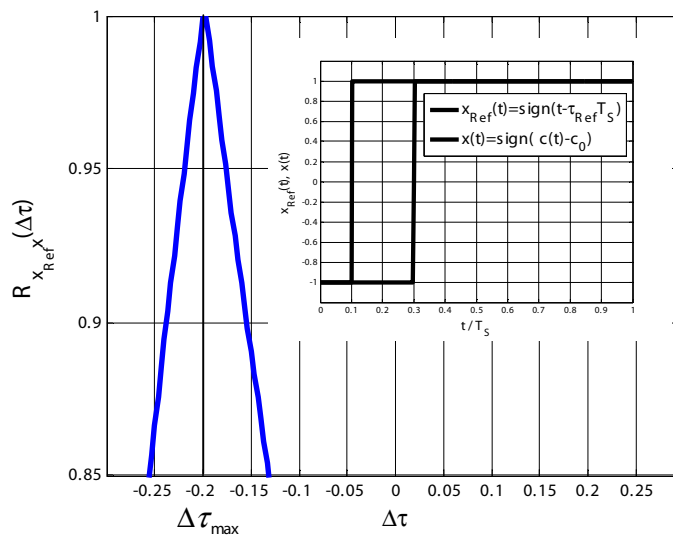

Figure 4.16: On cross correlation of two phase shifted sign signals.

Control Loop Description

Finally, the full program for the extract side is presented here to clarify the proposed control concept.

1. Compute normalized residence times and purity from concentration measurements at the extract drain.

$$y_1(k), \quad y_2(k), \quad P_{Ex}(k), \quad y_{1,ref}, \quad P_{Ex,ref}$$

2. Compute the predicted outputs:

$$\hat{y}_1(k) = \frac{\hat{\theta}_1(k-1) - \hat{u}_2(k-2)\left[1 - y_1(k-1)\right]}{\hat{u}_1(k-1)},$$

$$\hat{y}_2(k) = 1 + \frac{\hat{u}_2(k-2)\, y_2(k-1) - \hat{\theta}_2(k-1)}{\hat{u}_1(k-1)}.$$

3. Compute prediction errors:

$$\varepsilon_i(k) = y_i(k) - \hat{y}_i(k), \quad i = 1, 2.$$

4. Compute parameter errors:

$$\tilde{\theta}_1(k-1) = \hat{u}_1(k-1)\,\varepsilon_1(k),$$

$$\tilde{\theta}_2(k-1) = -\hat{u}_1(k-1)\,\varepsilon_2(k).$$

5. Compute parameter estimates:

$$\hat{\theta}_i(k) = \hat{\theta}_i(k-1) + (1 - a_\theta)\,\tilde{\theta}_i(k-1), \quad i = 1, 2, \quad |a_\theta| < 1.$$

6. Compute control errors:

$$e_1(k) = y_{1,ref} - y_1(k),$$

$$e_2(k) = -\vartheta_{Ex}\left(\frac{1 - P_{Ex,ref}}{P_{Ex,ref}} - \frac{1 - P_{Ex}(k)}{P_{Ex}(k)}\right), \quad \vartheta_{Ex} = \frac{c_{B,Fe}}{c_{A,Fe}}\, y_{1,ref}.$$

7. Compute virtual control signals:

$$w_i(k) = a\, w_i(k-1) + (1 - a)\, w_i(k-2) + (1 - a)\, e_i(k), \quad i = 1, 2, \quad |a| < 1.$$

8. Compute normalized control signals:

$$\hat{u}_1(k) = \frac{w_2(k-2)\,\hat{\theta}_1(k) - [1 - w_1(k-2)]\,\hat{\theta}_2(k)}{w_1(k-1)\, w_2(k-2) - [1 - w_1(k-2)]\,[1 - w_2(k-1)]},$$

$$\hat{u}_2(k) = \frac{w_1(k)\,\hat{\theta}_2(k) - [1 - w_2(k)]\,\hat{\theta}_1(k)}{w_1(k)\, w_2(k-1) - [1 - w_1(k-1)]\,[1 - w_2(k)]}.$$

9. Apply a similar procedure (1-8) for the raffinate side.

10. Compute switching time:

$$T_S\left(k\right) = \frac{\widehat{u}_3\left(k\right) - \widehat{u}_2\left(k\right)}{\dot{V}_{Fe}}.$$

11. Compute internal volumetric flow rates for each zone:

$$u_i\left(k\right) = \frac{\widehat{u}_i\left(k\right)}{T_S\left(k\right)}, \quad i = 1, 2.$$

12. Compute volumetric flow rates for the specific SMB configuration and apply the quantities computed for one switching time.

As stated above, the proposed adaptive control loop for adjusting the purities of a SMB plant makes use of the *certainty equivalence* concept, [58]. It means that the control loop without estimator, as well as the estimator alone, is stable. If one puts both parts together, stability cannot be guaranteed. However, as indicated by simulations, it was always possible to get a stable overall system for a proper choice of the poles, a and a_θ.

4.2.3 Simulation Results

In order to give a first impression of the efficiency of the adaptive controller developed here, a simulation of the control loop using the full model was carried out. The system of partial differential equations was transferred into ordinary differential equations with aid of the method of lines, [54]. In this case, 51 base points per column length were used. The equations of the full model and all its parameters were taken from [49] (same as in Tab. A-2 but $c_{A,Fe} = c_{B,Fe} = 1.5\frac{mol}{m^3}$); only the modeling of the dispersion was neglected. Further, a four-column SMB was used. The volumetric flow rates as well as the switching time, and thus the parameters of the reduced model were initialized with the equations for complete separation, as indicated in [49]. The controller pole was chosen as $a = 0.75$ and the estimator pole as $a_\theta = 0.40$. The outer normalized residence times were taken to be $\tau_{B,I,ref} = \tau_{A,IV,ref} = 0.95$ and the purity references, $P_{Ex,ref} = P_{Ra,ref} = 0.98$.

In Fig. 4.12 on page 103, the concentration profiles at cyclic steady state for drain purities of 98% are represented. Fig. 4.13 on page 103 and Fig. 4.14 on page 104 are the associated time trajectories of the concentrations at the drains.

In addition to the startup process, the behavior of the system for a counter step in the feed concentrations was also investigated. The step was simulated after 58 min, at which the feed concentrations were changed by 25 % from their nominal values. In Fig. 4.17, the time trajectories of the purities at the drains are represented. After approx. 45 switches, the purities have converged to their reference values. The counter step, which is indicated in Fig. 4.17 by a vertical line, leads only to a small departure from the desired purity set points, which are regulated back in approx. 20 switches to the nominal values. The great impurity during the startup phase is necessary in order to give the parameter estimator enough time for the determination of the process parameters. Especially in the outer
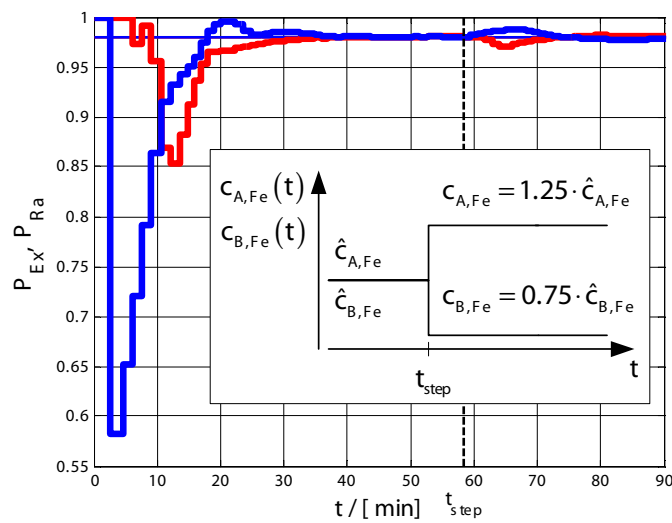

Figure 4.17: Adjustment of the purities at the drains during startup phase and a counter step disturbance in the feed.

normalized residence times, one recognizes the forced exponential behavior of the closed loop, as shown in Fig. 4.18. The parameter estimator works first if the concentration fronts appear at the drains. After the occurrence of the step in the feed concentrations, the plateau values of the concentration profiles and thus the parameters of the process change themselves, as pointed out in Fig. 4.19. As seen in Fig. 4.20, the switching time starts with a high value. This is desired since the concentration fronts should appear at the drains as fast as possible. After 45 switches, the optimal switching time is settled down. The step change in the feed concentration leads to a different switching time. Therefore, the control of the switching time ensures a constant feed flow rate, which is desired in practice.
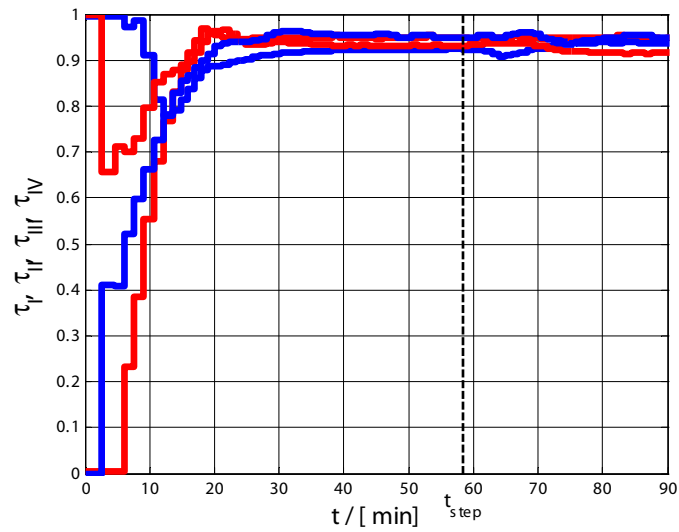
Figure 4.18: Adjustment of normalized residence times during startup phase and a counter step disturbance in the feed.
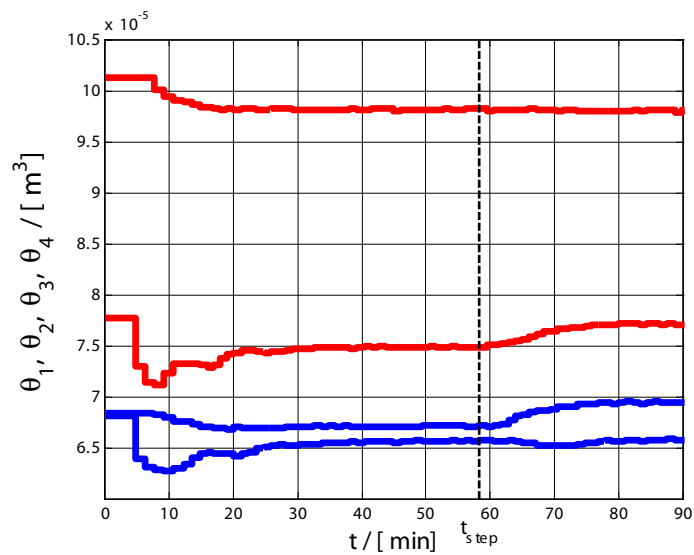

Figure 4.19: Adjustment of parameters during startup phase and a counter step disturbance in the feed.
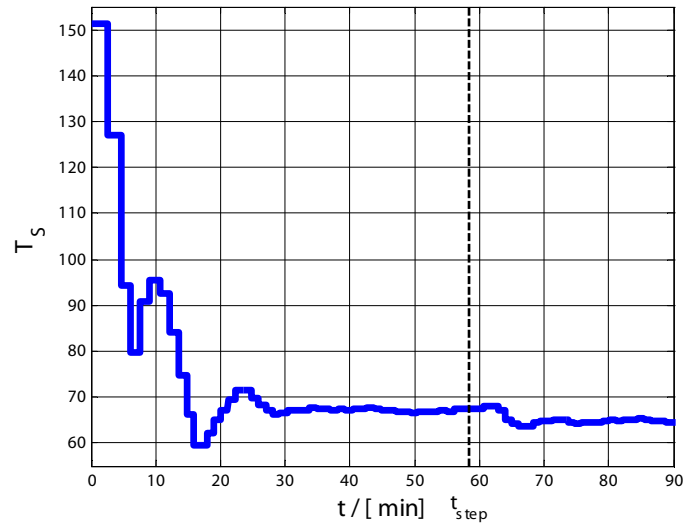
Figure 4.20: Adjustment of switching time during startup phase and a counter step disturbance in the feed.

4.2.4 Summary

A new adaptive control concept for adjusting the purities of SMB plants was presented here. It is based on a simple nonlinear model for the movements of the foot points of the concentration fronts. The proposed controller works independently of the adsorption behavior. In this section, the adsorption behavior was modeled by Langmuir isotherms. However, a simulation study with Henry, [57], and Bi-Langmuir isotherms, (not published), turns out to give similarly good results. A further advantage of this control concept lies in the robust determination of the normalized residence times. This procedure is also applicable for discontinuous concentration fronts.

The advantages of the proposed control concept are pointed out particularly well by a general control loop representation as shown in Fig. 4.21. The purities as well as the outer normalized residence times are adjusted by measuring the four concentrations at the drains. Since a time-discrete description was used, the time-discrete response can be assigned independently of the actual parameters of the SMB process. A time consuming tuning procedure of the controller to different SMB processes is therefore avoided. The controller is parameterized

only with a rough knowledge about the volumetric flow rates, the switching time, and the feed concentrations for ideal complete separation. Usually the operators of SMB plants already know this information. The set points for the outer normalized residence times are a measure of robustness with respect to step disturbances. These should be selected close to one according to a low solvent consumption. A choice of 0.95 is usually sufficient. The set points are fixed by the operator of the plant depending on his special interest and specifications. The regulation serves to adhere to his specifications. Sometimes one would like
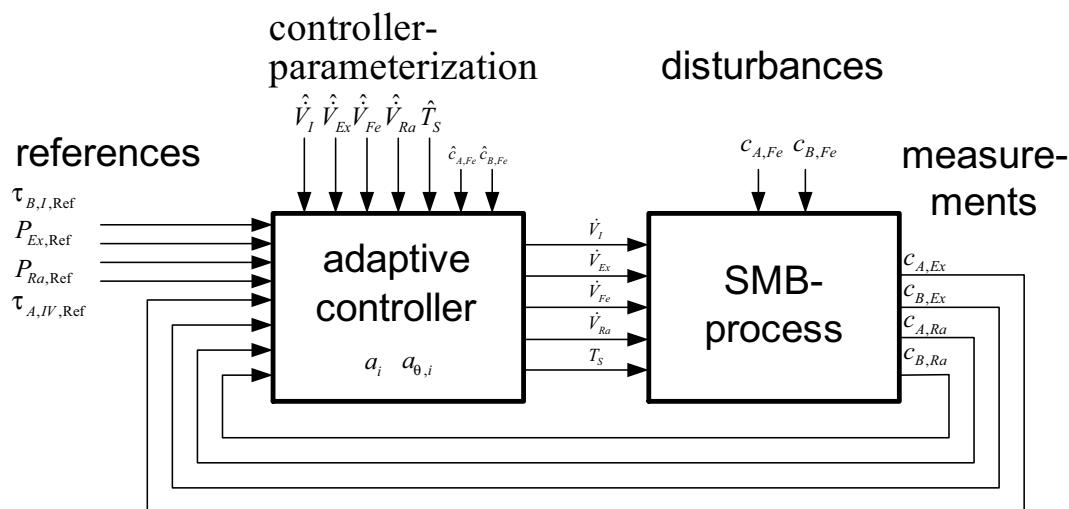
Figure 4.21: General control loop to adjust the purities of SMB plants.

to separate binary mixtures, where the concentrations are not separately measurable. If only the sum of both concentrations is available, no direct control of the purities can be realized. However, placements of the concentration fronts can be realized. In this case, one has to select two suitable points from the sum of the concentration profiles with the aid of the sign function, as shown in [56]. Under the assumption that the feed concentrations remain constant, one can guarantee an equal quality of the purities without having to determine their values exactly. Thus, the proposed control concept is ideally suited for industrial use.

4.3 Conclusion

In this chapter, two new control concepts were introduced. According to a simple and clear representation, controllers of low order were used. An improve-

ment in the control accuracy can easily be obtained by increasing the order, [57], [61].

The major advantage with these control concepts is the usage of a simple time-discrete description of the process. This led to simple models, which describe the essential dynamics sufficiently well. The adjustment of the flow rates and the switching time is carried out at the same time. No hybrid modeling of a continuous and time-discrete subsystem is necessary. The parameters of the simplified models can be derived directly from the parameters of the complete model. This allows to already get good initial estimates if the parameters of the complete model are known. The parameters can also be calculated using former measurements. Thus, extremely robust and self-adjustable controllers can be constructed. The control law can be expressed directly in dependence of the model parameters, because of the low model order. The dynamics can already be assigned in form of the transition sequence without knowing the nominal parameters in advance. A time-consuming calibration of the controller for different SMB processes is avoided through that.

Another essential advantage lies in the kind of the measuring principle. If purity control is not explicitly required, these control concepts do not use the concentrations directly as variables to be controlled. What is done instead is that the time-distance between the measured concentration fronts to a pre-defined reference is determined from the concentration dependent signals. The application of the correlation technique leads to an extremely robust determination of the variables that one likes to control.

Upper constraints of the volumetric flow rates can be taken into account easily as already shown. To this, no iterative method of computation is necessary. The control concepts are real time capable and can be easily implemented by using cheap micro controllers.

In practice, it makes sense to combine both concepts. In other words, the user decides whether a complete or incomplete separation is desired. A positioning of UV- sensors in the middle of the four zones also improves the regulation at incomplete separation. In this case, the control variables can be adjusted in time if insufficient parameter knowledge is present. Thus, no higher impurities than allowed will occur during the startup phase. Both concepts may serve as a base for further developments and an industrial application.

Bibliography

[1] D. Broughton, C. Gerhold, Continuous sorption process employing fixed bed of sorbent and moving inlets and outlets, US Pat. 2,985,589.

[2] G. Storti, M. Mazzotti, M. Morbidelli, S. Carrà, Robust design of binary countercurrent adsorption separation processes, AIChE J. 39 (3) (1993) 471–492.

[3] M. Mazzotti, G. Storti, M. Morbidelli, Optimal operation of simulated moving bed units for nonlinear chromatographic separations, J. Chromatogr., A 769 (1) (1997) 3–24.

[4] Z. Ma, N. Wang, Standing wave analysis of smb chromatography: Linear systems, AIChE J. 43 (10) (1997) 2488–2508.

[5] T. Mallmann, B. D. Burris, Z. Ma, N. H. L. Wang, Standing wave design of nonlinear smb systems for fructose purification, AIChE J. 44 (12) (1998) 2628–2646.

[6] M. Kaspereit, A. Seidel-Morgenstern, A. Kienle, Design of simulated moving bed processes under reduced purity requirements, J. of Chromat. A 1162 (1) (1998) 2–13.

[7] A. Rajendran, Equilibrium theory-based design of simulated moving bed processes under reduced purity requirements: Linear isotherms, J. of Chromat. A 1185 (2) (2008) 216–222.

[8] O. Ludemann-Hombourger, R. Nicoud, M. Bailly, The 'varicol' process: A new multicolumn continuous chromatographic process, Separation Science and Technology 35 (12) (2000) 1829–1862.

[9] H. Schramm, A. Kienle, M. Kaspereit, A. Seidel-Morgenstern, Improved operation of simulated moving bed processes through cyclic modulation of

feed flow and feed concentration, Chem. Eng. Sc. 58 (23-24) (2003) 5217–5227.

[10] M. Kearney, K. Hieb, Time variable simulated moving bed process, US Pat. 5,102,553.

[11] Y.Kawajiri, L. T.Biegler, Optimization strategies for simulated moving bed and powerfeed processes, AIChE J. 52 (4) (2006) 1343–1350.

[12] A. Toumi, S. Engell, M. Diehl, H. Bock, J. Schlöder, Efficient optimization of simulated moving bed processes, Chem. Eng. and Processing 46 (11) (2007) 1067–1084.

[13] G. B. Cox (Ed.), Preparative Enantioselective Chromatography, Blackwell Publishing Ltd., Oxford, 2005.

[14] P. S. Gomes, M. Minceva, A. E. Rodrigues, Simulated moving bed technology: Old and new, Adsorption 12 (5) (2006) 375–392.

[15] A. Seidel-Morgenstern, L. C. Keßler, M. Kaspereit, New developments in simulated moving bed chromatography, Chem. Eng. Technol. 31 (6) (2008) 826–837.

[16] E. Kloppenburg, E.-D. Gilles, Automatic control of the simulated moving bed process for c8 aromatics separation using asymptotically exact input/output-linearization, J. Process Control 9 (1) (1999) 41–50.

[17] E. Kloppenburg, Modellbasierte Prozessführung von Chromatographieprozessen mit simulierten Gegenstrom, VDI- Fortschritt- Bericht, R. 3 Nr. 661, Düsseldorf, 2000.

[18] H. Schramm, S. Grüner, A. Kienle, Optimal operation of simulated moving bed chromatographic processes by means of simple feedback control, J. Chromatogr., A 1006 (1-2) (2003) 3–13.

[19] H. Schramm, Neue Betriebsweisen und Prozessführungskonzepte für chromatographische Prozesse mit Simulierten Gegenstrom, Dissertation Universität Magdeburg, Shaker Verlag, Aachen, 2005.

[20] G. Erdem, S. Abel, M. Morari, M. Mazzotti, M. Morbidelli, J. H. Lee, Automatic control of simulated moving beds, Ind. Eng. Chem. Res. 43 (2004) 405–421.

[21] G. Erdem, On-line Optimization and Control of Simulated Moving Bed Processes, Diss. ETH No. 15867, Zürich, 2004.

[22] A. Toumi, Optimaler Betrieb und Regelung von Simulated-Moving-Bed-Prozessen, Dissertation Universität Dortmund, Shaker Verlag, Aachen, 2005.

[23] M. Alamir, F. Ibrahima, J. P. Corriou, A flexible nonlinear model predictive control scheme for quality/performance handling in nonlinear smb chromatography, J. Process Control 16 (4) (2006) 333–344.

[24] K. Klatt, F. Hanisch, G. Dünnebier, Model-based control of a simulated moving bed chromatographic process for the separation of fructose and glucose, J. Process Control 12 (2) (2002) 203–219.

[25] C. Wang, K. Klatt, G. Dünnebier, S. Engell, F. Hanisch, Neural network-based identification of smb chromatographic processes, Control Engineering Practice 11 (8) (2003) 949–959.

[26] T. Kleinert, J. Lunze, Modelling and state observation of simulated moving bed processes based on an explicit functional wave form description, Math. Comput. Simul. 68 (3) (2005) 235–270.

[27] T. Kleinert, J. Lunze, Decentralised control of chromatographic simulated moving bed processes based on wave front reconstruction, J. Process Control 18 (7-8) (2008) 780–796.

[28] T. Kleinert, Modelling, State Observation and Control of Simulated Counterflow Chromatographic Separations, Dissertation Ruhr- Universität Bochum, Logos Verlag, Berlin, 2006.

[29] H. Rhee, R. Aris, N. Amundson, First Order Partial Differential Equations, Part I and Part II, Prentice-Hall, New Jersey, 1986.

[30] J. Logan, Applied Partial Differential Equations, Springer, New York, 1998.

[31] J. Logan, Transport Modeling in Hydrogeochemical Systems, Springer, New York, 2001.

[32] G. Guiochon, B. Lin, Modeling for Preparative Chromatography, Academic Press, San Diego, 2003.

[33] M. Johannsen, Modeling of Simulated Moving Bed Chromatography, in Modeling of Process Intensification edited by F.J.Keil, Wiley-VCH Verlag GmbH & Co. KGaA, Weinheim, 2007.

[34] D. M. Ruthven, Principles of Adsoption and Adsorption Processes, John Wiley & Sons Inc., New York, 1984.

[35] G. Vogel, Lehrbuch Chemische Technologie, Wiley-VCH Verlag GmbH & Co. KGaA, Weinheim, 2004.

[36] L. Debnath, Nonlinear Partial Differential Equations for Scientists and Engineers, Birkhäuser, Boston, 1997.

[37] C. B. Laney, Computional Gasdynamics, Cambridge University Press, Cambridge, 2007.

[38] R. Courant, K. Friedrichs, Supersonic Flow and Shock Waves, Interscience Publishers, New York, 1948.

[39] G. Whitham, Linear and Nonlinear Waves, John Wiley & Sons Inc., New York, 1974.

[40] P. Sachdev, Self-Similarity and Beyond, Exact Solutions of Nonlinear Problems, Chapman & Hall/ CRC, Boca Raton, Florida, 2000.

[41] P. Prasad, Nonlinear Hyperbolic Waves in Multi-Dimensions, Chapman & Hall/ CRC, Boca Raton, Florida, 2001.

[42] F. G. Helfferich, Non-linear waves in chromatography i. waves, shocks, and shapes, J. Chromatogr., A 629 (1) (1993) 97–122.

[43] F. G. Helfferich, R. D. Whitley, Non-linear waves in chromatography ii. wave interference and coherence in multicomponent systems, J. Chromatogr., A 734 (1) (1996) 7–47.

[44] F. G. Helfferich, Non-linear waves in chromatography iii. multicomponent langmuir and langmuir-like systems, J. Chromatogr., A 768 (1) (1997) 169–205.

[45] F. G. Helfferich, G. Klein, Multicomponent Chromatography, Marcel Dekker, New York, 1970.

[46] A. Polyanin, V. F. Zaitsev, Handbook of Exact Solutions for Ordinary Differential Equations, pp.97, CRC Press, New York, 1995.

[47] M. Fütterer, Ein Beitrag zur Einstellung von Simulated Moving Bed- Anlagen, Chem. Ing. Tech. 80 (5) (2008) 601–606.
URL `http://dx.doi.org/10.1002/cite.200700177`

[48] Comsol Multyphysics Users Guide, Comsol AB, 2005.

[49] M. Fütterer, Finding optimal operating conditions for smb plants using comsol, Proc. of the European COMSOL Conf. 2007 2 (2007) 846–850.
URL `http://www.comsol.se/academic/papers/3309`

[50] G. Zhong, G. Guiochon, Analytical solution for the linear ideal model of simulated moving bed chromatography, Chem. Eng. Sc. 51 (18) (1996) 4307–4319.

[51] M. Fütterer, Design of simulated moving bed plants by using noncompetitive langmuir isotherms, Chem. Eng. Technol. 32 (10) (2009) 1535–1541.
URL `http://dx.doi.org/10.1002/ceat.200800397`

[52] M. Fütterer, Design of simulated moving bed plants for reduced purities, Chem. Eng. Technol. 33 (1) (2010) 21–34.
URL `http://dx.doi.org/10.1002/ceat.200900319`

[53] M. Fütterer, Die Einstellung von Simulated-Moving-Bed-Anlagen mit Hilfe des Coherence-Konzepts, Chem. Ing. Tech. 81 (3) (2009) 311–322.
URL `http://dx.doi.org/10.1002/cite.200800124`

[54] W. E. Schiesser, Computational Mathematics in Engineering and Applied Science, CRC Press, Florida, 1994.

[55] M. Fütterer, Homepage.
URL `http://ifatwww.et.uni-magdeburg.de/~futterer/`

[56] M. Fütterer, An adaptive control concept for simulated moving bed plants in case of complete separation, Chem. Eng. Technol. 31 (10) (2008) 1438–1444.
URL `http://dx.doi.org/10.1002/ceat.200800277`

[57] M. Fütterer, Ein Regelungskonzept zur Einstellung der Abzugsreinheiten von Simulated Moving Bed- Anlagen, Chem. Ing. Tech. 80 (12) (2008) 1767–1774.
URL `http://dx.doi.org/10.1002/cite.200800077`

[58] J.-J. Slotine, W. Li, Applied Nonlinear Control, Prentice- Hall, 1991.

[59] M. Fütterer, Adaptive control of simulated moving bed plants using comsol's simulink interface, Proc. of the European COMSOL Conf. 2008.
URL `http://www.comsol.se/academic/papers/5043/`

[60] M. Fütterer, An adaptive control concept for simulated moving bed plants under reduced purity requirements, Chem. Eng. Technol. 31 (12) (2008) 1816–1823.
URL `http://dx.doi.org/10.1002/ceat.200800373`

[61] M. Fütterer, Ein Adaptiver Regler zur Einstellung der Abzugsreinheiten von SMB- Anlagen, at Automatisierungstechnik 57 (4) (2009) 195–205.
URL `http://dx.doi.org/10.1524/auto.2009.0762`

Appendix

Notation

Table A-1: Notation

c	$\left[\frac{mol}{m^3}\right]$	Fluid concentration (volumetric)
q	$\left[\frac{mol}{m^3}\right]$	Adsorbed concentration (volumetric)
H	$[-]$	Henry constant
K	$\left[\frac{m^3}{mol}\right]$	Langmuir constant
v_l	$\left[\frac{m}{s}\right]$	Liquid velocity
v_s	$\left[\frac{m}{s}\right]$	Shock velocity
v_c	$\left[\frac{m}{s}\right]$	Concentration velocity
$\dot{V}$	$\left[\frac{m^3}{s}\right]$	Volumetric flow rate
T_S	$[s]$	Switching time
τ	$[-]$	Time normalized to switching time
P_{Ex}	$[-]$	Extract purity
P_{Ra}	$[-]$	Raffinate purity
NC		Number of columns
c_{Fe}	$\left[\frac{mol}{m^3}\right]$	Feed concentration

Model Parameters

Table A-2: Model parameters

Column length	L	0.12m
Column diameter	d	0.02m
Cross section area	A	$\frac{\pi}{4} d^2$
Void fraction	ε	0.7407
Package ratio	F	$\frac{1-\varepsilon}{\varepsilon}$
Henry constant A	H_A	5.0
Henry constant B	H_B	7.5
Langmuir constant A	K_A	0.15 $\frac{m^3}{mol}$
Langmuir constant B	K_B	0.30 $\frac{m^3}{mol}$
Column configuration	cfg	$[N_I, N_{II}, N_{III}, N_{IV}]$
Feed concentration of component A	$c_{A,Fe}$	1.5 $\frac{mol}{m^3}$
Feed concentration of component B	$c_{B,Fe}$	1.25 $\frac{mol}{m^3}$
Feed flow rate	$\dot{V}_{Fe}$	10 ml/min

COMSOL Implementation of SMB Process

To simulate the SMB process the finite element software package COMSOL, [48], is used, since it is a standard package that is broadly available. If implementing the system of equations, one needs to compare the model equations with COMSOL's PDE equation in general form, as stated below.

$$\mathbf{d_a} \cdot \frac{\partial \mathbf{u}}{\partial t} + \nabla \cdot \boldsymbol{\Gamma} = \mathbf{F} \tag{A-1}$$

COMSOL's vector variables are identified to be:

$$\mathbf{u} = \left(\begin{array}{cc} c_A & c_B \end{array} \right)^T, \quad \mathbf{d_a} = \left(\begin{array}{cc} 1 + F \frac{\partial q_A}{\partial c_A} & \frac{\partial q_A}{\partial c_B} \\ \frac{\partial q_B}{\partial c_A} & 1 + F \frac{\partial q_B}{\partial c_B} \end{array} \right), \tag{A-2}$$

$$\boldsymbol{\Gamma} = \left(\begin{array}{cc} \frac{\dot{V}}{\varepsilon A} \cdot c_A - D \frac{\partial c_A}{\partial z} & \frac{\dot{V}}{\varepsilon A} c_B - D \frac{\partial c_B}{\partial z} \end{array} \right)^T, \quad \mathbf{F} = \left(\begin{array}{cc} 0 & 0 \end{array} \right)^T. \tag{A-3}$$

The boundary condition in general forms are:

$$-\mathbf{n} \cdot \boldsymbol{\Gamma} = \mathbf{G} + \left(\frac{\partial \mathbf{R}}{\partial \mathbf{u}} \right)^T, \quad \mathbf{R} = \mathbf{0}. \tag{A-4}$$

One possible solution is:

$$\mathbf{G}_{|z=0} = \left(\begin{array}{cc} \frac{\dot{V}}{\varepsilon A} c_{A,in} & \frac{\dot{V}}{\varepsilon A} c_{B,in} \end{array} \right)^T, \quad \mathbf{G}_{|z=L} = \left(\begin{array}{cc} -\frac{\dot{V}}{\varepsilon A} c_A & -\frac{\dot{V}}{\varepsilon A} c_B \end{array} \right)^T, \tag{A-5}$$

$$\mathbf{R} \Big|_{\substack{z=0 \\ z=L}} = \left(\begin{array}{cc} 0 & 0 \end{array} \right)^T. \tag{A-6}$$

The coupling of the chromatographic columns can be done in COMSOL by extrusion or identity coupling variables.

Solution for Anti- Langmuir Isotherms

Given a specific feed composition, $c_{A,Fe}$ and $c_{B,Fe}$ and feed flow rate, $\dot{V}_{Fe}$, the velocity equations for Anti-Langmuir isotherms for complete separation and for complete regeneration, [53], can be solved for the unknown volumetric flow rates, $\dot{V}_I$, $\dot{V}_{Ex}$, $\dot{V}_{Ra}$ and switching time T_S, where some arbitrary normalized residence times, $0 \ll \tau_{B,I} \leqslant 1$ and $0 \ll \tau_{A,IV} \leqslant 1$, can be chosen to increase robustness.

$$1 + K_A\, c_{A,Fe} + K_B\, c_{B,Fe} > 0, \quad K_A < 0, \quad K_B < 0$$

$$\alpha = H_B\, (1 + K_A\, c_{A,Fe}) - H_A\, (1 + K_B\, c_{B,Fe})$$

$$C_2 = \frac{\alpha - \sqrt{\alpha^2 + 4\, H_A\, H_B\, K_A\, K_B\, c_{A,Fe}\, c_{B,Fe}}}{2\, H_B\, K_A\, c_{B,Fe}} \tag{A-7}$$

$$c_{A,4} = -\frac{H_B - H_A}{H_B\, K_A\, C_2 + H_A\, K_B}\, C_2 \tag{A-8}$$

$$c_{B,2} = \frac{H_B - H_A}{H_B\, (1 + K_A\, c_{A,4} - K_B\, c_{B,Fe}) - H_A}\, c_{B,Fe} \tag{A-9}$$

$$\dot{V}_I = \frac{1}{\tau_{B,I}} \frac{(\tau_{B,I}\, (1 + K_B\, c_{B,2}) + F\, H_B)\, (1 + K_A\, c_{A,4}) - F\, H_A\, (1 - \tau_{B,I})}{F\, [H_B\, (1 + K_B\, c_{B,2}) - H_A]}\, \dot{V}_{Fe} \tag{A-10}$$

$$\dot{V}_{Ex} = \frac{1}{\tau_{B,I}} \frac{H_B\, (1 + K_A\, c_{A,4}) - H_A}{H_B\, (1 + K_B\, c_{B,2}) - H_A}\, \dot{V}_{Fe} \tag{A-11}$$

$$\dot{V}_{Ra} = \frac{1}{\tau_{A,IV}} \frac{H_B - H_A\, (1 + K_A\, c_{A,4})}{H_B\, (1 + K_B\, c_{B,2}) - H_A}\, (1 + K_B\, c_{B,2})\, \dot{V}_{Fe} \tag{A-12}$$

$$T_S = \frac{F}{1 + F} \frac{A\, L}{\dot{V}_{Fe}} \frac{H_B\, (1 + K_B\, c_{B,2}) - H_A}{(1 + K_A\, c_{A,4})\, (1 + K_B\, c_{B,2})} \tag{A-13}$$

Solution for Henry Isotherms without Complete Regeneration

It is useful to define the following intermediate variables.

$$\gamma_{Ex} = \frac{1 - P_{Ex}}{P_{Ex}} \frac{c_{B,Fe}}{c_{A,Fe}}, \quad \gamma_{Ra} = \frac{1 - P_{Ra}}{P_{Ra}} \frac{c_{A,Fe}}{c_{B,Fe}} \tag{A-14}$$

Given the feed concentrations, $c_{A,Fe}$ and $c_{B,Fe}$, the feed flow rate, $\dot{V}_{Fe}$, the desired purities, P_{Ex} and P_{Ra}, and the inner normalized residence times, $(1 - \gamma_{Ex}) \leq \tau_{A,II} \leq 1$ and $(1 - \gamma_{Ra}) \leq \tau_{B,III} \leq 1$, one can compute the necessary volumetric flow rates, $\dot{V}_I$, $\dot{V}_{Ex}$, $\dot{V}_{Ra}$ and switching time, T_S, for $H_A < H_B$ and incomplete regeneration in the following way.

$$\dot{V}_I = \frac{\tau_{A,II}\,(1-\gamma_{Ra})\,(1+F\,H_B) + (\tau_{B,III} - (1-\gamma_{Ra}))\,(1-\gamma_{Ex})\,(1+F\,H_A)}{F\,(H_B - H_A)\,(1 - \gamma_{Ex}\,\gamma_{Ra})}\,\dot{V}_{Fe} \tag{A-15}$$

$$\dot{V}_{Ex} = \frac{1 - \gamma_{Ra}}{1 - \gamma_{Ex}\,\gamma_{Ra}}\,\dot{V}_{Fe} \tag{A-16}$$

$$\dot{V}_{Ra} = \frac{1 - \gamma_{Ex}}{1 - \gamma_{Ex}\,\gamma_{Ra}}\,\dot{V}_{Fe} \tag{A-17}$$

$$T_S = \frac{\frac{(1-\varepsilon)\cdot A\,L}{\dot{V}_{Fe}}\,(H_B - H_A)}{\cdot\,\frac{1 - \gamma_{Ex}\cdot\gamma_{Ra}}{\tau_{A,II}\,(1-\gamma_{Ra}) + \tau_{B,III}\,(1-\gamma_{Ex}) - (1-\gamma_{Ra})\,(1-\gamma_{Ex})}} \tag{A-18}$$

Self-similarity solutions for Langmuir isotherms at high extract purity:

$$
c_{A,Ex}(t) = \begin{cases} \frac{1}{\tilde{K}_A} \left[\sqrt{\dfrac{\left(1+\tilde{K}_A\, c_{A,0}\right)^2 (1-\tau_{A,II})\, T_S}{\left(2+\tilde{K}_A\, c_{A,0}\right) \tilde{K}_A\, c_{A,0}\, t + (1-\tau_{A,II})\, T_S}} - 1 \right] & 0 \le t \le (1-\tau_{A,II})\, T_S \\[2ex] 0 & (1-\tau_{A,II})\, T_S < t \le T_S \end{cases}
\tag{3.121}
$$

$$
c_{B,Ex}(t) = \begin{cases} c_{B,2} + \frac{1}{\tilde{K}_B} \left[\sqrt{\dfrac{\left(1+\tilde{K}_B\, (c_{B,0}-c_{B,2})\right)^2 (1-\tau_{A,II})\, T_S}{\left(2+\tilde{K}_B\, (c_{B,0}-c_{B,2})\right) \tilde{K}_B\, (c_{B,0}-c_{B,2})\, t + (1-\tau_{A,II})\, T_S}} - 1 \right] & 0 \le t \le (1-\tau_{A,II})\, T_S \\[2ex] c_{B,2} & (1-\tau_{A,II})\, T_S < t \le \tau_2\, T_S \\[2ex] \frac{1}{K_B} \left[\sqrt{\dfrac{(1+K_B\, c_{B,2})^2 (\tau_{B,I}-\tau)\, T_S}{(2+K_B\, c_{B,2})\, K_B\, c_{B,2}\, (t-\tau_2\, T_S) + (\tau_{B,I}-\tau)\, T_S}} - 1 \right] & \tau_2\, T_S < t \le \tau_{B,I}\, T_S \\[2ex] 0 & \tau_{B,I}\, T_S < t \le T_S \end{cases}
\tag{3.122}
$$

Self-similarity solutions for Langmuir isotherms at low extract purity:

$$
c_{A,Ex}(t) = \begin{cases}
c_{A,3} & 0 \leq t < \tau_3\, T_S \\[2ex]
\dfrac{1}{\tilde{K}_A} \left[\sqrt{\dfrac{\left(1+\tilde{K}_A\, c_{A,3}\right)^2 \left(1-\tau_{A,II}-\tau_3\right) T_S}{\left(2+\tilde{K}_A\, c_{A,3}\right)\tilde{K}_A\, c_{A,3}\left(t-\tau_3\, T_S\right)+\left(1-\tau_{A,II}-\tau_3\right) T_S}} - 1 \right] & \tau_3\, T_S \leq t < \left(1-\tau_{A,II}\right) T_S \\[2ex]
0 & \left(1-\tau_{A,II}\right) T_S \leq t < T_S
\end{cases}
\tag{3.128}
$$

$$
c_{B,Ex}(t) = \begin{cases}
c_{B,3} & 0 \leq t < \tau_3\, T_S \\[2ex]
c_{B,2} + \dfrac{1}{\tilde{K}_B} \left[\sqrt{\dfrac{\left(1+\tilde{K}_B\left(c_{B,3}-c_{B,2}\right)\right)^2 \left(1-\tau_{A,II}-\tau_3\right) T_S}{\left(2+\tilde{K}_B\left(c_{B,3}-c_{B,2}\right)\right)\tilde{K}_B\left(c_{B,3}-c_{B,2}\right)\left(t-\tau_3\, T_S\right)+\left(1-\tau_{A,II}-\tau_3\right) T_S}} - 1 \right] & \tau_3\, T_S \leq t < \left(1-\tau_{A,II}\right) T_S \\[2ex]
c_{B,2} & \left(1-\tau_{A,II}\right) T_S \leq t < \tau_2\, T_S \\[2ex]
\dfrac{1}{K_B} \left[\sqrt{\dfrac{\left(1+K_B\, c_{B,2}\right)^2 \left(\tau_{B,I}-\tau\right) T_S}{\left(2+K_B\, c_{B,2}\right) K_B\, c_{B,2}\left(t-\tau_2\, T_S\right)+\left(\tau_{B,I}-\tau\right) T_S}} - 1 \right] & \tau_2\, T_S \leq t < \tau_{B,I}\, T_S \\[2ex]
0 & \tau_{B,I}\, T_S \leq t \leq T_S
\end{cases}
\tag{3.129}
$$

Table A-3: Definition of sign function.

$$sign\,(x) = \begin{cases} +1 & x > 0 \\ 0 & x = 0 \\ -1 & x < 0 \end{cases}$$